Journal of Nuclear Materials 625 (2026) 156512

Contents lists available at ScienceDirect

Journal of Nuclear Materials

journal homepage: www.elsevier.com/locate/jnucmat

Review

State of the art, gaps, and prospects in fusion materials theory and modelling

Luca Reali [a,b,*], Mark R. Gilbert [a,c,*], David Cereceda [d], Krishna Chaitanya Pitike [e], Sergei L. Dudarev [a,c], Philip Edmondson [f], Shin Kajita [g], Jae-Min Kwon [h], Byeongchan Lee [i], Jaime Marian [j], Daniel R. Mason [a], Samuel T. Murphy [k], Duc Nguyen-Manh [a,c], Takuji Oda [l], Pär Olsson [m], Wahyu Setyawan [e], Sophia O. Von Tiedemann [n], Chenxu Wang [o], Yugang Wang [o], Andrew R. Warwick [a], Jan S. Wróbel [p], Hong-Bo Zhou [q], Steven J. Zinkle [r]

[a] United Kingdom Atomic Energy Authority, Culham Campus, OX14 3DB, Abingdon, Oxon, UK
[b] Department of Civil and Environmental Engineering, Politecnico di Milano, Piazza Leonardo da Vinci 32, 20133, Milan, MI, Italy
[c] Department of Materials, University of Oxford, Parks Road, OX1 3PH, Oxford, UK
[d] Department of Mechanical Engineering, Villanova University, 19085, Villanova, PA, USA
[e] Pacific Northwest National Laboratory, Richland WA, USA
[f] University of Manchester, Oxford Road, M13 9PL, Manchester, UK
[g] Graduate School of Frontier Sciences, The University of Tokyo, 5-1-5 Kashiwanoha, 277-8561, Kashiwa, Chiba, Japan
[h] Korea Institute of Fusion Energy, Korea
[i] Kyung Hee University, 17104, Gyeonggi, Republic of Korea
[j] Department of Materials Science and Engineering, University of California, Los Angeles, CA, USA
[k] Engineering Department, Lancaster University, LA1 4YW, Bailrigg Lancashire, UK
[l] Department of Nuclear Engineering, Seoul National University, 1 Gwanak-ro Gwanak-gu, 08826, Seoul, Republic of Korea
[m] Nuclear Science and Engineering, KTH Royal Institute of Technology, SE-106 91, Stockholm, Sweden
[n] School of Metallurgy and Materials, University of Birmingham, B15 2TT, Birmingham, UK
[o] Peking University, China
[p] Faculty of Materials Science and Engineering, Warsaw University of Technology, ul. Wołoska 141, 02-507, Warsaw, Poland
[q] Beihang University, China
[r] University of Tennessee-Knoxville, Knoxville, TN, USA

ARTICLE INFO

Keywords:
Fusion materials
Transmutations
Radiation defects
High-performance computing
ML potentials

ABSTRACT

Advancing the theory and simulation of materials for fusion applications remains a key component of global roadmaps aimed at delivering much-needed fusion power. Especially as the drive for commercial application increases, prototypes must be designed against radiation damage before the relevant experimental data can be collected and cost reductions that are possible by testing materials *in silico* become even more important. Here, we summarise the state of the art as it emerged during the 7th Fusion Materials Theory & Modelling Workshop that took place in 2024, with the aim to highlight present gaps and future directions for the fusion materials modelling community. Of particular interest were the effects of transmutations, chemical complexity with the development of novel alloys and interatomic potentials, advancements in modelling high-dose microstructures, comparison with experimental data and multiscale models for structural assessment relying on high-performance computing and virtual reality.

* Corresponding authors.
E-mail addresses: luca.reali@polimi.it (L. Reali), mark.gilbert@ukaea.uk (M.R. Gilbert), david.cereceda@villanova.edu (D. Cereceda), krishnachaitanya.pitike@pnnl.gov (K.C. Pitike), sergei.dudarev@ukaea.uk (S.L. Dudarev), philip.edmondson@manchester.ac.uk (P. Edmondson), kajita@k.u-tokyo.ac.jp (S. Kajita), jmkwon74@kfe.re.kr (J.-M. Kwon), airbc@khu.ac.kr (B. Lee), jmarian@ucla.edu (J. Marian), daniel.mason@ukaea.uk (D.R. Mason), samuel.murphy@lancaster.ac.uk (S.T. Murphy), duc.nguyen@ukaea.uk (D. Nguyen-Manh), oda@snu.ac.kr (T. Oda), polsson@kth.se (P. Olsson), wahyu.setyawan@pnnl.gov (W. Setyawan), sov737@student.bham.ac.uk (S.O. Von Tiedemann), cxwang@pku.edu.cn (C. Wang), ygwang@pku.edu.cn (Y. Wang), andrew.warwick@ukaea.uk (A.R. Warwick), jan.wrobel@pw.edu.pl (J.S. Wróbel), hbzhou@buaa.edu.cn (H.-B. Zhou), szinkle@utk.edu (S.J. Zinkle).

https://doi.org/10.1016/j.jnucmat.2026.156512
Received 30 October 2025; Received in revised form 20 January 2026; Accepted 5 February 2026
Available online 20 February 2026
0022-3115/Crown Copyright © 2026 Published by Elsevier B.V. This is an open access article under the Open Government License (OGL) (http://www.nationalarchives.gov.uk/doc/open-government-licence/version/3/).

1. Introduction

This article provides a review of the status of fusion materials theory and modelling, largely drawn from the Fusion Materials Technology Collaboration Program (FM TCP) workshop held in January 2024 in the Republic of Korea. The workshop was organised with topical sessions covering the development of fusion materials theory and models, computational optimisation of the models, as well as their experimental validation. In particular, the meeting focused on materials response theory, application of machine learning (ML) with a focus on ML interatomic potentials, and modelling of neutron-induced transmutation and the effect of neutron impacts on materials properties and behaviour. The FM TCP is part of a network of autonomous collaborative partnerships focused on a wide range of energy technologies. The TCPs are organised under the auspices of the International Energy Agency (IEA), where the TCPs themselves remain functionally and legally autonomous. Views, findings and publications of the Fusion Materials TCP do not necessarily represent the views or policies of the IEA Secretariat or its individual member countries.

The 2024 workshop was held at the Yonsei University Global Campus, Songdo in Incheon, Republic of Korea. It is the 7th meeting on fusion materials theory and modelling organised under the auspices of Fusion Materials TCP. The outcomes of the previous meeting were captured in a review paper published in 2021 [1]. The workshop involved 40 participants with 30 presentations that provided a review of the key research activities within the fusion materials modelling community and, in particular, highlighted the areas where research challenges remain.

Fig. 1 presents a selection of key issues and outstanding questions that were discussed in the workshop and that form the broad backbone of this review. The final summary section outlines current trends and new directions in the development of models for fusion materials, highlighting the continuing extensive effort on the development of new fusion systems and applications of fusion technologies.

2. Transmutation effects

2.1. Gaps and opportunities identified since the last workshop

Exposure of plasma-facing materials (PFMs) and first wall/ blanket structural materials to high neutron fluxes induces nuclear reactions that change their nuclide composition over time. These reactions produce radionuclides, leading to material activation, and generate nuclides of new elements through transmutation, which can modify material properties. It is then critical to enhance our understanding of these phenomena and their impact on selecting structural materials for fusion energy. For example, H and He transmutation products can stimulate cavity swelling at intermediate temperatures (potentially leading to unacceptable dimensional changes) [2–4], and solute transmutations typically lead to pronounced degradation in thermal conductivity and may induce embrittlement [5–8].

Another phenomenon which had previously been overlooked is the generation of energetic γ-photons by materials under fusion neutron irradiation. Of particular interest is the sensitivity of the fraction of neutron energy converted into photon energy on the material being irradiated. For example, Reali et al. calculated this value for the two candidate plasma-facing materials for ITER, namely Be and W (before the choice ultimately fell on W). While Be converts a negligible fraction of neutron power into gamma heating (0.1%), W does the same with an efficiency approaching 99% [9]. This has implications both for obtaining an accurate description of the neutron heating and for the behaviour of the plasma. Materials in the tokamak chamber may in fact radiate high energy photons or electrons back into the plasma [9,10].

Experimentally, neutron irradiation campaigns at the fast test reactor Joyo [11–16], the Japan Materials Testing Reactor (JMTR) [15–17], and the High Flux Isotope Reactor (HFIR) [5,15,16,18–20] have investigated the microstructural evolution of tungsten and tungsten alloys. Their findings suggest that the influence of transmutant *Re* and Os on the properties of irradiated materials is at least as significant as the effects caused by displacement damage.

Experimental reactor irradiation studies on W have also reported significant *Re* and Os solute segregation and precipitation for solute concentrations that should be uniformly dissolved in solid solution according to equilibrium phase diagrams [5,21]. Still, the absence of experimental reactors and materials testing facilities that accurately replicate the conditions required for making fusion a commercially viable energy source has driven the need for further modeling studies to examine the anticipated effects of irradiation and temperature in fusion power plants [1,22–40].

Of particular relevance are those using inventory codes that solve a set of coupled differential equations describing the rate of change of all possible nuclides, thus evolving the nuclide composition of materials exposed to a specific neutron irradiation field [41]. As well as quantifying that evolution under a given neutron environment, inventory calculations performed with codes such as the FISPACT-II developed and maintained by the United Kingdom Atomic Energy Authority over the last 30 years [41,42], can also explore how the spatial variation in the neutron environment can lead to similarly large variations in material response. For example, variations in the thermal neutron environment, caused by moderators such as water, can create localised, on mm length scales, increases in transmutation in elements such as W [43]. Over greater lengths the variations are no less extreme in a fusion environment because of the essential need to slow, stop, and absorb all energy from, the 14 MeV neutrons produced by deuterium-tritium reactions. Fig. 2

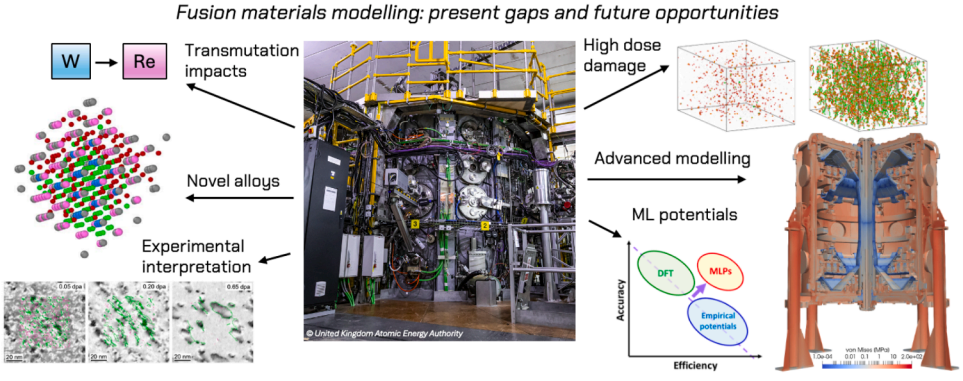

Fig. 1. Theory and modelling of fusion materials will necessarily play a part in transitioning from present, experimental devices to future fusion reactors. In this review, we highlight examples from the state-of-the-art alongside the areas where we see gaps that should soon be addressed (central image: ©2023 United Kingdom Atomic Energy Authority).

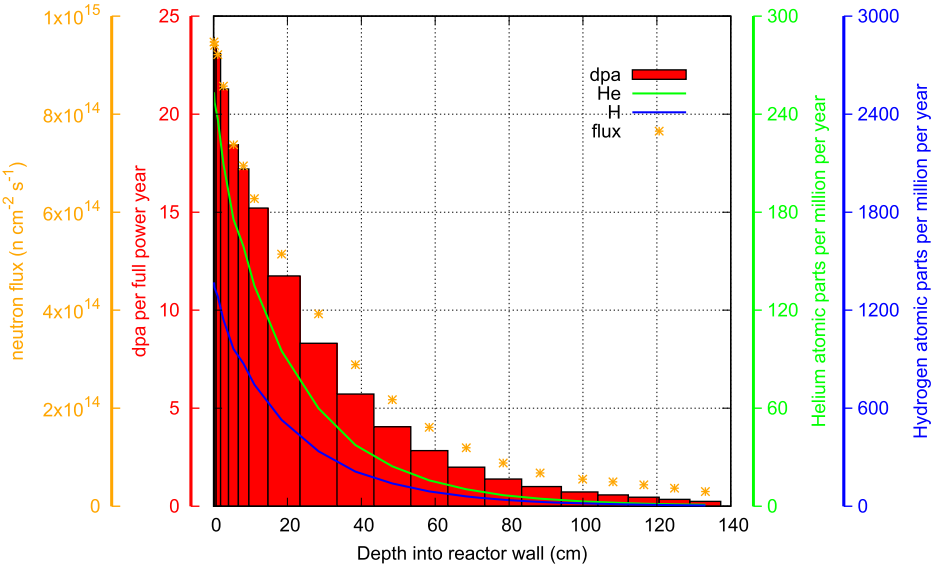

Fig. 2. Variation in the predicted damage dose rate (measured according to the NRT-displacements per atom or dpa per unit time), and helium and hydrogen production per year that would be experienced in pure Fe as a function of depth into the plasma-facing wall of a typical fusion tokamak design. Also shown is the variation in total neutron flux over the same depth for the design (an early concept of the STEP prototype [44,45]) that included other materials, such as tungs10 armour and tritium breeding materials. The neutron fluxes are the volume averages in voxels of a rectangular mesh superimposed over the underlying (STEP) tokamak geometry and include the accumulated contributions from all nuclear interactions, including neutron scattering, multiplication, and absorption. This large variation of neutron-exposure-related phenomena on the engineering component-scale highlights the heterogeneous modelling challenge that must be solved to predict material performance at this scale.

demonstrates this, showing the predicted variation in displacements per atom (dpa), helium and hydrogen production per year in Fe as a function of depth into plasma-facing wall of a fusion system.

In addition to enhancing our understanding of how the thermo-mechanical behavior of PFMs changes due to nuclear transmutation, further investigation into the uncertainty and sensitivity of the various techniques used to study these transmutation effects is needed. These factors play a critical role in defining safety margins for the design of fusion power plants.

2.2. Current modelling activities

2.2.1. Impact of transmutation on the mechanical behavior of W-based plasma facing materials

It is known that Re, either as a transmutated or an alloying element, reduces the mobility of self-interstitial atoms (SIAs) [46]. Furthermore, Re, when combined with another element other than W, can form a strong alloy-SIA complex, further reducing the mobility of SIAs [47]. This in turn can buy time for Frenkel pairs to recombine during recoil events, and reduce the number of residual defects. Recently, Qian et al. [48,49] have presented a novel computational approach that integrates inventory codes, uncertainty quantification, and first-principles DFT electronic structure calculations to investigate how the bulk mechanical properties of tungsten-based (W-based) materials evolve over time under neutron irradiation-induced transmutation.

In particular, they investigated pure W, two W-based high-entropy alloys (W-HEAs), and two W-based "SMART alloys" (W-SAs), where SMART stands for Self-passivating Metal Alloys with Reduced Thermo-oxidation.

Their approach starts by calculating the evolution of the chemical composition of the candidate materials as they are exposed to the fusion-like environments expected in DEMO, as shown in Fig. 3. Such calculations are carried out using the FISPACT-II inventory code and the analysis also included the evaluation of uncertainties for the production of stable nuclides of the main transmutant elements.

Then, they performed first-principles Density Functional Theory (DFT) calculations to investigate the mechanical response of the candidate materials at the beginning of their operational life and as their chemical composition changes due to nuclear transmutation.

Their results, some of which are shown in Fig. 3, include the evolution of the lattice constant, elastic properties, density of states, generalized stacking fault energies, unstable stacking fault energies, gamma surface, and dislocation-based ductility parameter.

The approach presented in these first works uses the simplistic Virtual Crystal Approximation (VCA) [50], but it sets the foundation for investigating these transmutation effects using other DFT techniques that could explore the heterogenous distribution of alloying elements [51–53].

2.2.2. Nuclear data uncertainty propagation

In the nuclear fusion community, the determination and communication of uncertainties associated with any calculated radiological parameter is of particular importance, due to an inherent lack of experimental data for effects of long-term exposure to high-energy neutrons on material evolution, from a materials properties as well as radiological safety perspective.

The UK has set the goal for its fusion programmes to achieve low-level waste (LLW) within 100 years of reactor end-of-life (EOL) for any radioactive waste produced, where LLW is defined as below 1.2×10^7 Bq/kg for any $\beta + \gamma$ activity. While studies have shown that this aim will not be feasible for all reactor components [54–57], it is instrumental to be able to accurately predict factors such as material activity, heat output, and dose rate to enable efficient decommissioning post-EOL alongside appropriate waste handling and disposal. Therefore, corresponding uncertainties must be quantified with any parameter value as a measure to assess accuracy, reliability and potential needs for further investigation. Demonstrating an independent methodology for conducting a sensitivity and uncertainty (S/U) analysis was the subject of a recent study presented at the FM TCP workshop [58]. Radioactivity levels and their associated uncertainties in decay time were calculated for several nuclear steels after a 20-year DEMO irradiation schedule, in order to estimate necessary safety margins for the mean decay time to reach LLW levels. In this method, uncertainties in nuclear cross-sections of 'dominant radionuclides' responsible for high material activity levels

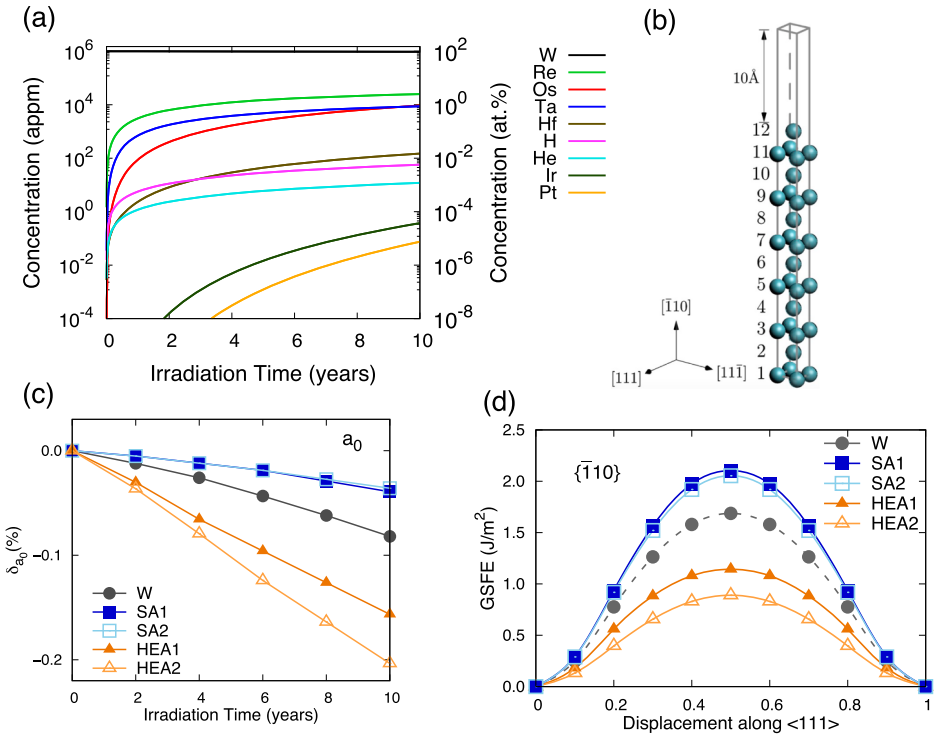

Fig. 3. (a) Transmutation of W after 10 years of continuous exposure to the plasma-facing conditions expected in a prototype fusion reactor; (b) Atomic arrangement of the surface models used to calculate the general stacking faults energy (GSFE) on the $\langle 111 \rangle \{\bar{1}10\}$ slip system; (c) Evolution of the lattice constant in transmuted W-alloys during the first ten years of continuous exposure to EU-DEMO conditions, in terms of the relative difference $\delta_{a_0} = \frac{a_0' - a_0^0}{a_0^0}$; and (d) GSFE for the slip along $\langle 111 \rangle$ direction in $\{\bar{1}10\}$ plane after 5 years of irradiation. Figure adapted from [48,49].

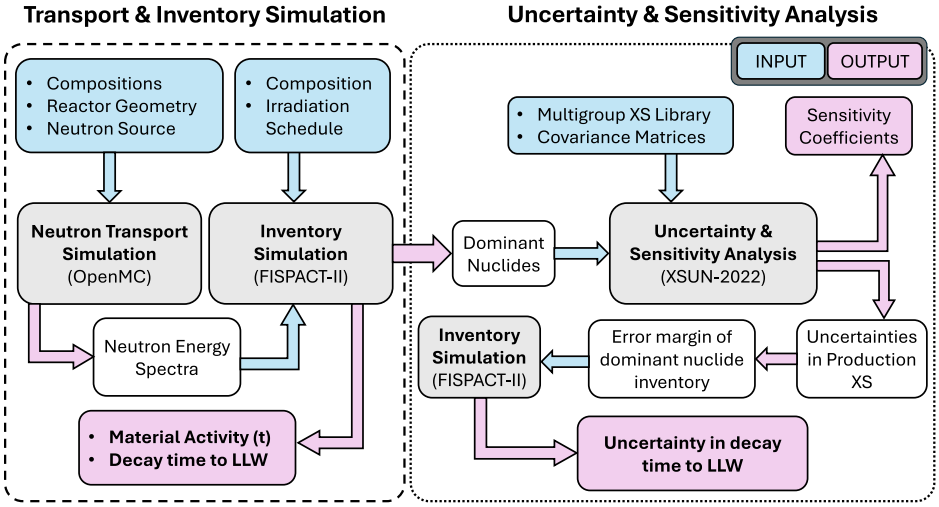

Fig. 4. Summary of method combining transport and inventory calculation to investigate material activity with independent uncertainty analysis on relevant nuclear data.

were propagated through to upper and lower margins of $(\beta + \gamma)$ activity ($\pm$ [Bq/kg]) at certain points in time post-EOL, which were subsequently propagated to uncertainties in required decay time to reach a specified activity level ($\pm$ [years]). A schematic of the methodology is shown in Fig. 4.

First, transport and inventory simulations were carried out to calculate the parameter of interest - in this case material activity - for which uncertainties due to nuclear cross-section data were to be determined. Neutron transport calculations were conducted with OpenMC [59], inventory simulations were carried out using FISPACT-II [41].

Outputs of the latter included total material $(\beta + \gamma)$ activity levels as a function of time, alongside individual radionuclide contributions, rendering a list of 'dominant' nuclides which were produced during irradiation. The XSUN-2022 code package [60] was then used to conduct an independent sensitivity and uncertainty analysis of the relevant cross-sections relating to the production of each dominant nuclide. This code-package comprises a suite of deterministic codes: TRANSX-2.15 [61] to prepare cross-section data compatible with the discrete-ordinate transport code PARTISN [62], and SUSD3D [63] which calculates sensitivities and uncertainties in parameters of interest stemming from input nuclear data. The resulting uncertainties in nuclide production cross-sections where then propagated into an error margin in dominant nuclide inventory present in the material composition of interest. Subsequently, FISPACT-II was used again to calculate the decay time-to-LLW

for each upper and lower margin of dominant nuclide inventory in the material, providing uncertainties for each nominally calculated time-to-LLW.

A one-dimensional, cross-sectional reactor geometry was used, finding that differences in the type of dominant nuclides produced and their associated uncertainties varied between structures closer to the neutron source and further outboard of the blanket for several reasons: (1) Different nuclear cross-sections dominate in deeper regions in the blanket due to flux softening occurring from neutron-material interactions, resulting in different dominant nuclides in the first wall (FW) compared to the blanket back-structure; (2) uncertainties are generally higher towards the rear of the blanket compared to the FW, because uncertainties in transmutation cross-sections dominate closer to the source, whereas contributions from transport cross-section uncertainties increase towards the rear. The calculated error margins in time-to-LLW were comparatively small, and did not change predicted waste classifications within 100 years for any of the assessed steels. It is however noted that the uncertainties studied in this case were derived from nuclear data only, and therefore account only for a small part of a large number of uncertainty contributors affecting reactor lifetime, activity, dose level, operational and decommissioning time schedules and costs.

The XSUN-2022 code package can be used to carry out S/U analyses in one, two and three-dimensional transport geometries for numerous parameters of interest, such as reaction rates, gamma-dose output, decay heat output, etc. One of the main limitations of S/U analyses is the quality and availability of relevant covariance matrix data, which has improved significantly with releases of recent evaluations, e.g. ENDF/B-VIII.0 [64] and JEFF-3.3 [65]. However, further development in this area is still required to ensure mathematical verification of the available covariance matrices and ultimately consistency between calculated and experimental results. Such S/U analyses as outlined above should be conducted periodically as covariance data continues to be improved and reactor design parameters become more mature. Validated and accurate nuclear data is critical for making reliable predictions needed for the design, operation and ultimate decommissioning of future fusion power plants, determined by transmutation and materials degradation. Some successful validation of nuclear data libraries as well as inventory codes used to make these predictions has recently been demonstrated, and needs for expansion of fusion-relevant experiments on appropriate timescales have been highlighted [66].

3. Advances in conventional and novel alloys

3.1. Modelling of void decoration by Re and Os in neutron irradiated W

Development of predictive schemes for understanding microstructure evolution and compositionally phase stability of plasma facing materials under fusion environment represents one of the most challenging gaps to link materials theory and modelling from atomistic scale to engineering application. On the other hand, the kinetic models are conventionally deterministic assuming that the equilibrium phases are known a priori and will finally appear after long-time simulations involving nucleation and growth accelerated by defect diffusion in materials under irradiation. On another hand, more general models are based on statistical physics to investigate free energies of different phases in the presence of radiation induced defects and quasi steady-state configurations can be obtained by minimisation of the total free energy of the considered system [67]. To avoid big uncertainties due to empirical parametrization, a first-principles approach in determining the free energy of multi-element materials including vacancy and self-interstitial defect components on equal footing, has been developed combining DFT, Cluster Expansion Hamiltonian (CEH) with large-scale Monte-Carlo simulations [68,69]. The CEH can be written in the following formula [68]:

$$\Delta H_{mix}^{CEH}(\vec{\sigma}) = \sum_{\omega,n,s} J_{\omega,n}^{(s)} m_{\omega,n}^{(s)} \langle \Gamma_{\omega',n'}^{(s')}(\vec{\sigma}) \rangle_{\omega,n,s}, \quad (1)$$

where the summation is performed over all the clusters, distinct under symmetry operations in the BCC lattice for the present study. $\vec{\sigma}$ denotes the ensemble of occupation variables in the lattice. ω and n are the cluster size and its shell label, respectively. $m_{\omega,n}^{(s)}$ denotes the site multiplicity of the decorated clusters (in per-lattice-site units); and $J_{\omega,n}^{(s)}$ represents the many-body effective cluster interaction (ECI) energy corresponding to the same (s) decorated cluster. In Eq. (1), $\langle \Gamma_{\omega',n'}^{(s')}(\vec{\sigma}) \rangle_{\omega,n,s}$ denotes the cluster function, averaged over all the clusters of size, ω', and label, n', decorated by the sequence of point functions,(s'). Within the matrix formulation of CEH for a system with K elements, the cluster function is related to the probability function of finding a given cluster via the formula [70]:

$$y_{\omega,n}^{(AB\cdots)} = \overbrace{(\bar{\bar{\tau}}_K^{-1} \otimes \cdots \otimes \bar{\bar{\tau}}_K^{-1})}^{\omega}{}_{AB\cdots,ij\cdots} \langle \Gamma_{\omega,n}^{(ij\cdots)} \rangle \quad (2)$$

where the matrix elements of the inverse of the $(\bar{\bar{\tau}}_K)$ matrix are defined by the expression [70]:

$$(\bar{\bar{\tau}}_K^{-1})_{ij} = \begin{cases} \frac{1}{K} & \text{if } j = 0\,, \\ -\frac{2}{K}\cos\left(2\pi\lceil\frac{j}{2}\rceil\frac{\sigma_i}{K}\right) & \text{if } j > 0 \text{ and } j-1 < K \text{ and j odd}, \\ -\frac{2}{K}\sin\left(2\pi\lceil\frac{j}{2}\rceil\frac{\sigma_i}{K}\right) & \text{if } j > 0 \text{ and j even}, \\ -\frac{1}{K}\cos\left(2\pi\lceil\frac{j}{2}\rceil\frac{\sigma_i}{K}\right) & \text{if } j-1 = K \text{ and j odd}. \end{cases} \quad (3)$$

and $i, j = 0, 1, 2, \ldots (K-1)$, j and $\lceil\frac{j}{2}\rceil$ stands for the ceiling function - rounding up to the closest integer. From Eq. (2), the point probability function is written as:

$$y_{1,1}^{A} = \sum_{s} (\bar{\bar{\tau}}_K^{-1})_{A,(s)} \langle \Gamma_{1,1}^{(s)} \rangle, \quad (4)$$

and the pair probability function is determined by the following formula :

$$y_{2,n}^{AB} = \sum_{s} (\bar{\bar{\tau}}_K^{-1} \otimes \bar{\bar{\tau}}_K^{-1})_{A,B,(s)} \langle \Gamma_{2,n}^{(s)} \rangle. \quad (5)$$

Eq. (5) allows the two-body cluster probability to be linked with the Warren-Cowley short-range order (SRO) parameter, $\alpha_{2,n}^{(AB)}$, via the definition [71,72]:

$$y_{2,n}^{AB} = x_A x_B (1 - \alpha_{2,n}^{AB}) \quad (6)$$

where x_A and x_B denote the bulk concentration of the chemical species A and B, respectively. In the case where $\alpha_{2,n}^{AB} = 0$, the pair probability is given by the product of their concentrations $x_A x_B$ corresponding to random configuration of A and B species in an alloy system. In the case of $\alpha_{2,n}^{AB} > 0$, clustering or segregation between A-A and B-B pairs is favoured and for $\alpha_{2,n}^{AB} < 0$, the chemical ordering of A-B pairs occurs. By combining Eqs. (4),(5 and (6), the SRO parameters for K-component system can be calculated by the general expression as follows [68]:

$$\alpha_{2,n}^{AB} = 1 - \frac{\sum_{s} (\bar{\bar{\tau}}_K^{-1} \otimes \bar{\bar{\tau}}_K^{-1})_{A,B,(s)} \langle \Gamma_{2,n}^{(s)} \rangle}{\left(\sum_{s} (\bar{\bar{\tau}}_K^{-1})_{A,(s)} \langle \Gamma_{1,1}^{(s)} \rangle\right)\left(\sum_{s} (\bar{\bar{\tau}}_K^{-1})_{B,(s)} \langle \Gamma_{1,1}^{(s)} \rangle\right)}. \quad (7)$$

The CEH, defined by Eq. (1) can be used to explicitly determine the configuration entropy of a K-component system via the thermodynamic integration method [73,74]. Here the entropy is computed from fluctuations of the enthalpy of mixing at a given temperature using the following formula

$$S_{conf}[T] = \int_0^T \frac{C_{conf}(T')}{T'} dT' = \int_0^T \frac{\langle [\Delta H_{mix}^{CEH}(T')]^2 \rangle - \langle [\Delta H_{mix}^{CEH}(T')] \rangle^2}{T'^3} dT', \quad (8)$$

where $\langle [\Delta H_{mix}^{CEH}(T')]^2 \rangle$ and $\langle [\Delta H_{mix}^{CE}(T')] \rangle^2$ are the square of the mean and mean square enthalpies of mixing, respectively. The statistical average over configurations at finite temperature in Eq. (8) can be performed by combining the CEH with atomistic Monte Carlo (AMC) technique.

The above modelling scheme has been employed to simulate transmutation induced segregation effects in neutron irradiated tungsten

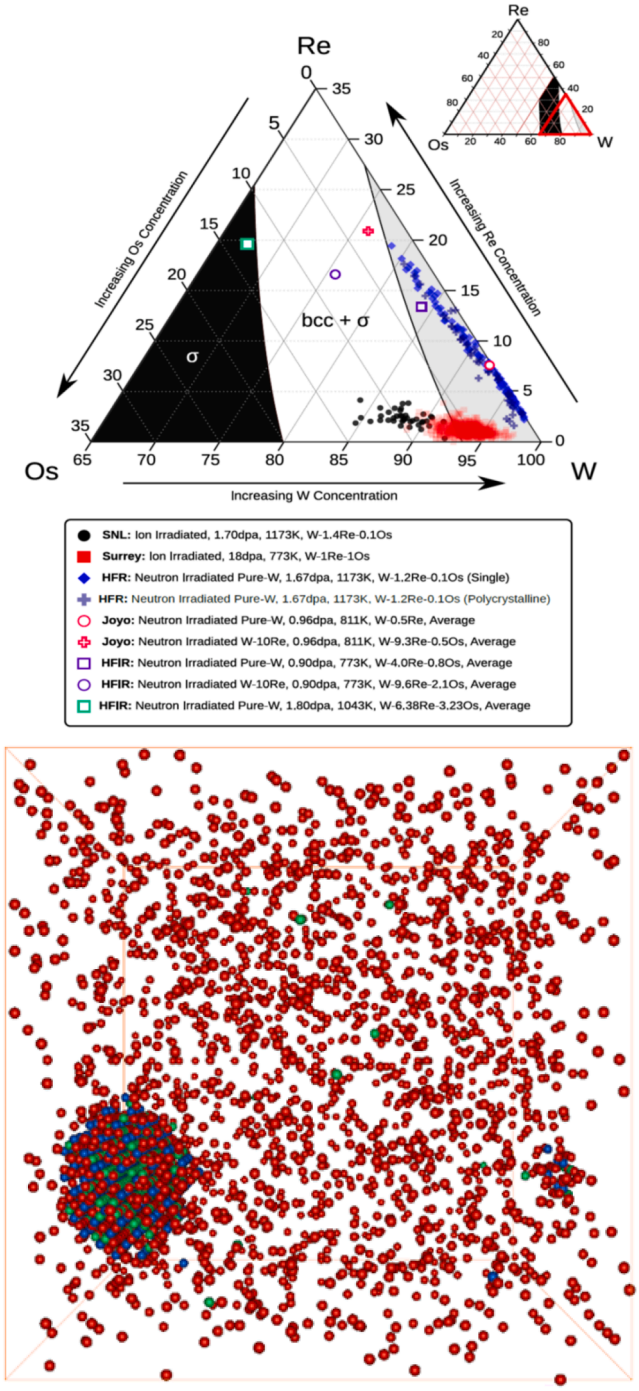

Fig. 5. Top: A section of phase diagram containing Re, Os cluster concentration determined from experimental data for neutron irradiated W and for ion irradiated W-Re-Os with similar alloy composition and dose [75–78]. Bottom: First principles based Monte Carlo simulations in a bcc 30x30x30 supercell containing voids (blue) decorated by *Re* (red) and Os (green) in W with 2at% *Re* and 0.2at% Os and 0.2 at% vacancy at 1173K [68,69]. (For interpretation of the references to colour in this figure legend, the reader is referred to the web version of this article.)

where the phenomenon is strongly pronounced at radiation dose [75–78]. Finite-temperature analysis shows that voids are decorated by *Re* and Os, but there is no decoration by tantalum (Ta). The difference between the elements is correlated with the DFT prediction of solute-vacancy binding energies as well the sign of the short range order (SRO) parameter between *Re* and Os as function of solute and vacancy concentrations, in agreement with Atom Probe Tomography (APT) observations. Statistical analyses of *Re* and Os impurities in vacancy-rich tungsten show that the SRO effects involving the two solutes are highly sensitive to the background concentration of the different species. In quaternary W-Re-Os-vacancy alloys containing 1.5% *Re* 0.1% Os and 0.1% vacancy, the SRO Re-Os parameter is negative at 1200K, driving the formation of concentrated *Re* and Os precipitates. Comparison with experimental Transmission Electron Microscopy (TEM) and APT data on W samples irradiated at the High Flux Reactor (HFR) shows that the model explains the origin of anomalous segregation of transmutation products (Re,Os) to vacancy clusters and voids in the high temperature limit pertinent to the operating conditions of a fusion power plant.

The top Fig. 5 shows the cross-section of ternary phase diagram W-Re-Os in which the neutron-induced precipitations in W containing *Re* and Os have been collected from previous experimental studies reported for different fission reactors. It is found from our analysis that the cluster size of these precipitations is larger for the reactor materials with higher transmutation rate. The bottom Fig. 5 shows results from our Monte-Carlo simulation with the higher Re, Os concentrations applied for the high-flux isotope reactors (HFIR) [69].

3.2. Models for phase decomposition of SMART alloys

Tungsten alloys have been selected as a potential first wall material for DEMO and other near-term fusion reactors. Tungsten is a good candidate due to its high melting point, low sputtering by plasma particles, relatively short-term activation, low tritium retention, and high thermal conductivity. However, pure tungsten behaves poorly in loss-of-coolant accident scenarios, where contact with the surrounding atmosphere causes rapid oxidation releasing radioactive tungsten dust into the air or form hazardous gaseous tungsten volatile oxides. To tackle this, Self-passivating Metallic Alloys with Reduced Thermo-oxidation (SMART) have been suggested that incorporate additions of Cr, Y, and Zr that, will preferentially form protective scales of their own oxides on the surface, inhibiting the tungsten oxide formation.

Combining first-principles CE Hamiltonian with MC simulations, a constrained thermodynamic approach is developed to predict the composition stability in defective multi-component alloys for which the short-range order (SRO) are directly derived for investigating the strong impact on microstructural phase decomposition as a function of elemental concentrations and temperatures in SMART W-Cr-Y [82] and W-Cr-Y-Zr materials [80]. In fig. 6, the SRO parameter values are calculated for different pairs in the two quaternary W-Cr-Y-Zr alloys with strongly negative SRO for Y-Zr pair while the SRO of the remaining pairs had the positive values. These predictions lead to the co-segregation of Y and Zr in the considered SMART systems and the enhancement of spinonal phase decomposition between W and Cr in a comparison with the SMART ternary system W-Cr-Y.

These modelling results reveal a significant impact on understanding the role of phase decomposition on microstructural evolution in the integration with engineering and technology manufacturing of SMART materials [83]. Importantly, the impact of phase decomposition is recently validated by experimental observations from EELS, TEM and in-situ STEM as well as from systematic study of oxidation properties of W-Cr-Y SMART materials under annealing conditions [84,85].

3.3. Modelling of highly radiation-resistant W-based high-entropy alloys

Recently, tungsten-based low-activation high-entropy and medium-entropy alloys have been proposed as possible candidates for next-generation fusion reactors due to their exceptional tolerance to irradiation. These alloys have been developed and designed via a strong integration between predictive modelling and experimental studies carried at the US national laboratories [79,86–89].

The top panel of Fig. 7 shows the result of atomistic modelling from exchange Monte Carlo simulations obtained for the specific composition

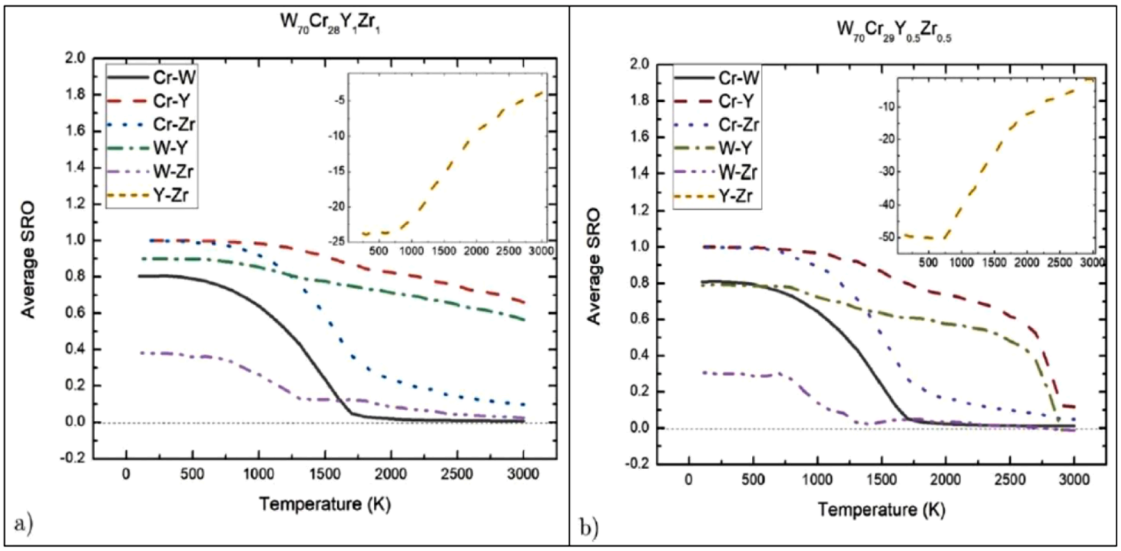

Fig. 6. Short-range order evolution in W-Cr-Y-Zr SMART materials as function of alloy compositions—a) being $W_{70}Cr_{28}Y_1Zr_1$ and b) being $W_{70}Cr_{29}Y_{0.5}Zr_{0.5}$—showing the phase decomposition between W and Cr whereas the SRO between Y and Zr (insert figures) is strongly negative [79–81].

$W_{0.38}Ta_{0.36}Cr_{0.15}V_{0.11}$ alloy at 1100 K in a 30x30x30 supercell using CEH (Eq. 1) and thermodynamic integration technique (Eq. 8). It was found that inside of the second-phase bcc precipitate there was a very high concentration of Cr and V atoms with a very low (up to 5%) concentration of W and Ta atoms. The resulted concentration profile (not shown here) along the arrow direction was in an excellent agreement with the profile measured by Atom Probe Tomography (APT) experimental analysis from [86].

Chemical complexity and nano-crystallinity enhance the radiation tolerance of the refractory HEAs, but their multi-element nature, including low-melting Cr, complicates bulk fabrication and limits practical applications. In [88], it is demonstrated that reducing the number of alloying elements while retaining high-radiation tolerance is possible within the binary system W–Ta tailored by small additions of V. The experimental results were validated with theoretical analysis of chemical short-range orders (CSRO), combining ab-initio atomistic Monte-Carlo modeling with machine-learning-driven molecular dynamics (MD) simulations of radiation damage. It is found from computational analysis that a small change in V concentration has a significant effect on the Ta-V CRSO between $W_{53}Ta_{44}V_3$ and $W_{53}Ta_{42}V_5$ leading to radiation-resistant microstructures in these medium-entropy alloys. Furthermore, MD simulations using machine-learned potentials (see the bottom Fig. 7) directly support and explain the experimental observations, showing drastic differences in the radiation response between W–Ta and W–Ta–V with only small additions of V.

3.4. Modelling of radiation damage in Fe-Cr alloys and composition dependence in Fe-Cr-Mn-Ni high-entropy alloys

Fe-Cr alloys form the basis of many industrially important steels. Ferritic/martensitic steels with 7–12 wt% Cr are candidates for the internal structures of future fusion power plants because of their remarkable resistance to swelling. Because magnetism plays an important role in understanding of structural phase stability between ferritic (bcc) and austenitic (fcc) steels, an ab-initio database taking into consideration of electron spin polarization is indispensable for modelling not only for thermodynamic but also radiation damage properties in these materials [22,90–98].

Using exchange Monte Carlo (MC) simulations based on an DFT parameterized CEH model, the phase stability of low-Cr Fe-Cr alloys under irradiation as a function of vacancy (Vac), carbon, and nitrogen content has been explored. In the presence of vacancies, C/N aggregate to the core regions of vacancy clusters, making segregation of Cr-rich clusters less pronounced (see top Fig. 8). The structure of Cr-rich clusters varies significantly, depending on the concentration of interstitial atoms and on the ratio of N to C. Predictions derived from MC simulations agree with experimental observations of Fe-Cr alloys exposed to ion irradiation. The concentration of Cr found in clusters containing C and N interstitial atoms is in qualitative agreement, and the absolute Cr content found in the clusters simulated at 650 K is in quantitative agreement with experimental APT observations of Fe-3.28 at.%Cr alloys irradiated at 623 K. The measured C and N content of 42±5 and 151±3 at. ppm likely results from the contamination that occurred during ion beam irradiation.

Fe-Cr-Mn-Ni HEAs with higher radiation and corrosion resistances can potentially replace the austenitic 304 and 316 steels, which are used, for example, as advanced structural materials for fast breeder and light water fission reactors. The relative phase stability of fcc and bcc Cr-Fe-Mn-Ni alloys has been investigated using a combination of DFT, CEH, and Monte Carlo (MC) simulations in an integration with the thermodynamic databases within the OpenCalphad approach. The results obtained using this approach are in qualitative agreement with the available experimental data from the literature and the experiments performed within this work for the samples of Fe-Cr-Ni-Mn alloys synthesized using arc-melting and annealed at 1273 K for 48 h. The Gibbs free energy analysis has enabled the identification of the alloys that are predicted to be single fcc phase for a wide range of temperatures. The bottom Fig. 8 shows the temperature dependence of phase stability between fcc and bcc within the quaternary HEAs as a function of alloy compositions from these simulations.

4. Modelling high dose damage

4.1. Defect production, ballistic mixing and microchemical and microstructural evolution: State of the art, gaps and opportunities

A comprehensive and quantitatively accurate understanding of primary damage events is essential for the development of robust predictive models of high-dose damage in materials. It is now well established that the traditional international benchmark for quantifying displacement damage, the venerable Norgett-Robinson-Torrens displacements per dpa (NRT dpa) model [100], significantly under-predicts, by a factor of 2-50 (depending on PKA energy), the amount of radiation mixing (replacements per atom, RPA) and over-predicts the surviving defect

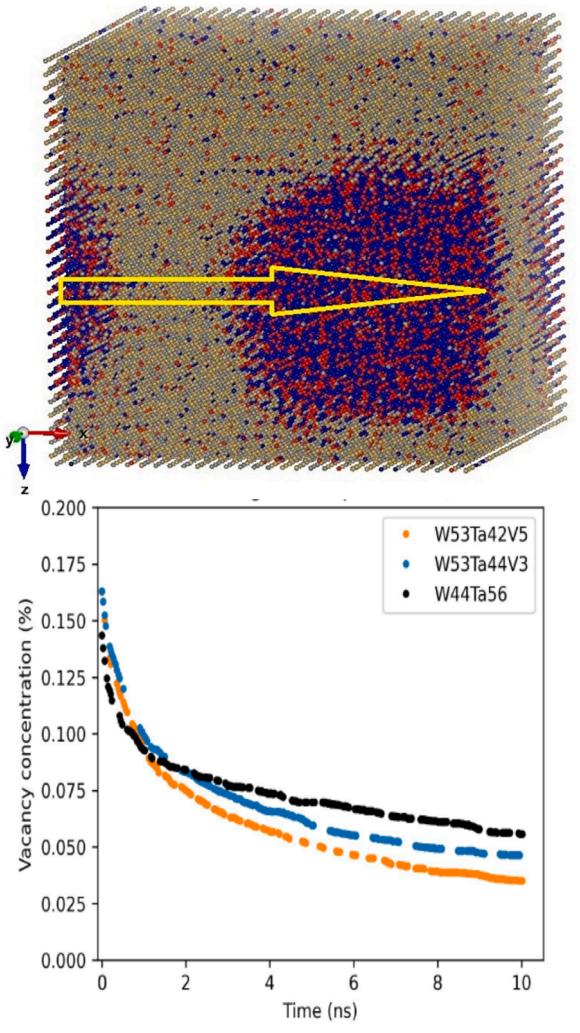

Fig. 7. Top: Modelling of co-segregation of Cr (blue) and V (red) from W (yellow) and Ta (green) in high-entropy alloys $W_{38}Ta_{36}Cr_{15}V_{11}$ [79]. The arrow shows a direction where the predicted composition partitioning changes between the matrix and the Cr-V-rich precipitates. Bottom: Reduction of void density from binary W-Ta to W-Ta-V alloys with 3% and 5% at. of V obtained from overlapping cascade molecular dynamics simulations in combination with annealing using machine-learning potentials [88]. (For interpretation of the references to colour in this figure legend, the reader is referred to the web version of this article.)

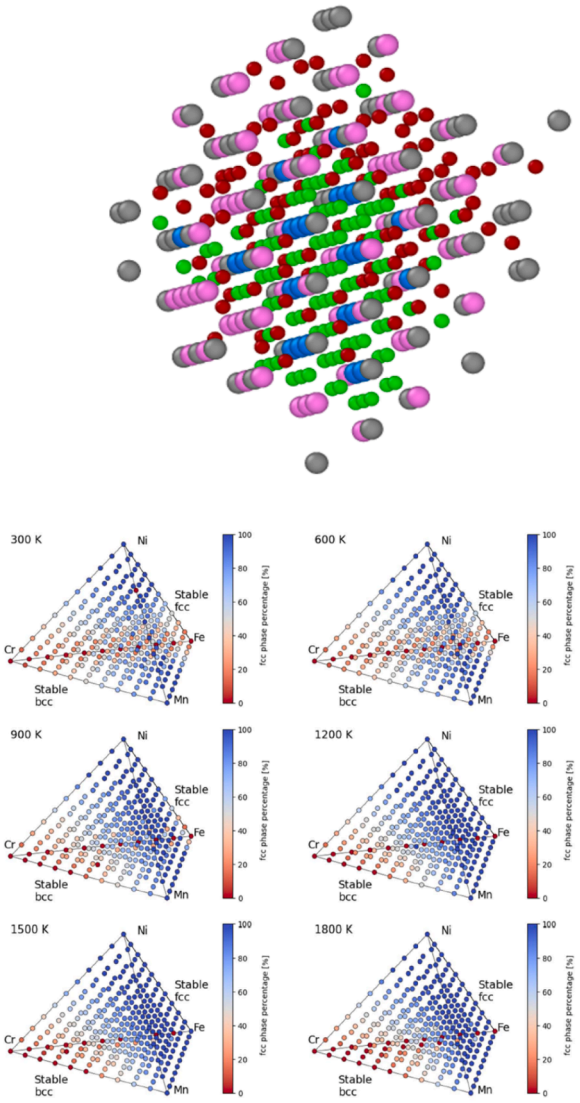

Fig. 8. Top: Formation of Cr (grey atoms) clustering predicted and extracted from modelling of Fe-alloys with nominal 3at.%Cr alloys containing Fe (pink) containing C (red), N (green) impurities interacting with vacancies (blue) [98]. Bottom: Temperature and composition maps showing fcc (blue) and bcc (red) phases of Fe-Cr-Ni-Mn high entropy alloys from Monte-Carlo simulations using cluster expansion Hamiltonian [96,97,99].. (For interpretation of the references to colour in this figure legend, the reader is referred to the web version of this article.)

production at near-zero temperatures where thermally activated point defect migration is negligible (athermal recombination corrected dpa, ARC-DPA) for energetic displacement cascade conditions due to limitations inherent in the binary collision approximation for defect production [101,102]. This leads to about a factor of 3 difference in the surviving defect fraction (relative to the NRT dpa) for near-threshold PKA (e.g., electron or proton) irradiations vs. energetic PKA (e.g., fast neutron or heavy ion) conditions. At temperatures where interstitials are mobile, experimental and modeling studies have found that thermally-activated correlated recombination corrections to the dpa (CRC-DPA) cause a pronounced additional reduction in surviving defects (particularly for low-PKA damage events), such that the surviving defect fraction for irradiations above the onset temperature for long range interstitial motion (recovery Stage ID [103]) is 20-25% of the NRT dpa value, independent on PKA energy [104]. At higher temperatures where thermally activated vacancy migration occurs, there is insufficient experimental and modeling studies to accurately predict the additional correlated defect recombination that occurs. Limited studies suggest the CRC-DPA could be reduced to as low as 10% of the NRT dpa value, independent of PKA energy [104]. Fig. 9 summarizes experimental estimates for the surviving defect fraction in Cu after corrections for athermal and thermal-activated correlated recombination within individual PKA collisions for electron and fast reactor neutron irradiations [104]. Quantification of the long-term correlated defect recombination associated with isolated PKA events as a function of PKA energy for multiple materials (using kinetic Monte Carlo or other modeling tools) would be valuable for developing improved predictive models of radiation damage.

Radiation mixing is a key contributor to the stability of nanoscale precipitates in irradiated alloys. A moderate number of experimental studies have investigated radiation mixing in ordered alloys [102,105]. Additional fundamental experimental and modeling studies of radiation mixing within isolated PKA events would be valuable to more accurately quantify the radiation mixing as a function of PKA energy, target mass, and exposure temperature. It has been empirically observed

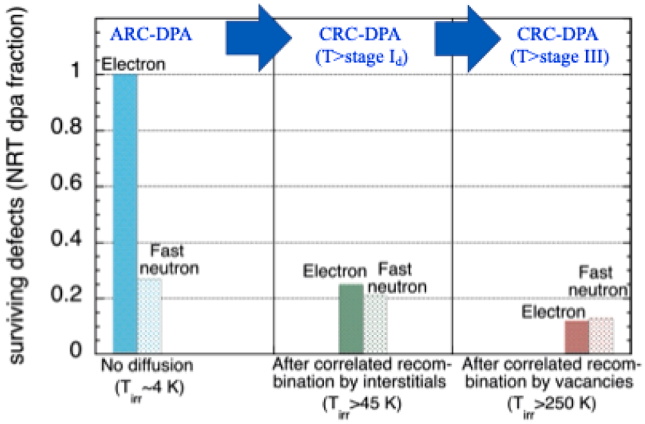

Fig. 9. Temperature dependence of surviving defect fraction (normalized to NRT dpa) in Cu considering athermal recombination corrections (ARC-DPA) and thermal-activated correlated recombination (CRC-DPA) for defects produced within individual PKA events, based on damage rate or correlated defect recovery experimental measurements [104].

that nanoscale precipitate stability is suppressed for high damage rates (increased frequency of ballistic collision events) and low irradiation temperatures (decreased diffusional renucleation and/or self-healing of radiation mixed nanoprecipitates). Several phase stability models have been developed to semi-quantitatively describe precipitate evolution under a variety of irradiation conditions [67,106–111]. However, additional work is needed to include appropriate radiation mixing values and solute intermixing of precipitate and matrix elements, along with precipitate nucleation and growth/coarsening phenomena. An additional important phase stability activity is improved predictive modeling of radiation induced solute segregation (RIS), which can lead to localized chemical segregation that exceeds solid solution phase stability limits and thereby causes radiation induced precipitation (RIP). Depending on the RIP microstructural location (grain boundaries, matrix), intergranular or intragranular embrittlement might be induced. Fig. 10 shows an example of matrix Re-rich precipitation that is induced in neutron irradiated W [5] at solute concentrations far below the predicted solubility limit obtained from the equilibrium phase diagram [112]. Due to the presence of multiple RIS mechanisms (inverse Kirkendall diffusion, solute-defect coupled diffusion, etc.) it has been elusive to achieve quantitatively reliable RIS predictions of the solute enrichment or depletion evolution as a function of spatial location and dose in the vicinity of radiation defect sinks.

Further research is needed on the evolution of dislocation loops and creation of network dislocation structures during irradiation. In many elemental metals and simple alloys, saturation in the loop number density is typically achieved within ~0.1–5 dpa [113]. The potential impact of 1-D glissile point defect clusters vs. random walk diffusion monodefects on the dislocation loop evolution needs further modeling. The potential impact of elastic strain fields from other microstructural features on the migration and trapping of 1D glissile clusters needs further modeling analysis. Numerous studies have shown that intermediate levels of He/dpa lead to maximized cavity swelling during irradiation [2], and this has been attributed to achievement of a balance between biased (loops, small cavities) and unbiased (void) microstructure features in terms of preferential absorption of interstitials [2,3,114–116]. A recent experimental dual ion beam (heavy ion + He) study reported that the He/dpa level corresponding to peak swelling tended to decrease with increasing dose in ferritic-martensitic steels irradiated at 445 or 460 °C [117]. Further research and modeling is needed to determine whether the evolution of cavities or other microstructural features might lead to a shift in the He/dpa ratio that produces peak swelling in irradiated materials with increasing dose. The change in hardening accompanying irradiation-induced microstructural changes has traditionally been analyzed using dispersed barrier hardening models [118,119]. For accurate predictions of hardening, it is essential to use size-dependent barrier strengths for the various dislocation obstacles [120,121] rather than assuming an empirical size-independent barrier strength. Another important aspect is that hardening superposition relations need to be calculated by grouping "weak" dislocation barriers and "strong" dislocation barriers using root sum square (RSS) relationships for similar-strength obstacles and linear superposition to subsequently combine the grouped weak and strong composite obstacles strengthening contributions [122–127]. Therefore, in contrast to current widespread practice in the radiation effects research community, it is generally inappropriate to calculate the change in hardness after irradiation by only considering the irradiation-induced microstructural features since that methodology implicitly (and often incorrectly) assumes the preirradiation and irradiation dislocation obstacle strengths have similar values [128,129]. Assuming linear superposition for the irradiation-modified component of the microstructure can lead to hardening overpredictions errors up to 50% for typical irradiation studies in the irradiation hardening regime [128]. Instead, the hardness due to various microstructural features needs to be separately calculated for all microstructural features in the unirradiated and irradiated conditions (using appropriate RSS and linear superposition relations), and then the radiation-induced hardness change can be calculated from the difference in the unirradiated and irradiated calculated composite strengths. For the case of multiple weak and strong obstacles in the unirradiated and irradiated microstructures, the unirradiated and irradiated strengths (σ_{unirr}, σ_{irr}) are given by

$$\sigma_{\text{unirr}} = \sqrt{\sigma_{w1}^2 + \sigma_{w2}^2 + \dots} + \sqrt{\sigma_{s1}^2 + \sigma_{s2}^2 + \dots} \tag{9}$$

$$\sigma_{\text{irr}} = \sqrt{\sigma_{w1}^2 + \sigma_{w2}^2 + \sigma_{iw1}^2 + \dots} + \sqrt{\sigma_{s1}^2 + \sigma_{s2}^2 + \sigma_{is1}^2 + \dots} \tag{10}$$

where σ_{w1} and σ_{s1}, etc. are the strength contributions associated with weak and strong obstacles, respectively, and σ_{iw1} and σ_{is1}, etc. are the corresponding irradiation-induced weak and strong obstacles. Fig. 11 summarizes the comparison between microstructure-predicted and measured hardness for two ferritic/martensitic steels irradiated at 369–520 °C with fast reactor neutrons or dual ions to 16–72 dpa [129]. Good quantitative agreement (within 5–10% accuracy) was obtained for the predicted strength based on microstructure characterization and the measured strength when size-dependent dislocation obstacle strengths and appropriate hardening superposition rules (linear vs. root sum square) were used. The predicted hardness in Fig. 11 involved contributions from 9 different obstacles (several precipitates, dislocations, cavities, etc.).

4.2. Atomistic simulation of high-dose damage

To understand the evolution of irradiated microstructure, we are faced with an enormous complexity in possible metastable atomistic and chemical configurations and their thermally-activated transformations [130,131]. For many years, mean field rate theory (MFRT) [132] was the principal method for understanding irradiated microstructural evolution at experimental timescales. MFRT replaces the complexity of irradiation defects with independent idealised defect objects, and so explores the competition between diffusion, coalescence, annihilation, and sinks. Because evolution is determined by diffusion, it is most obviously applicable where the mean free path between defects is long, and MFRT returns the same dynamics if spatial correlation is explicitly introduced using object Kinetic Monte Carlo with the same Hamiltonian [133]. But where the local density of objects is such that elastic interactions are strong, different conclusions are reached about the self-trapping of defects [134–136] and the atomic degrees of freedom become important for evolution to the point where idealising defects into objects is more of a hindrance than an advantage [137].

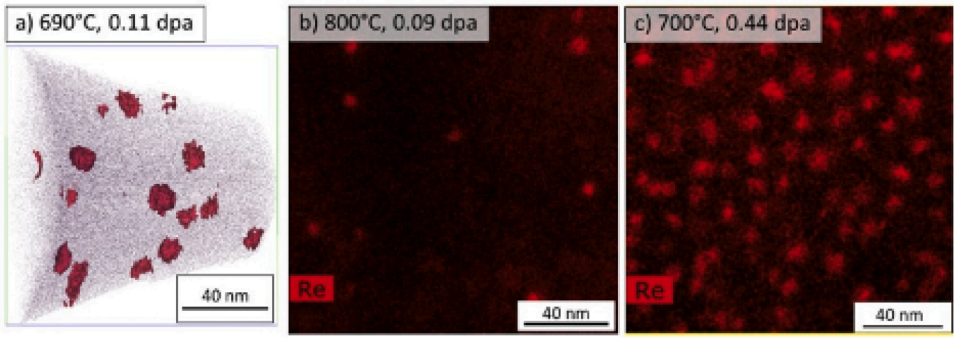

Fig. 10. Re-enriched matrix precipitates in pure W irradiated in a mixed spectrum reactor at 590–700 °C [5]. The measured and calculated transmutant *Re* content is far below the 25% *Re* equilibrium phase stability limit for W-Re at these temperatures [112].

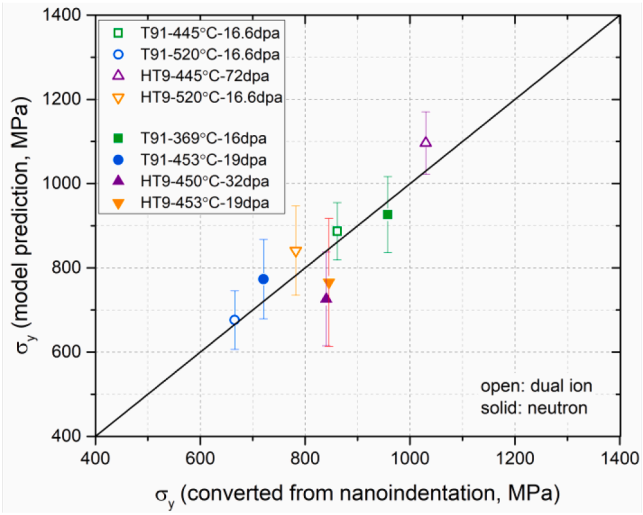

Fig. 11. Comparison of predicted and measured hardening of HT9 and T91 ferritic/martensitic steels following fast reactor or dual ion irradiation [129].

One could simulate the sequence of displacements initiated by primary knock on atoms and subsequent recovery directly. However, this approach also presents significant challenges. A single collision cascade produces less than 10^{-4} dpa. Thus, accumulating doses on the order of 100 dpa would require more than $\sim 10^6$ cascades [138,139]. Clearly, it is impractical to perform brute force ab initio molecular dynamics simulations of a single cascade event, let alone over multiple cascades, even with optimized state of the art density functional theory code. Furthermore, simulation cells typically probe short length scales in DFT simulations, containing at most $\mathcal{O}(100)$ atoms. Unfortunately, simulating a large number of cascades sequentially is also computationally demanding with molecular dynamics. Hence, more efficient algorithms are required to investigate the evolution of microstructure at high dose.

The creation relaxation algorithm (CRA) [39], or Frenkel pair accumulation method [140,141], are efficient techniques for simulating the evolution of microstructure to high dose at atomistic length scale resolution with reasonable computational effort. These methods represent the ballistic transport of atoms in a collision event with a simple process and, in the most reduced form, may be described in a few steps. Starting with a simulation cell of perfect crystal containing N_{cell} atoms:

1. Select an atom at random, and move it to a new position in the simulation cell.
2. Relax the energy of the system *via*, for example, the conjugate gradient method.
3. Repeat steps 1 and 2 until a specified dose ϕ_F is achieved.

The system relaxation has to be performed in a physically consistent way for the simulation to be meaningful. The most common approach is to use interatomic potentials and rely on standard molecular statics or molecular dynamics relaxation[39,141–144]. However, given the high efficiency of the method, it is also tractable to apply electronic structure theory methods such as DFT to relax the system and evolve the microstructure [145,146]. In a similar spirit to conventional definitions of dose, the 'canonical displacement per atom' (cdpa) the simulation cell is 'exposed' to in the algorithm is measured by $\phi = N_D/N_{cell}$ cdpa, where N_D is the number of atoms selected and displaced thus far. Canonical dose and NRT dpa are qualitatively similar notions, and it has been shown that the microstructural properties evolved as a function of cdpa can be mapped linearly to the NRT dose scale [147]. In this form, no additional effort is required to advance the system in time and the energy minimisation offers a fast and insightful route to producing high dose microstructures.

There are multiple variations of the CRA approach that optimise the algorithm or account for dynamical effects. For instance, one may create multiple Frenkel pairs in a single iteration, although not so many as to amorphize the entire simulation cell. As a rule of thumb, accumulating a dose of 0.005 cdpa per creation-relaxation cycle results in an evolution of microstructure similar to displacing one atom at a time [142]. Chartier and Marinica [141] simulated irradiation damage of iron by relaxing the system with molecular dynamics for 2 ps at 300 K between Frenkel pair insertions as opposed to the aforementioned energy minimisation schemes [39]. Reali et al. [148] introduced the 'molten spheres' algorithm, where the Frenkel insertion step is replaced with replacing spherical regions in the crystal with a molten configuration of the atoms, so as to mimic the melt that is created in the wake of a collision cascade. All of these athermal simulations of irradiation damage to an initially perfect single crystal result in broadly similar microstructures and defect statistics treated as a function of dose.

An obvious limitation of MD simulation is the system size available. Simulations of irradiation damage with tens of millions of atoms or more [149,150] are now relatively common, but still this corresponds only to simulation boxes with sides 50–100 nm. Moving to GPU-based clusters can increase this simulation size to some extent, but practically researchers are often more limited by the data-storage requirements of the trajectory [151].

The important question to ask therefore is whether a 100 nm length-scale is relevant to simulating fusion materials, and the answer is a (qualified) yes. Displacement cascades characteristic of neutron damage are typically lower energy than those produced by ion-irradiation [152], the practical upshot of which is that cascade splitting is less prevalent [153], and so thermal heat spike regions more spatially contained [154]. The individual lattice defects observed in displacement cascades are typically under 10 nm diameter [155,156], similar in size to the cascade extent [135], so we conclude MD lengthscales to be entirely appropriate for understanding the defect generation process.

In the case of massively overlapping cascade simulations [139,157] at low homologous temperatures, individual defects are mobilised by nanoscale fluctuating stresses to coalesce into larger, complex dislocation structures [39]. If the simulation cell is relatively small (order 1 million atoms, equivalent to a cube with linear dimensions of about a hundred interatomic distances), complete crystal planes will form [158], rather than a dislocation network [159] that spontaneously evolves if the simulation cell contains 10 M or more atoms. The formation of a dislocation network has been detected in experimental observations of ion-irradiated materials [160]. There is also evidence from Electron channelling contrast imaging (ECCI) and High angular resolution electron backscatter diffraction (HR-EBSD) for the possible emergence of an even larger length-scale, order 1 μm, appearing in the spatial correlations of strain [161], which may be due to the loop rafting occurring on the scale of over hundred of nanometres. We conclude that large MD simulations are suitable for high-dose low-temperature irradiation simulations, but could miss long-range elastic strain correlations brought about by defect diffusion [162,163]. The significance of the emergent strain-driven length scales over 50 nm requires further analysis.

The initial structure used in MD simulations does not need to be a perfect single crystal – a highly idealised approximation. Recent work has explored the evolution of polycrystalline nano-grain tungsten [164]. It was found that smaller grains swell less than larger grains and suppress the transient peak of dislocation density at low doses. With increasing dose, the size distribution of the grains broadens together with an upward shift in the mean grain size.

With regard to timescales, the characteristic timestep of MD simulations, order 1fs, is short compared to the inverse Debye frequency, and simulations are rarely extended beyond 1μs. So how can simulated irradiation with a dose rate of 1 dpa/μs be compared even to high dose rate experiments closer to 1 dpa/h? One way to view the problem was proposed by Boleininger et al. [143]. Recovery events affecting the microstructure do not occur at the Debye frequency, but rather with an Arrhenius rate, with a mean time for a process with activation energy E_A given by $\tau_A = \nu_D^{-1} \exp\left[E_A/(k_B T)\right]$. These can be fast or slow compared to the characteristic time for a cascade heat spike to impact a given atomic site. If the dose rate is $\dot{\phi}$, each cascade displaces N_d atoms in the ballistic phase, and the heat spike affects N_{melt} atoms, then the characteristic cascade mixing time is order $\tau_C = N_d/(\dot{\phi} N_{melt})$. We can therefore define a *thermal factor* ξ as the ratio of these times, which we can interpret as the number of times a defect will hop before it is hit by another cascade,

$$\xi = \frac{\tau_C}{\tau_A} = \frac{\nu_D N_d}{\dot{\phi} N_{melt}} \exp\left(-\frac{E_A}{k_B T}\right). \tag{11}$$

If the thermal factor is small, then cascades are impacting faster than the recovery events with activation energy E_A, and the system becomes insensitive to dose rate. Conversely, if ξ is large then defect diffusion and recovery dominates. The crossover point is strongly dependent on temperature. At the most extreme limit, CRA [39] introduces damage completely athermally, by displacing an atom then relaxing the microstructure with conjugate gradients solely. This has no diffusion-enabled defect recovery, and so generates a very dense damage microstructure. However, in fusion materials the key recovery stages are visibly separable [165], with wide temperature gaps between observations of stage I recovery (movement of self-interstitial atoms), stage II recovery (movement of interstitial clusters), and stage III recovery (monovacancy movement) [166]. The activation barrier for (a carbon or nitrogen-decorated) monovacancy migration event in steels requires the dissociation of vacancy-carbon and vacancy-nitrogen complexes resulting in the effective energy of 1.3 eV [167]. In pure tungsten, the vacancy migration energy is 1.7 eV [168,169], compared to the value of 1.78 eV derived from ab initio calculations [27,170]. We can therefore perform atomistic simulations at a temperature where ξ is large for self-interstitial movement, but small for vacancies. What happens to the interstitials when given time to diffuse can vary according to their local environment. In the low dose limit, the mean free path for interstitial cluster diffusion can be long, leading to loss of interstitials at sinks [171], especially under conditions of production bias [172]. While not fundamentally excluded from MD simulation, typically the simulation time used for overlapping cascade simulations is insufficient to model this long-range diffusion, and other methods such as object kinetic Monte Carlo [173,174] or stochastic cluster dynamics [175,176] are more appropriate. At high doses, the movement of interstitial clusters is constrained by local elastic fields [39,134], and so for high dose simulation, the fast movement of interstitial clusters manifests as local recombination, possible to simulate within the MD timeframe [177]. This gives a wide temperature window of validity for MD cascade simulations, so that direct comparisons can be made to experiments near room temperature. This temperature is also technologically relevant, as it includes actively-cooled regions of a fusion device.

We might then ask what is the expected asymptotic consequence of a system of atoms driven by successive cascades? An MD simulation just before one cascade can be defined by a (high dimensional) state vector $\mathbf{x}$ [151], and after the cascade and a few ps of annealing by the new state $\mathbf{x}'$. Granberg et al. [178] argued that as the simulation is inherently stochastic, there is a probability distribution for a state $p(\mathbf{x})$, and therefore the cascade event is represented by an unknown Markov matrix $\mathbf{M}$ describing the evolution of the probability distribution, $p(\mathbf{x}') = \mathbf{M}_{\mathbf{x}',\mathbf{x}} p(\mathbf{x})$. Successive cascade events will drive the system to a steady state, whose probability distribution is a right eigenvector of $\mathbf{M}$. This eigenvector may even be unique if $\mathbf{M}$ has strictly positive elements [179], but no guarantees can be made that the steady state is reached quickly. The existence of the steady state does, however, mean that any route to steady state is acceptable [178], allowing for high dose simulations to be accelerated by starting 'near' the steady state and performing a smaller number of full cascades [147]. A further advantage of the steady state is that it has the greatest density of defects, and therefore the greatest microstructural stabilisation through elastic interactions. The steady state is therefore also likely to show the slowest recovery processes, and so be the most accurately described by MD.

In general, the irradiation damaged microstructure that develops under athermal modes is characterised by a transient over small doses of ~ 0.1 dpa, followed by a defect evolution and growth stage into an eventual steady state at high doses of the order of 1 dpa [39,142,143,145,158]. The steady state is characterised by a global change in dimensions and dense fluctuating defect configurations supported by a spatially varying internal stress field.

At higher temperatures, we should expect higher energy barrier events to be activated within characteristic experimental times. Chief amongst those absent in MD simulations is vacancy migration, which should lead to void formation or further defect recovery through annihilation, and the balance between these two paths is critical to understanding high dose - high temperature evolution. Explicit Hamiltonian dynamics must be abandoned to model longer times if the such events are expected, and so while atomistic resolution seems to be important to correctly model strongly interacting defects, maintaining this atomistic resolution is very challenging due to the explosion in number of possible events. This restricts the applicability of on-the-fly kinetic Monte Carlo [131,137,180] to small defects or individual cascades. Very recent progress has been made explicitly evolving interstitial clusters with MD and slower processes with kMC [181,182], but there is no generally established procedure for simulating the high-dose, high-temperature limit, and further work in this area is important.

4.3. Athermal defect accumulation in the CRA approximation

The most simple methods for athermally accumulating defects have very few adjustable parameters, perhaps only a restriction on the minimum separation on displaced atoms, so results are a function of the interatomic potential energy surface. CRA has been performed using

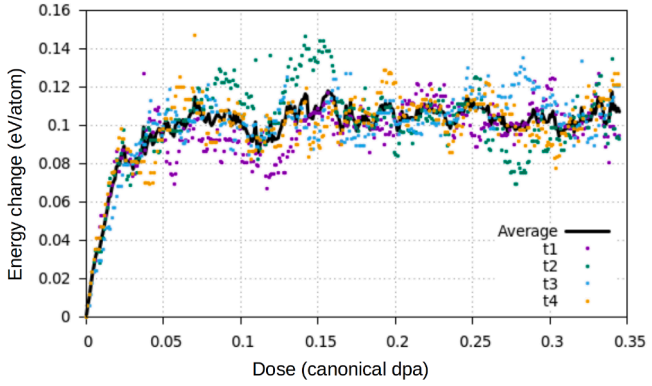

Fig. 12. DFT-CRA trajectories of microstructural evolution in bcc Fe. The evolution of the total energy for four trajectories (t1-t4) and their average is shown, data from [145].

density-functional calculations for the energy (DFT-CRA). This offers a ground-truth for dense defect interactions against which empirical or machine-learned interatomic potentials can be validated. For DFT-CRA, given the limited supercell size, it is important to perform several CRA trajectories to gather statistically significant results. Fig. 12 shows the total energy change for four distinct trajectories, including their average, for a DFT-CRA simulation of single Frenkel pair insertion in bcc Fe[145]. One can here clearly see the linear growth and subsequent transformation into a saturation stage of the implanted energy.

Below $\sim 10^{-3}$ dpa, the inserted Frenkel pairs are well separated and thus their concentration increases linearly as a function of dose. Shortly after, self interstitial atoms interact and coalesce into small clusters and dislocation loops whilst a vacancy atmosphere remains. The population of isolated loops grows and coalesces into a dense dislocation network at doses of the order of 0.1 dpa. In the limit of large doses above 1 dpa, loops expand further and dissociate the percolating network into new crystallographic planes and isolated loops, significantly reducing the total dislocation density. In Fig. 13, a typical evolution of microstructure under the molten spheres algorithm is shown with doses increasing from 0.01 dpa to 1 dpa where the dislocation structure is overlaid on simulated TEM images [148,183].

These stages, as elucidated using IAP-driven CRA, have been confirmed in bcc Fe using DFT-driven CRA [145]. The maximally useable supercell sizes using DFT-CRA do not, however, allow for simulating the appearance of the dislocation network, but instead saturates in a dislocation loop dominated steady state, in all other aspects very similar to the steady state achieved in the IAP-CRA simulations.

The use of DFT-CRA allows for analysis of electronic structure effects on the evolving microstructure, beyond the capabilities of classical methods. The evolution of local magnetization in an evolving microstructure has shown how important local magnetic moments are in stabilizing 3D defect clusters such as the C15 Laves phase structures that have been modelled separately before [184,185]. Under DFT-CRA in bcc Fe, C15 grows spontaneously and dynamically, and it has also been indicated that alloying elements such as Cr allow for increased stabilization of these clusters, see Fig. 14. The C15 cluster structures display local ferromagnetic ordering, anti-parallel to the host Fe lattice, and analysis of the local stresses in the evolving microstructure show how the constrained environment promotes different defect cluster types to form and grow[144].

Typically, the development of these defects results in a net swelling of the crystal lattice as the expansive relaxation volumes of interstitial type defects are generally larger in magnitude than the contracting relaxation volumes of a mono vacancy [186–188]. On average, the dimensional changes of cubic metals are purely dilatational. However, in anisotropic materials, such as Zr, the dimensional change contains a shear component in a phenomenon known as irradiation induced growth [142]. X-ray Laue diffraction measurements of lattice strains in ion-irradiated tungsten were found to be in qualitative agreement with CRA simulations, with an initial low-dose phase of positive strain due to interstitials giving way to a high-dose phase of negative strain due to the vacancies as the interstitials form a dislocation network or form complete planes [158] as shown in Fig. 15. This validates the basic evolution phases observed in CRA, but it should be noted that as CRA represents cryogenic accumulation, it overestimates the defect density by an order of magnitude. Similar strain curves have been subsequently observed with massively-overlapping molecular dynamics cascade algorithms at room temperature, and these produce the same qualitative trends, but with quantitative accuracy [148,189].

In the CRA limit, where no thermal evolution takes place, the irradiated system displays responses and statistics that are signatures of self organised criticality. The distribution of change in total energy of a system as a result of one Frenkel pair insertion was found to be distributed according to a power law. Rare high energy events were highly non-local such that a single displacement iteration could induce a change in dislocation structure far away from the insertion location [39]. In addition, the size distribution of dislocation loop diameters has been found to be distributed according to a power law whose exponents are consistent with experiment [190]. Overlapping cascade simulations are expected to deviate from purely critical behaviour, yet retain heavy tailed defect size and response distributions.

4.4. Modelling the influences of He and H on defect evolution in iron-based materials

In iron-based blanket structural materials, substantial transmutation He and H atoms will be produced via nuclear reactions induced by high-energy fusion neutrons [191]. Experimental studies have demonstrated that He and H can impose significant influences on cavity evolution, reflected by the size and density of cavities [192–199]. Moreover, the coexistence of He and H may synergistically result in more complex evolutionary behaviors of cavities [4,198,200–202]. Mesoscale simulations, such as kinetic Monte Carlo (KMC) and cluster dynamics (CD) methods, provide feasible pathways to model the long-term evolution of irradiation-induced defects and high dose damages. To elucidate the physical mechanisms by which He and H influence cavity evolution, it is essential to acquire the fundamental parameters for the interactions among He, H and cavities at the atomic scale as key inputs into mesoscale simulations. These physical parameters primarily include the diffusion barriers of mobile defects, the interaction radii between defects, and the binding energies for defect clusters (associated with their dissociation rates) [203].

Significant challenges remain in understanding the synergistic effects of H and He on cavity evolution in iron-based materials using mesoscale simulations. Over the past few decades, substantial ab-initio calculations and molecular dynamics simulations have been conducted to investigate the interactions among He, H and cavities in BCC iron [115,204–217], while the comprehensive parameters for the ternary interactions among He, H and cavities remain lacking. Helium is shown to inhibit the diffusion of vacancy-type defects more effectively than H [204–206]. Both He and H can enhance the thermal stability of cavities by increasing vacancy binding energies to cavities [204,208,209,213,214], which is predicted to increase cavity density by enhancing cavity nucleation [194–199]. The synergistic influence of He and H on the thermal stability of He-H-cavity ternary systems remains underexplored, and the reasonable predictive models need to be developed for accurate mesoscale modelling. The impacts of He and H on the capture radii of cavities for displacement defects have received relatively less attention. Molecular statics calculations show that He can increase the spontaneous capture radii of cavities for vacancies and weakly alter those for interstitials [115]. This can increase the vacancy flux into cavities, thereby altering their long-term evolution. Future efforts are needed to explore H effect

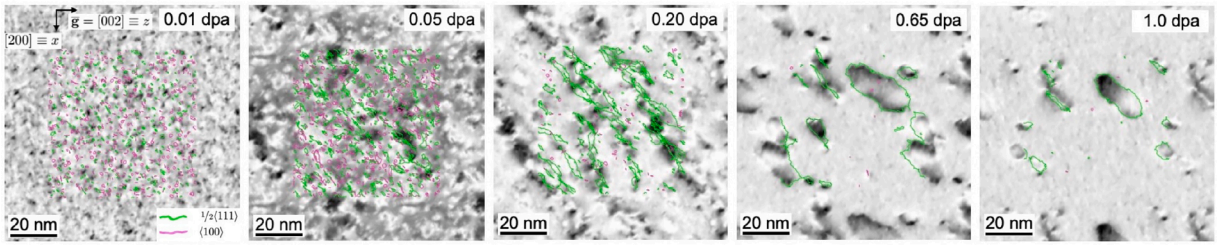

Fig. 13. Simulated TEM images of high energy irradiated sheared tungsten with increasing dose from left to right under the molten spheres algorithm. The dislocation structure is overlaid on each TEM image, showing the evolution from small isolated loops to a network that dissociates into larger loops. Figure adapted from [148].

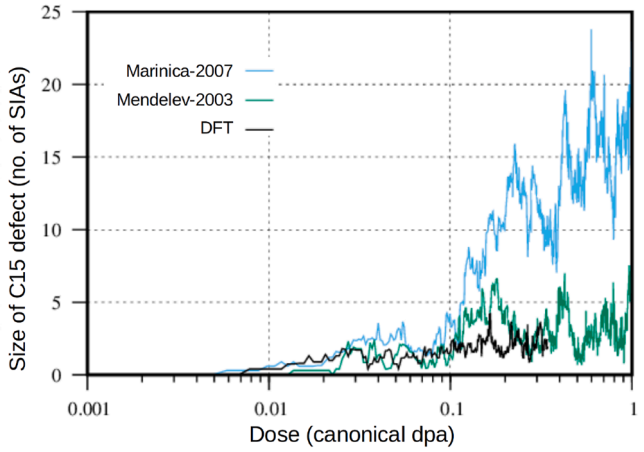

Fig. 14. The largest C15-type structures, dynamically formed under CRA conditions, as a function of irradiation dose predicted by different methodologies [145].

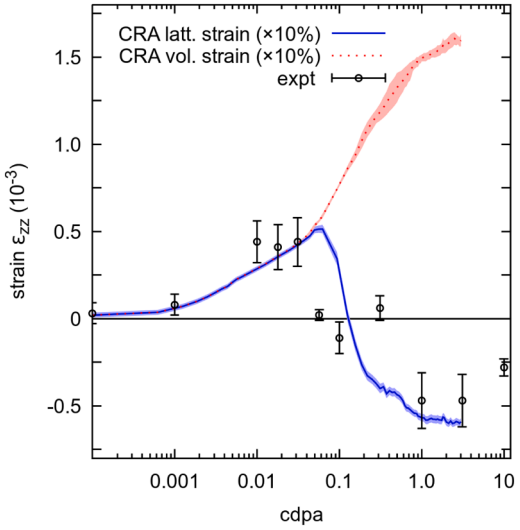

Fig. 15. Variation of lattice strain and volume strain of a ion irradiated tungsten sample. The scatter plot shows X-ray Laue diffraction measurements of the lattice strain along the irradiation direction. Lattice strain and volumetric strain derived from CRA simulations are shown in solid and dashed curves respectively. Figure adapted from [158].

and H-He synergistic effect on the capture radii of cavities for displacement defects.

In Object kinetic Monte Carlo (OKMC) simulations, the rapid diffusion of interstitial He and H atoms (with the diffusion barriers lower than 0.10 eV in BCC iron [204,211,215]) increases the overall event rate of the simulated system and may significantly limit the applicability to low-dose scenarios. This effect is more pronounced for H than He since the binding energies of H to cavities are significantly lower than those of He to cavities (less than 1.0 eV vs. several eV in BCC iron [204,210–213,215,216]), Consequently, a high concentration of interstitial H atoms persists when cavities can effectively trap interstitial H atoms. Recently, a quite simplified approach to this issue is to treat interstitial H atoms as immobile [218], and preliminarily demonstrates the synergistic effects of He and H on the long-term evolution of displacement defect. However, this approach may underestimate the frequency of the interaction between H and displacement defects. The kinetic trapping process of H by cavities involving spatial information may require implicit treatment for improved computational efficiency.

Meanwhile, CD based on the mean-field rate theory can model defect evolution in high doses sacrificing spatial information on defects. Nonetheless, the binding of He and H to cavities will remarkably increase the number and complexity of master equations that depict the concentrations of cavities and thus limit the available timescales and achievable irradiation dose. An effective method is to reduce the dimension of the phase space representing cavities containing He and H. Specifically, taking He as an example, small cavities containing He are completely depicted by a two-dimensional (2D) phase space defined by the number of vacancies and He. For larger cavities of the same size, one master equation governs the evolution of their total concentration, and another calculates the time-dependent average number of He per cavity. This approach effectively reduces the phase space to be one-dimensional (1D), as illustrated in Fig. 16(a). Using the above model, Brimbal et al. demonstrated He can evidently promote cavity nucleation in austenitic stainless steels at elevated temperatures [219], as shown in Fig. 16(b). Due to the lack of interaction parameters for H-cavity binary system and He-H-cavity ternary system, CD simulations examining the influences of H and the coexistence of He and H on cavity evolution remain rudimentary [175,191,216]. Future simulations using reasonable interaction parameters are valuable for elucidating the physical mechanisms for He and H to alter cavity evolution in fusion reactor environments.

5. New developments in machine learning interatomic potentials

Computational methodologies, such as DFT, MD, KMC, CD methods, etc. are routinely used to investigate the materials' behavior. *Ab initio* based DFT provides an accurate potential energy surface (PES) to understand the behavior of the material in such a complex chemical environment. However, the computational cost associated with the *ab initio* methods is prohibitively expensive for simulation domains with >2 nm or 1000 atoms.

PES for larger simulation domains is routinely obtained from empirical and semiempirical interatomic potentials for simulating materials at higher length scales ranging up to 1000 nm. However, for materials with complex chemical interactions, such as interactions between material defects, transmutation gases, and interfacial effects, the formulation of these classical potentials with a fixed mathematical form may not be sufficient to provide an accurate PES description. Unlike classical potentials, machine learning-based potentials (MLPs) provide a highly flexible mathematical formulation, allowing for an accurate description

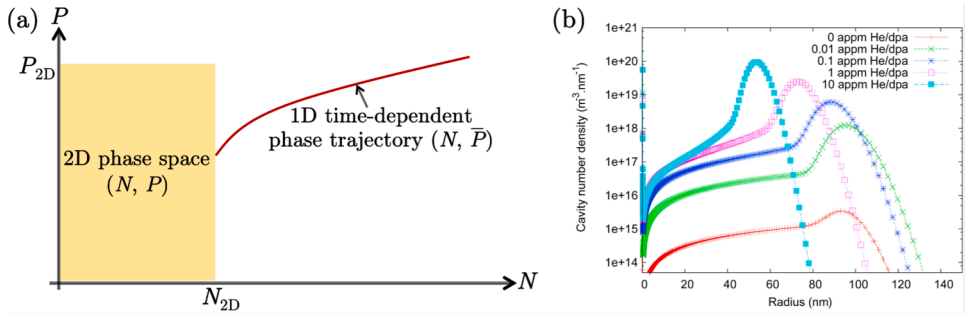

Fig. 16. Cluster dynamics simulations on He effect on cavity evolution. (a) An effective method to reduce the number of master equations when modelling the influence of He on cavity evolution. In the 2D domain (the yellow region), cavities containing He are depicted by the 2D phase space (N, P), with N and P being the number of vacancies and He, respectively. In the 1D domain (the red line), cavities containing He are depicted by the simplified phase trajectory $(N, \overline{P})$ that evolves with time, where $\overline{P}$ represents the average number of He per cavity containing N vacancies. (b) The influence of He on cavity evolution in austenitic stainless steels [219], with the dose rate 10^{-8} dpa/s, the irradiation temperature 500 deg C, and the irradiation dose 100 dpa. (For interpretation of the references to colour in this figure legend, the reader is referred to the web version of this article.)

of complex chemical interactions. When these MLPs are trained with *ab inito* data, the PES calculated by MLPs will have *ab initio*-level accuracy at a fraction of computational cost, leading to accurate simulations of chemically complex interactions in long-length scale domains.

In the past decade, significant progress has been made in developing MLPs. A key step in developing an MLP is defining structural descriptors invariant to symmetry operations, such as translation, rotation, and permutation of chemically equivalent atoms. Eliminating the necessity for *in-house-code* development for training and utilizing MLPs, several open source packages are available that streamline this process and also have an interface with popular molecular dynamics codes, such as LAMMPS [220]: Gaussian approximation potential (GAP) [221–223], spectral neighbor analysis potential (fitSNAP) [224–227], moment tensor potential (MLIP) [228–231], the atomic energy network (AENET) [232–235], and deep neural network potentials (DeePMD-kit) [236–240]. Here, we briefly review several developments on MLPs that help in the investigation and the development of advanced radiation-resistant materials for fusion applications by extending our understanding of fundamental atomistic interactions.

5.1. Accurate prediction of He and vacancy binding energies with He bubbles in BCC-Fe

Fe-He MLP was developed in 2023 to investigate the clustering behavior of He atoms in BCC-Fe that leads to bubble formation and growth [241]. Specifically, the work focused on obtaining accurate binding energies of He with He_{n-1} clusters and $He_{n-1}V$ bubbles with monovacancy. ~10,000 at. configurations required to achieve this were carefully selected for training the MLP. Configurations include relaxation of point defects (vacancy and self interstitial), He clusters, He bubbles, lattice strains, etc. The deep neural network potential code, DeePMD-kit, was used to train the potential, run structural optimization and molecular dynamics simulations.

$$E_b[\mathrm{He}_{n-1} + \mathrm{He}] = E[\mathrm{He}_{n-1}] + E[\mathrm{He}_{\mathrm{tet}}] - E[\mathrm{He}_n] - E[\mathrm{Fe}_{\mathrm{P}}] \quad (12)$$

$$E_b[\mathrm{He}_{n-1}V_m + \mathrm{He}] = E[\mathrm{He}_{n-1}V_m] + E[\mathrm{He}_{\mathrm{tet}}] - E[\mathrm{He}_nV_m] - E[\mathrm{Fe}_{\mathrm{P}}] \quad (13)$$

$$E_b[\mathrm{He}_nV_{m-1} + V] = E[\mathrm{He}_nV_{m-1}] + E[V] - E[\mathrm{He}_nV_m] - E[\mathrm{Fe}_{\mathrm{P}}] \quad (14)$$

Fig. 17 compares the binding energies of He with He_{n-1} clusters and $He_{n-1}V$ bubbles with monovacancy using Eq 12 and 13. $E_b[D_1 + D_2]$ is the binding energy of the defect D_1 with defect D_2, $E[D]$ is the total energy of BCC-Fe containing defect D and $E[\mathrm{Fe_P}]$ is the total energy of pristine BCC-Fe. D represents defects such as He_n (He cluster with n number of He atoms), He_nV_m (He bubble with n number of He atoms and m number of vacancies).

Fig. 17(a) compares DFT versus MLP binding energies in a 4×4×4 supercell (SC4). In addition, comparison of binding energies calculated with relaxed cells (RCBE) and fixed cells (FCBE) is studied. The difference between RCBE and FCBE is due to the periodic effects of the small SC4. The difference between RCBE and FCBE progressively diminishes for bigger 8×8×8 and 12×12×12 supercells, shown in Fig. 17(b) and Fig. 17(c), respectively.

The impact of developing a Fe-He machine learning potential is discussed in the following. Several works have reported $E_b[\mathrm{He}_{n-1}V_m + \mathrm{He}]$ value, calculated using DFT and interatomic potentials (IAP). However, a one-to-one comparison between the DFT and IAP computed binding energy values was not possible because DFT calculations were limited to small SC4 supercells, while IAP values were typically computed using a large 10×10×10 supercells. In Ref. [241], we have estimated that the mean absolute error (MAE) of IAPs ranges between 0.33 and 0.57 eV, compared to MLP binding energies computed using 12×12×12 supercells.

5.2. Ta-Ti-V-W high entropy alloys

As noted in Ref. [242], understanding the eigenstrains of radiation-induced defects is essential for simulations using the finite element method. While MD is a powerful tool for determining eigenstrains efficiently, the accuracy of its predictions heavily depends on the quality of the interatomic potentials used. This challenge becomes especially pronounced in multicomponent systems such as high-entropy alloys, where the energy landscape around irradiation defects is highly complex. Even for point defects, formation energies and relaxation volumes depend not only on the alloy's composition but also on the defect's local environment. For more intricate defect structures, the complexity of the energy landscape further increases. Therefore, the possibility of developing MLPs capable of accurately reproducing the formation energies and relaxation volumes of defects in irradiated multicomponent alloys is critically important.

This subsection demonstrates the ability of MLPs to accurately reproduce formation energies and relaxation volumes of point defects using the equiatomic Ta-Ti-V-W high-entropy alloy (HEA) as an example, a material considered promising for fusion applications. HEAs are attractive for high-temperature environments due to their exceptional yield strength, hardness, and superior irradiation resistance compared to pure elements and conventional alloys. The Ta-Ti-V-W system was selected based on theoretical studies of the Cr-Ta-Ti-V-W system, which combined DFT, cluster expansion, and Monte Carlo (MC) simulations [243]. These studies predicted that Ta-Ti-V-W solid solutions exhibit some of the lowest ordering temperatures [243], a finding validated experimentally, where TaTiVW formed a single bcc phase [244]. Consequently, two MLP versions were developed for Ta-Ti-V-W alloys: a linear ML

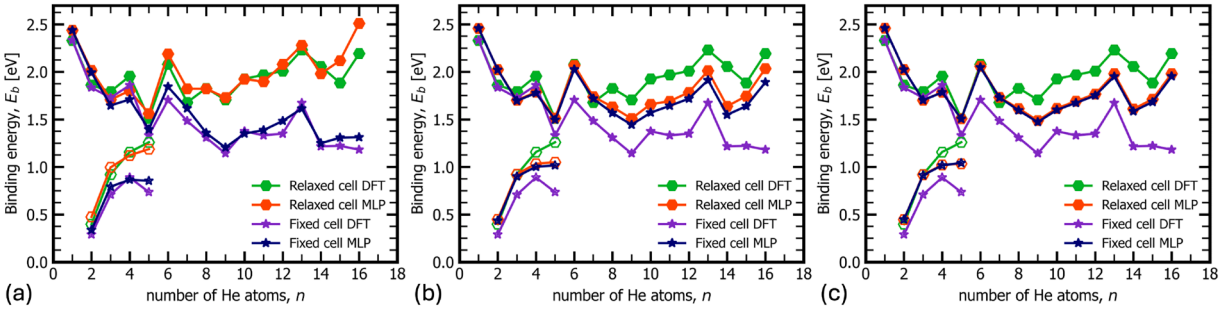

Fig. 17. Comparison of binding energies calculated with the MLP using (a) 4×4×4, (b) 8×8×8, and (c) 12×12×12 supercells. The DFT data (purple and green) in all panels is calculated using a 4×4×4 supercell. Binding energies calculated using fixed-cells (purple and blue star markers); relaxed-cells (green and red hexagon markers. Binding energies of He with $He_{n-1}V$ bubbles (solid markers) and with He_{n-1} clusters (open markers). (For interpretation of the references to colour in this figure legend, the reader is referred to the web version of this article.)

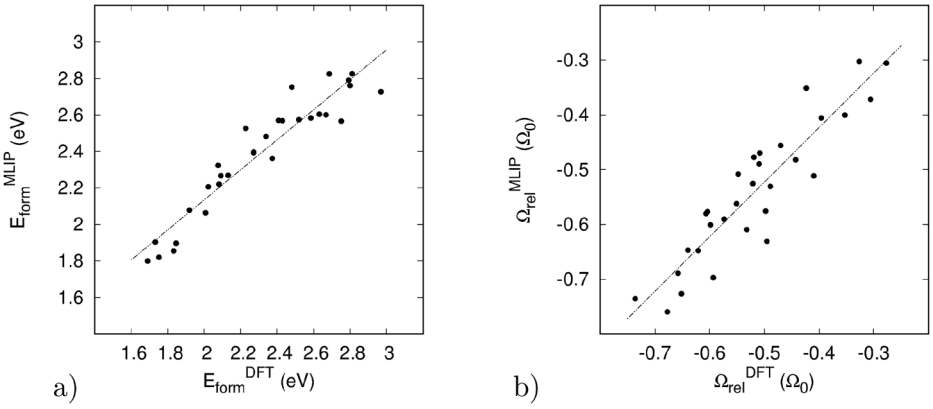

Fig. 18. Comparison of (a) formation energies and (b) relaxation volumes of vacancies in the equiatomic random Ta-Ti-V-W high-entropy alloy computed using DFT and MLP.

model with hybrid descriptors and a kernel-based approach (known as KNML) [245]. The linear model computes atomic potential energy as a weighted sum of descriptor components, while the KNML approach refines deviations from DFT predictions using a subset of DFT data points.

The comparison of vacancy formation energies and relaxation volumes in the equiatomic Ta-Ti-V-W HEA, as obtained from DFT and KNML, is presented in Fig. 18(a) and (b), respectively. The kernel ML accurately reproduces both properties, with vacancy formation energies ranging from 1.6 to 3.0 eV and relaxation volumes ranging from -0.8 to -0.3 at. volumes in both methods. A key advantage of MLPs is their ability to analyze much larger statistics of point-defect configurations. Fig. 19(a) and (b) show the distributions of formation energies and relaxation volumes of vacancies, respectively, for all possible vacancy configurations in a disordered equiatomic alloy structure containing 128 at. sites. These distributions exhibit Gaussian-like behaviour, with mean values of 2.5 eV for formation energy and -0.5 at. volumes for relaxation volume.

5.3. Hydrogen isotopes in metals

MLPs allow not only large-scale simulations with DFT accuracy, but also the application of more physically accurate theoretical methods. One such method is the path-integral (PI) method [246] to account for nuclear quantum effects (NQEs). It should be noted that ab initio molecular dynamics (AIMD) deals only with the quantum nature of electrons and ignores NQEs, such as zero-point vibration and quantum tunneling. NQEs are important for the simulation of light atoms, such as hydrogen isotopes, at low temperatures. Thanks to the isomorphism between quantum theory and classical statistical mechanics [247], the PI calculation can be performed by a relatively small extension of classical MD codes, as implemented in the LAMMPS code [248], as well as by a code designed for various PI methods, such as the PIMD code [249].

There are basically two types of PI methods: (i) for the calculation of thermodynamic properties at equilibrium, such as path integral molecular dynamics (PIMD) and path integral Monte Carlo (PIMC), and (ii) for the calculation of transport and dynamical properties, such as ring polymer molecular dynamics (RPMD) [250], centroid molecular dynamics (CMD) [251], and path integral quantum transition state theory (PI-QTST) [252]. For example, method type (i) can be used to calculate the solution enthalpy of hydrogen and the hydrogen distribution over lattice defects at a finite temperature, and method type (ii) can be used to calculate the diffusivity of hydrogen isotopes. Although the quantum dynamics obtained by CMD and RPMD are approximations, the two methods give similar results and achieve reasonable agreement with experiments within the limits of the deviation of the experimental results and the statistical precision of the calculation results for hydrogen diffusion in metals [253,254].

In practice, CMD and RPMD calculations are roughly 100–1000 times slower than classical MD calculations. Therefore, not only accurate but also efficient force fields are needed, and MLPs can satisfy these requirements. In previous studies, the moment tensor potential [255] and artificial neural networks [256] were used to calculate the diffusion coefficients of hydrogen isotopes in bcc metals (Fe, Nb, W) [254] and fcc metals (Pd) [253], respectively. Significant deviations from classical MD due to NQEs are typically observed by PI methods below about 500 K for protium (H) [253,254].

MLPs also allow us to accurately evaluate isotope effects in diffusion coefficients and then identify interesting physics in hydrogen dynamics. For example, even at high temperatures where NQEs are negligible, the isotope effects deviate from classical theory, i.e. $D_H/D_T = \sqrt{m_T/m_H} =$

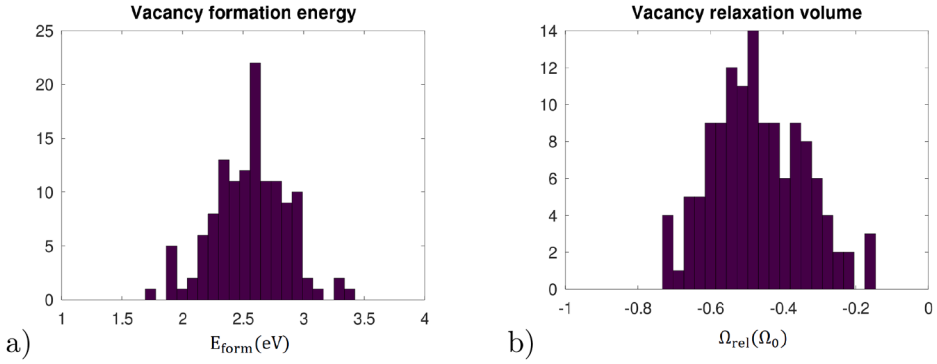

Fig. 19. Distribution of (a) formation energies and (b) relaxation volumes for vacancies computed using MLP for the structure of disordered equiatomic Ta-Ti-V-W alloy with 128 at. sites.

1.73, where D and m are the diffusion coefficient and atomic mass, respectively, and the subscript indicates the type of hydrogen isotope, for all calculated bcc metals (Fe, Nb, and W) [254]. This observation cannot be reproduced by empirical potential models, since not only the migration barrier but also the lattice vibrational frequencies associated with the hydrogen motion must be accurately described to correctly simulate the diffusion coefficients and isotope effects, which is a formidable task for empirical potentials [257]. NQEs become significant at lower temperatures for deuterium (D) and tritium (T) compared to H because the NQEs are mass-dependent, causing larger isotope effects at lower temperatures in bcc metals. In fcc metals, anomalous isotope effects characterized by a reversed-S shape on an Arrhenius plot have been identified: for example, the T diffusivity can be larger than the H diffusivity at 80–400 K in Pd [253,258].

It should be noted that for the materials in which the hydrogen solution energy is positive and the hydrogen solubility is low, such as Fe and W, accurate experimental measurements of the hydrogen diffusivity in the lattice are inherently difficult. This is because, as illustrated in Fig. 20(a), the majority of the dissolved hydrogen atoms are trapped at surfaces and lattice defects, such as grain boundaries, dislocations, and point defects (vacancies, impurities, etc). Consequently, except at high temperatures where the trapping effects of lattice defects become negligible due to the entropy effect, the measured hydrogen diffusivity is affected by lattice imperfections and has large deviations, for example below 500 K in Fe [259] and below 1000 K in W [260], depending on the microstructure [261] and defect concentrations [262] in a material, as depicted in Fig. 20(b). Therefore, atomistic simulation is an essential tool to study lattice diffusion. Since classical MD loses its accuracy at low temperatures due to the neglect of NQEs, the PI methods are also needed (Fig. 20(c)). The advent of MLPs, which has improved the accuracy-efficiency trade-off of atomistic simulations compared to DFT and empirical potentials (Fig. 20(d)), has greatly facilitated accurate PI simulations, which is expected to help improve our understanding and prediction of hydrogen diffusivity in broad classes of materials, including for the diffusivity of tritium for which the availability of experimental data is quite limited.

Meanwhile, another interesting application of MLPs is the simulation of hydrogen-defect interactions in nuclear fusion materials, especially in the plasma-facing components such as tungsten and its alloys. Although a well-trained empirical potential shows improved reproduction of hydrogen-defect interactions [263], MLPs can reproduce hydrogen-defect interaction energies obtained by DFT much better in W [264–266]. Nevertheless, these MLPs are not trained for all properties and phenomena, and thus are probably not sufficiently transferable to general simulations of tungsten-hydrogen systems: specifically, the deep neural network potential developed by Wang et al. was trained primarily for hydrogen blistering [264], the ANN potential developed by Xu et al. for hydrogen segregation in strained regions [265], and the MTP developed by Yang et al. for low-energy hydrogen implantation [266]. Further improvement of the accuracy, transferability, and speed of MLPs, including the development of methods to guarantee high accuracy of MLPs in atomic dynamics and rare events [267], is a key challenge and should be one of the core research topics in the coming decade.

5.4. Summary

In summary, the development of machine learning potentials has dramatically enhanced our ability to simulate complex materials phenomena with near-*ab initio* accuracy at a fraction of the computational cost. The examples discussed in this section, from accurately capturing He-defect interactions in BCC-Fe, to reproducing defect energetics in high-entropy alloys, and incorporating nuclear quantum effects for hydrogen isotopes–demonstrate the versatility and power of ML potentials. These advancements not only bridge the gap between quantum-mechanical accuracy and large-scale simulations but also pave the way for predictive modeling in challenging environments, such as those found in fusion reactors.

Yet some challenges persist in adoption machine learning potentials to further fusion materials understanding:
(1) Although the computational cost of neural network (NN) based MLPs is significantly lower than that of DFT, it remains approximately three orders of magnitude higher than that of EAM potentials [241]. Hence the computational cost of NN based MLPs may limit the simulation cell size to <1M atoms.
(2) Besides metals, ceramics such as, Li_4SiO_4 and Li_2TiO_3 are being explored to use as tritium solid breeder materials. The long range electrostatic interactions and changes in local ionic charges due to charged vacancies in ceramics adds additional complexity to the training of MLPs. Development of open source software packages that include long range electrostatic interactions with charge equilibration is crucial for developing MLPs for ceramics.

Looking forward, further improvements in accuracy, transferability, and computational efficiency will be critical for addressing remaining challenges, such as modeling rare events and extending these methods to even more complex materials systems.

6. Non-metallic materials for fusion

As a complex device, a fusion reactor will require functional materials that can perform a range of essential tasks. For example, a future tokamak may employ high temperature superconducting (HTS) magnets that may be exposed to neutron damage able to compromise the integrity of plasma confinement. Also, neutron irradiation induced defects in ceramic breeder materials may lead to tritium retention levels that makes the tritium cycle unsustainable. Clearly, then, considering the behavior of these materials is important and while modelling work

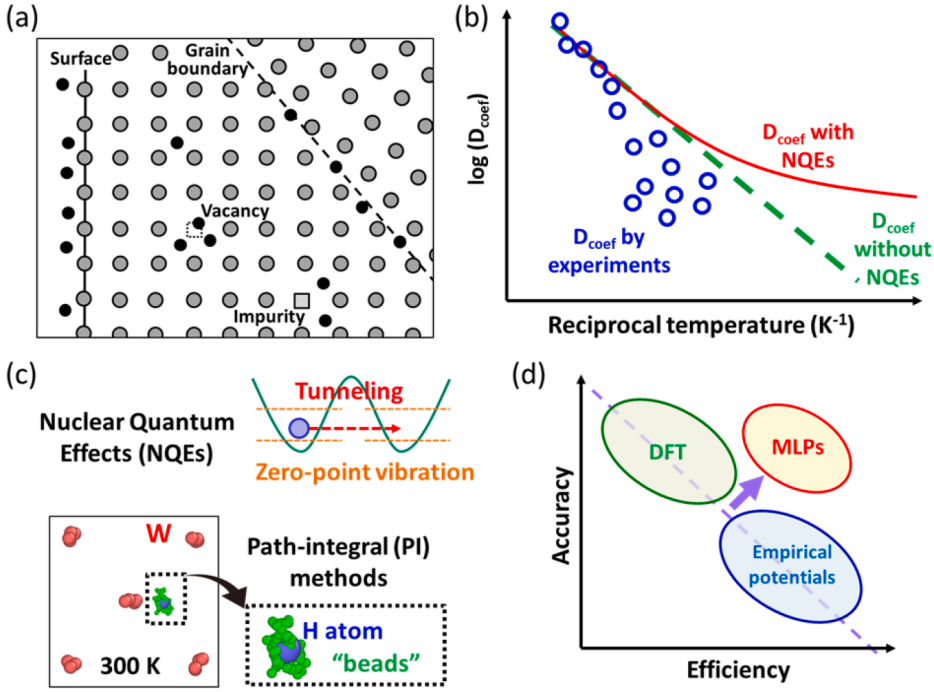

Fig. 20. (a) Hydrogen interacting with lattice defects in a material. (b) A typical Arrhenius plot of the diffusion coefficient of solute hydrogen in a metal. The blue open symbols represent experimental data, which often deviate at low temperatures due to the trapping effects of lattice defects. The red solid and green dashed lines show the diffusion coefficients with and without NQEs, respectively. (c) NQEs and their description by PI methods. (d) Improvements in the accuracy-efficiency trade-off thanks to MLPs. (For interpretation of the references to colour in this figure legend, the reader is referred to the web version of this article.)

here is less mature than elsewhere, there has been considerable progress, however, more needs to be done.

6.1. High temperature superconductors

For research purposes, tokamak reactors could employ copper magnets to provide the magnet field for plasma confinement. However, the next generation of devices have increased requirements in terms of plasma densities and confinement times, requiring higher strength magnetic fields. ITER will employ a mixture of Niobium-Tin (Nb_3Sn) and Niobium-titanium (NbTi) low temperature superconductors, providing magnetic field strengths up to 11.8 T and 6 T respectively. Both materials have critical temperatures below 18.3 K and therefore, require substantial cooling using liquid He, consuming a significant amount of energy. Many powerplant designs, including STEP, ARK, and others, envisage using high-temperature superconducting magnets, based around rare earth cuperates as these offer field strengths up to > 30 T and critical temperatures up to 133 K. Neutronics simulations by Torsello et al. predict a fluence of 1.6×10^{19} n cm^{-2} in the ARK reactor hitting the magnets with the anticipated accumulated dose reaching 0.52 dpa over 10 years [268].

The Rare Earth Barium Cuperates ($REBa_2Cu_3O_{7-x}$), where RE = Y, Gd and Eu, are a group of ceramic oxides that adopt a defective perovskite crystal structure as illustrated in Fig. 21. Within this structure the copper ions exhibit two different charge states, with the Cu2 ions adopting a 2+ charge state surrounded by five oxygen ions that form linked squared-based pyramids, the bases of which form the CuO_2 planes and the Cu1 ions exhibit a +3 charge and are co-ordinated to four oxygen ions to form the so-called chains. The x in the $REBa_2Cu_3O_{7-x}$ is accommodated by oxygen vacancy defects, which are predominantly on the O1 site in the CuO chain [269]. This observation is supported by DFT simulations, that indicate the formation energy for the O1 and O4 site are 0.6-0.8 eV lower than the O2 and O3 sites in the planes [270,271].

Neutron irradiation experiments of $REBa_2Cu_3O_{7-x}$ indicate that initially the critical temperature decreases linearly with fluence with a concomitant increase in the critical current, J_c [272–277]. It is thought that this increase in J_c is due to the formation of large amorphous regions that can act as flux pinning centres, while the decrease in T_c is associated with the creation of vacancy defects throughout the material. At a certain fluence, which depends on the initial defect structure of the HTS materials, there is a sharp drop in the superconducting properties [278].

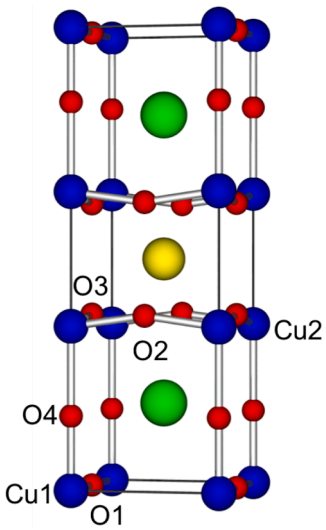

Fig. 21. Graphical representation of the $REBa_2Cu_3O_7$ unitcell, where red spheres represent oxygen ions and the blue, green and yellow spheres represent the copper, barium and rare earth cations respectively. (For interpretation of the references to colour in this figure legend, the reader is referred to the web version of this article.)

There have been a number of empirical potentials derived for the $REBa_2Cu_3O_7$ materials, particularly $YBa_2Cu_3O_7$ [279,280]. These mod-

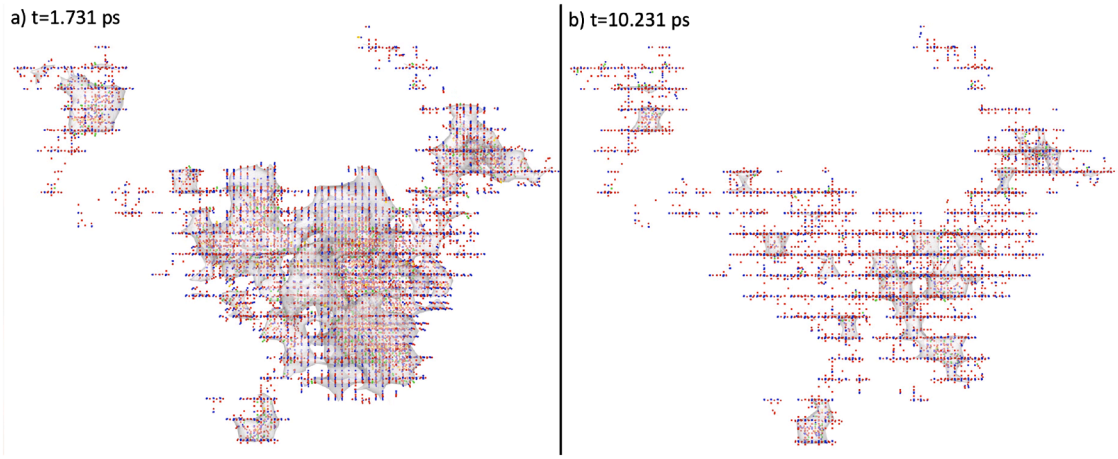

Fig. 22. Two images of the cascade progression in the x-z plane of a 20 keV cascade with pka launched in the x direction taken at the peak damage and final state. Vacancies are cubes, interstitial are spheres, antisites are spherocylinders with the colours the same as in Fig. 21 [283].

els are not suitable for use in MD simulations, where atoms may swap sites, as they represent the different Cu environments by either designating different charges for the Cu ions or by incorporating an extra interaction between the Cu and O atoms in the chains. Despite this limitation, these potentials have been adopted to perform small cascades in $YBa_2Cu_3O_7$, see for example Refs. [281,282]. To address this limitation, Gray et al. developed a model based on a simple Buckingham potential that did not distinguish between Cu ions to enable simulations of radiation damage [283].

Using this new potential Gray et al. suggest that the cascades result in the formation of amorphous regions with a periphery that contains oxygen and copper defects located predominantly in the chains, with a smaller number of oxygen defects in the planes as shown in Fig. 22. Results from a combined He irradiation and DFT study support the presence of defects in the plane region. [284]. An interesting observation from the MD simulations of Gray et al. and Torsello et al. is the relatively low level of recombination, at least on the timescales of an MD simulation. Experimentally, it has been observed that there is some recovery in the superconducting properties of tapes that have been irradiated at cryogenic temperatures and then allowed to return to room temperature before being tested again [285]. This recovery of superconducting properties is likely a result of rearrangement of the oxygen sublattice as it is mobile with activation energies for oxygen diffusion of 0.9-1.2 eV [286–288] from experiment and 0.4-1.19 eV from simulations [283,289].

While the potential of Gray et al. is a significant improvement as it allows the simulation of Cu exchange between the two sites, the potential is limited by use of the Buckingham form. Therefore, as proposed in the Roadmap of Torsello et al. [290], there is a requirement to develop a Machine Learned Potential to obtain a better understanding of these materials under irradiation.

6.2. *Li ceramics for tritium breeding*

Most conceptual designs for future fusion power plants employ the reaction between deuterium and tritium (see Eq. (15)). While deuterium can be readily extracted from seawater, there is a paucity of naturally occurring tritium. Therefore, to ensure a sustainable tritium economy, it must be bred *in-situ* from the transmutation of lithium via Eqs. (16) and (17).

$$^{2}_{1}\mathrm{H} + ^{3}_{1}\mathrm{H} \rightarrow ^{4}_{2}\mathrm{He} + ^{1}_{0}n \tag{15}$$

$$^{6}_{3}\mathrm{Li} + ^{1}_{0}n \rightarrow ^{4}_{2}\mathrm{He} + ^{3}_{1}\mathrm{H} \tag{16}$$

$$^{7}_{3}\mathrm{Li} + ^{1}_{0}n \rightarrow ^{4}_{2}\mathrm{He} + ^{3}_{1}\mathrm{H} + ^{1}_{0}n \tag{17}$$

Therefore, the reaction chamber in a fusion reactor must be wrapped in a breeder blanket containing lithium. The exact form the lithium takes depends on the blanket concept and can be either liquid (for example PbLi or FLiBe) or solid (typically Li_2TiO_3 and Li_4SiO_4). There have been some atomistic studies on liquid breeder materials, for example Refs. [291–294] for PbLi and Refs. [295,296] for FLiBe, however, this review will focus on the ceramics.

In typical solid breeder concepts the ceramic tritium breeder material will be in the form of pebbles of up to roughly 1 mm in diameter [297]. The neutrons ejected from the plasma will penetrate the pebbles and generate tritium in the middle of the material. Therefore, to ensure the fuel cycle is sustainable it is essential to be able to recover the tritium from the pebbles. Tritium will initially diffuse through the crystal matrix until it reaches a grain boundary. It then migrates along the grain boundary until it reaches the surface where it will undergo an isotope exchange reaction with H_2 in a helium purge gas. This process is illustrated in Fig. 23.

During operation, the transmutation of lithium and neutron irradiation will result in the introduction of defects into these materials and it is important to ensure that these defects do not trap tritium and compromise the fuel cycle. Therefore, there have been a number of studies of defects in the leading breeder candidates, Li_2O_3 [299–301] and Li_4SiO_4 [302] as well as some less well studied materials, including Li_8PbO_6 [303], $LiAlO_2$ [300,304] and Li_2ZrO_3 [305]. As would be expected for wide bandgap materials, these studies indicate that the defects, will predominantly exist in their formal charge state, for example the lithium vacancy will exhibit a -1 charge state, i.e.: V_{Li}^{-1} (Kroger-Vink notation [306]). Using DFT and a point defect model, Murphy proposed that non-stoichiometry in Li_2TiO_3 was accommodated via lithium and antisite defects. For example, excess lithium was incorporated via Li_i^{+1} and Li_{Ti}^{-3} defects, while a lithium deficiency was facilitated by a combination of V_{Li}^{-1} and Ti_{Li}^{+3} defects [301]. This conclusion was supported by an empirical pair study of Sanjeev et al. [307] and experiments from Vitins et al. [308] and Yu et al [309].

A number of studies have examined tritium accommodation in these complex ceramics, for example Refs. [310–315]. As an interstitial, tritium typically exhibits a +1 charge state and bonds to an oxygen atom forming a hydroxyl species with a bond length on the order to 1 Å. A similar hydroxide structure is created when tritium is placed on the lithium site, forming a $\{T_i^{+1} : V_{Li}^{+1}\}^{\times}$ defect cluster. By contrast, substitution onto the oxygen site exhibits a dominant +1 charge which corresponds to a hydride ion on a V_O^{+2} site, resulting in a T_O^{+1} defect [302,312]. What

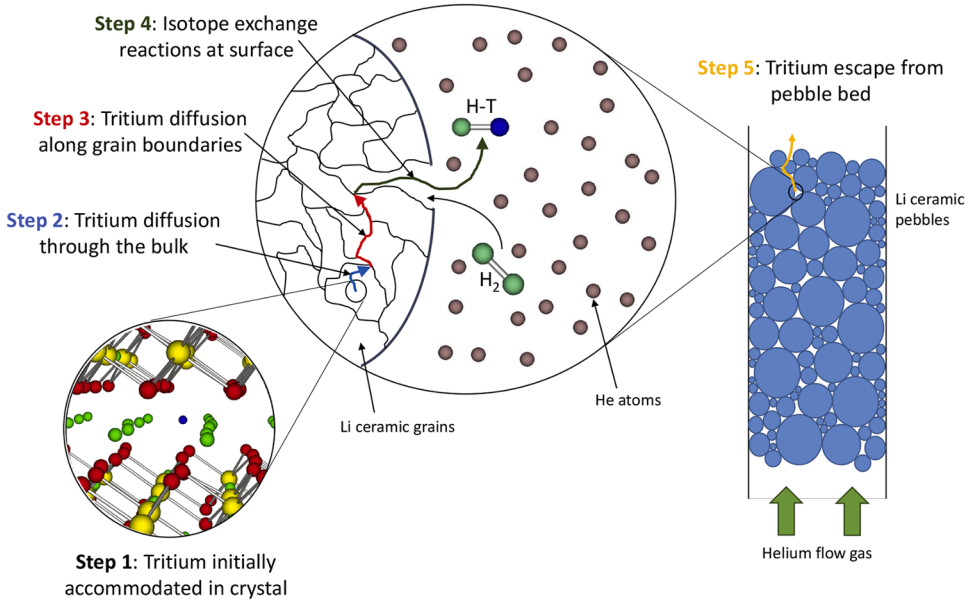

Fig. 23. Schematic of the tritium release process from lithium ceramic pebbles in the breeder blanket [298].

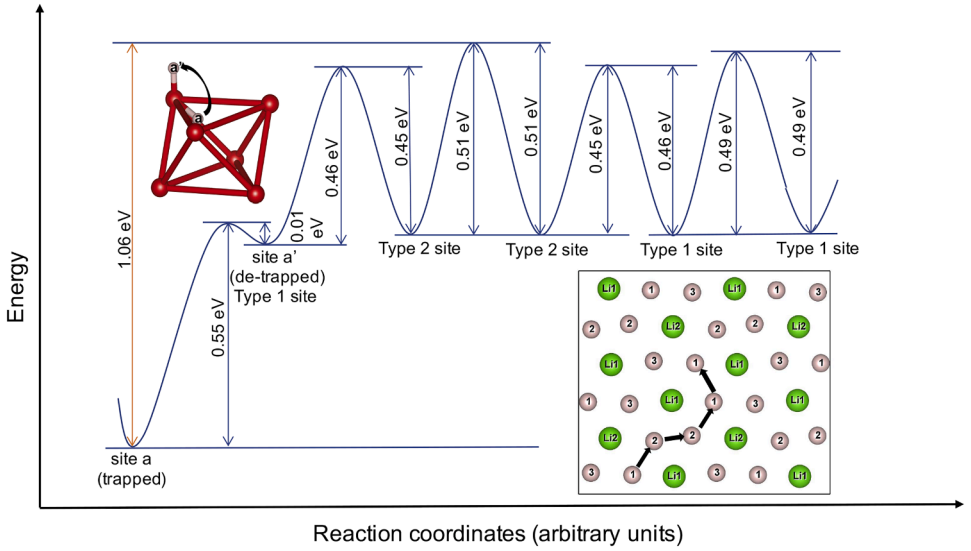

Fig. 24. Tritium escape from a lithium vacancy defect in Li_2TiO_3.

these results indicate is that the tritium ions can change charge state depending on where they are in the lattice.

As an interstitial, tritium will migrate through the material by hopping between oxygen ions as well as reorientations around the same oxygen ion [316,317]. Interstitial diffusion has been shown to be anisoptropic, with it being particularly difficult for tritium to cross the mixed cation layer in Li_2TiO_3 [316,317]. If the interstitial encounters a lithium vacancy defect it will bind to form the $\{T_i^{+1} : V_{Li}^{+1}\}^{\times}$ cluster [298]. This binding energy must be overcome to enable the continued diffusion of the tritium (see Fig. 24), which indicates that an increase in the lithium vacancy concentration may result in enhanced tritium retention. However, Goswami and Murphy identified collaborative process, whereby the vacancy and tritium move via a tethered mechanism. This implies that as tritium diffuses through the crystal it will bind to a lithium vacancy and the two will migrate together for a while before separating again. As explained elsewhere, these activation energies for diffusion can be input into kMC and while there has been some effort to do this [318], more should be done in this area.

While significant effort has been expended looking at the behaviour of tritium in these materials, there has been much less attention paid to the other transmutation product from reactions (16) and (17), which is helium. Murphy suggested that helium will be predominantly incorporated onto the oxygen site as an He_O^{+2} defect in Li-rich Li_2TiO_3, however, as the availability of lithium vacancies increase it can be accommodated on the lithium site, i.e. He_{Li}^{-1} [319]. Zhou et al. showed that it is possible to accommodated multiple He atoms on a single Li site [320] in Li_2TiO_3. To enable the simulation of the nucleation of He bubbles, a Lennard-Jones style potential was developed to represent the interactions between He and Li, Ti and O [321]. Using this potential, MD simulations suggested the clustering of He atoms in the pure lithium layers in Li_2TiO_3.

7. Multiscale models for plasma-facing materials

Plasma-facing materials (PFMs) are exposed to the most extreme service conditions in a fusion reactor, including not only the high energy

neutron irradiation, but also the high fluxes of hydrogen (H) isotopes and helium (He) ions from the plasma. This inevitably leads to the formation of displacement defects (e.g. vacancies, voids, self-interstitial atoms and dislocation loops), in addition to the transmutation elements and impurity elements in the materials, significantly affecting their thermo-mechanical properties. As highlighted by the previous review paper [1], the evolution of irradiation defects is a multiscale problem, spanning the scales from the microscopic scale (collision cascades) to the mesoscopic scale (defect evolution) and ultimately to the macroscopic scale (mechanical and thermal properties of the materials).

Despite advances in multiscale modelling, significant challenges remain in achieving predictive capabilities on the effects of He irradiation on PFMs. Experiments in linear plasma devices demonstrated that nanostructure formation in tungsten is strongly influenced not only by He ion bombardment but also by the deposited tungsten and small amounts of impurity gases such as argon and neon [322]. However, current modelling approaches often rely on idealized assumptions and therefore struggle to capture the transition from isolated bubbles to interconnected cavities and surface exfoliation observed experimentally. Moreover, the role of deposited material and impurities remains insufficiently incorporated in most of the existing frameworks. To overcome these limitations, multiscale modelling efforts must be coupled with experiments addressing the reactor relevant conditions. This will enable the development of a more comprehensive description of He retention, bubble evolution, and the associated material degradation.

7.1. Thermodynamic and kinetic behavior of irradiation defects in tungsten

The evolution of vacancies and self-interstitial atoms (SIAs) are pivotal in the context of treatments for predicting how the various properties and performance of materials change under irradiation. The properties of small vacancy clusters in tungsten (W) have been studied, revealing that their binding and formation energies increase with cluster size [323]. Recently, Hou et al. [324] proposed that the stable configurations of vacancy clusters in W can be effectively characterized by minimizing their Wigner-Seitz surface area. They further identified a linear correlation between the formation energy of vacancy clusters with stable structures and their Wigner-Seitz surface area, enabling precise prediction of the binding energy of these clusters [324]. Additionally, the interactions between vacancy clusters and impurities (such as H and He) have also been extensively studied. For example, Hou et al. investigated the binding between H and vacancy clusters in W, revealing adsorption of H atoms on Wigner-Seitz squares and providing a power-law function relationship describing the adsorption of H atoms [212]. Song et al. [325] systematically investigated the aggregation behavior of He in W monovacancies (Vac-He$_n$, n=1-13), showing that He atoms initially occupy the vacancy core and gradually diffuse outwards [325]. The migration and aggregation behaviours of SIA clusters in W have also been studied. It has been reported that the migration of interstitial defects in pure crystalline W changes from one-dimensional (1D) to three-dimensional (3D) movement with increasing temperature [23,326]. The stable configurations and binding energies of SIA clusters (SIA$_n$, n=1-7) have been examined, and the binding energy formulas have been extrapolated to predict larger clusters [327]. Impurity elements (such as H, He, Re, Os, and Ta) significantly affect the motion of SIA clusters. For example, He strongly attracts to SIA clusters, with binding energy increasing as the number of SIAs rises. This phenomenon alters the diffusion of SIAs from 1D to 3D, as shown in Fig. 25, which significantly reduces their mobility [328]. Recently, Bakaev et al. [329] reported that the mobility of dislocation loops is significantly affected by impurities, gradually decreasing with increasing impurity concentration [329].

7.2. Simulation of primary irradiation damage structures in tungsten

MD simulations have been extensively utilized to investigate primary irradiation damage caused by primary knock-on atoms (PKAs) with various energies, including a large number of studies focusing on energies below 100 keV and relatively few studies exploring higher energies up to 300 keV [35,102]. Fellman et al. [330] and Byggmästar et al. [150] examined how overlaps between cascade and pre-existing defect clusters in W influence defect evolution, finding that these overlaps significantly diminish the number of new defects. Additionally, simulations of collision cascades in W across different temperatures and PKA energies showed that the number of surviving defects strongly depends on PKA energy, but exhibits a weak dependence on temperature [331,332] and thermal conductivity [333]. Recently, Liu et al. [334] conducted extensive displacement cascade simulations in W, encompassing three temperatures, seven distinct primary PKA directions, and various PKA energies (1–300 keV). They established a comprehensive cascade simulation database in W, incorporating defects counts, types, and spatial distributions. Notably, four types of SIA clusters were identified in the final state: (a) $1/2\langle 111\rangle$ loops, (b) $\langle 100\rangle$ loops, (c) mixed loops, and (d) C15 clusters [15]. Among these, $1/2\langle 111\rangle$ loops dominate and can form not only directly within cascades but also through the collapse of C15 clusters via three possible transformation pathways [335].

7.3. Defect evolution under irradiation in tungsten

In this paper (see Section 4.2) we have outlined the modeling of high-dose radiation damage using a methodology, CRA, that overcomes the challenges of simulating the long-term evolution of defects created via cascade simulations in MD. However, there is still interest in accurate understanding of the stages of damage creation and evolution at lower doses; CRA may miss the real details of evolution since it doesn't explicitly model the creation of defects in cascades, even if it has been demonstrated in some cases to capture the changes in behaviour as a function of dose observed in experiments. Insight into those "real" details of evolution may lead to the development of mitigation solutions (e.g. impurity additives, microstructural design, etc.) for fusion materials in the future.

Both OKMC and CD simulation approaches are alternative methods for investigating irradiation defects behaviour under a variety of irradiation conditions; methods that can be more directly linked to the formation of defects by PKAs than the CRA. As effective sinks for irradiation defects, intrinsic defects (e.g., grain boundaries (GBs) and dislocations) have been also incorporated into OKMC and CD simulations through the sink strength model, enabling a more accurate representation of defect evolution under irradiation conditions [336,337]. For example, Castin et al. have studied the evolution of irradiation defects under fission neutron irradiation in reactors such as JOYO and BR2, as well as under ion irradiation using OKMC method, including the effects of irradiation dose, temperature, and PKA energy spectrum [338]. Additionally, the impact of impurity elements such as Re, C, H, and He on the evolution behaviour of defects has also been extensively investigated [339–342]. For instance, Niu et al. demonstrated that the strong attraction between carbon impurities and irradiation defects in irradiated tungsten leads to a higher number density of vacancies and SIA clusters, with this effect becoming more pronounced as the C concentration increases [341]. Furthermore, the formation process of void lattices, an interesting phenomenon observed under neutron irradiation, have been investigated using the OKMC method [343]. Recently, a method has been proposed to directly perform MD simulations of displacement cascades within cells generated by the OKMC model, enabling the consideration of cascade overlap effects and thereby providing a more accurate description of defect introduction at the atomic scale [344].

The CD method, based on mean-field rate theory, solves a series of diffusion-reaction master equations to simulate the evolution of defects, including generation, diffusion, and absorption. Recently, the CD method is widely applied to study the damage behavior of PFMs under various irradiation conditions, including defect evolution, He bubble formation, hardening and swelling of materials. For example, the effects of *Re* on the hardening of single-crystal W under neutron irradi-

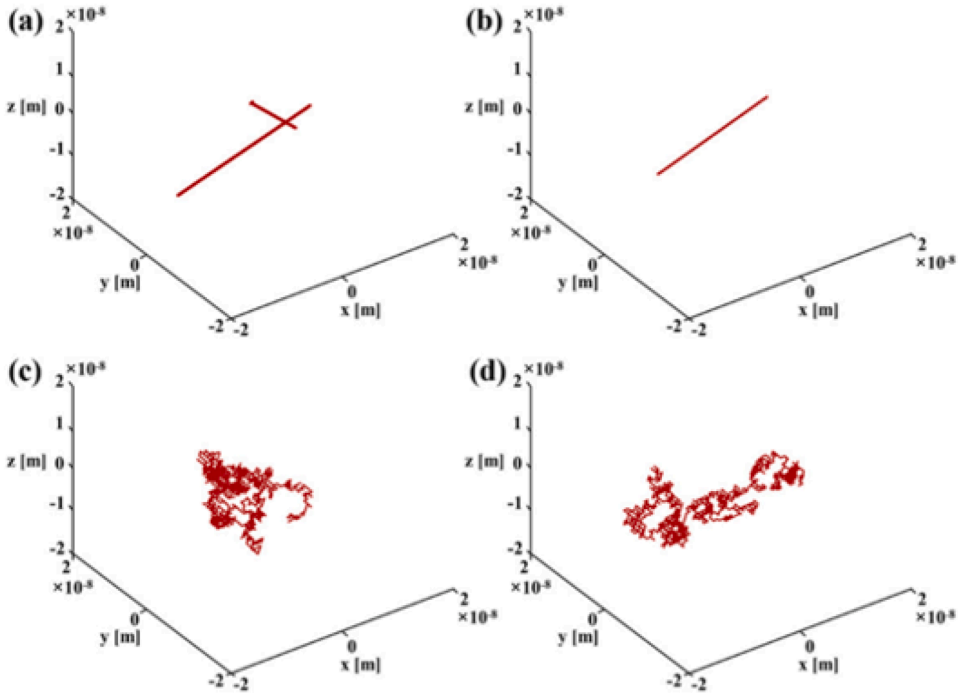

Fig. 25. Trajectories of migrating SIA_m defects and He-SIA_m ($m = 1, 2$) defects at 300 K. (a) SIA_1; (b) SIA_2; (c) He-SIA_1, and (d) He-SIA_2 [328].

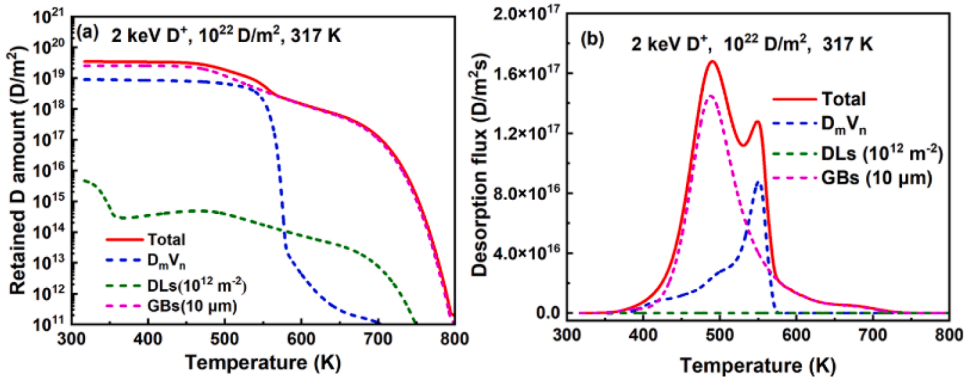

Fig. 26. (a) Simulated retention as a function of the annealing temperature after 2 keV D ion implantation with a fluence of 10^{22} D/m^2 at 317 K. (b) Simulated total and partial TDS spectra at the heating rate of 0.5 K/s [346].

ation of JOYO, HFIR and DEMO reactors were investigated, revealing a dominant role of *Re* clusters in irradiation hardening [345]. Recently, Chen et al. developed an improved CD model, IRadMat-TDS, which incorporates the saturation absorption and release mechanisms of H at GBs and dislocation lines, as well as the multiple trapping effect where deuterium (D) exhibits different trapping energies at various types of GBs [346]. Using this model, their simulations accurately replicated the experimentally observed thermal desorption spectroscopy (TDS) curve under 2 keV D ion implantation, attributing the primary peak at 490 K and the shoulder peak between 550 and 700 K to D trapping at GBs and vacancies (as shown in Fig. 26).

8. From microscopic models to a full device simulation

The timescale for the expected development and deployment of fusion power is short in relation to its technological complexity and readiness, and this timescale is becoming increasingly more compressed by the drive for commercial success. This is an opportunity for digital engineering, as reactors can in principle be built faster *in silico* than *in vivo*. The recognition of this fact is spurring substantial activity across the world to develop digital shadows, replicas, and twins of fusion systems. In particular, virtual shadows of existing fusion devices are under active development. We mention the example of the Virtual Korea Superconducting Tokamak Advanced Research tokamak (V-KSTAR) [347,348] and of the Mega Ampere Spherical Tokamak - Upgrade (MAST-U) spherical tokamak in the UK [349]. The two efforts have different emphases: the digital twin of KSTAR aims at integrating plasma simulations using the digital platform for monitoring and analysis purposes; the virtual model of MAST-U is focused on a finite element representation of the structure of the device that, although having a specific objective [349] of simulating the mechanical loads, illustrates the general capabilities of structural analyses that are now able to treat a variety of sources of stress in a fusion tokamak device. A mechanical model for MAST-U and the von Mises stress field arising from the gravitational load are shown in Fig. 27

In V-KSTAR it is possible to trace dynamical elements referring to fusion plasmas (e.g. particles, magnetic fields, and EM-rays) and analyze their interactions with the complex 3D structure of tokamak. For

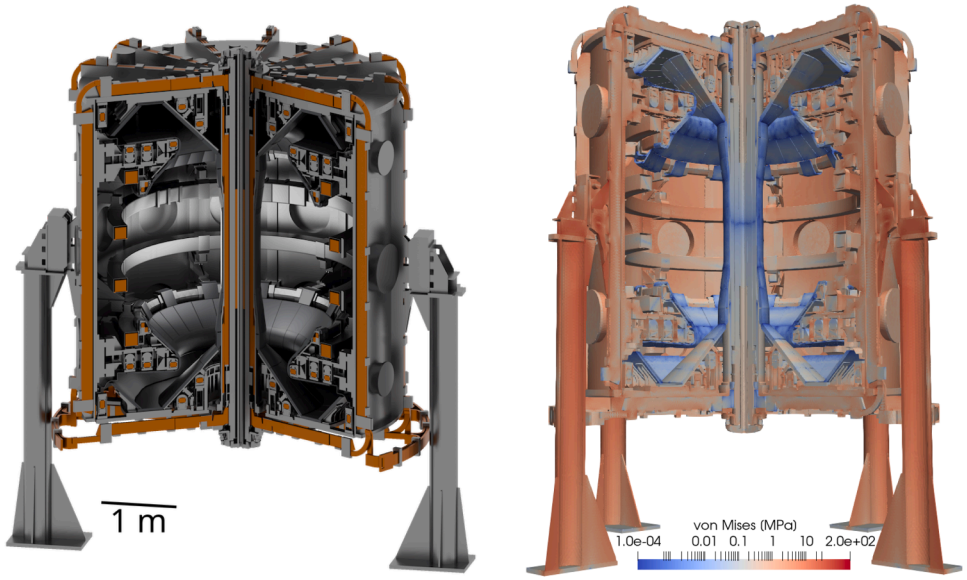

Fig. 27. (a) Analysis-ready CAD model of the MAST-U tokamak device. The associated finite element mesh involves 127 million elements. (b) for the purpose of demonstrating the capabilities of a full-scale FEM simulation, the tokamak is loaded with gravitational body forces, producing stresses in the structure illustrated here using the von Mises invariant of the stress field. Figures from [349].

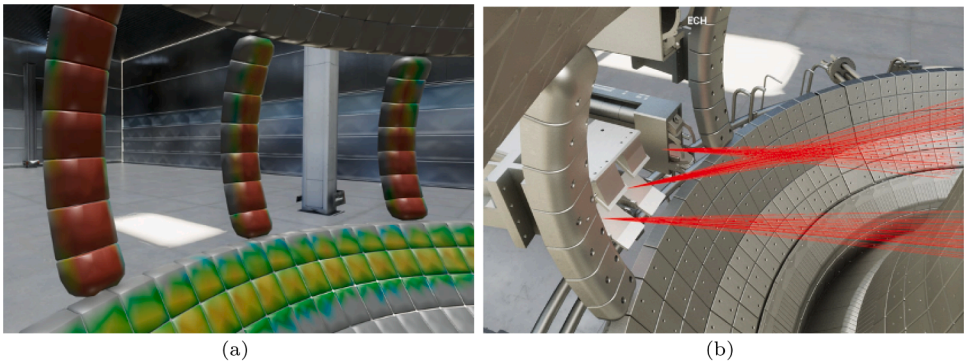

Fig. 28. A demonstration of the capabilities of V-KSTAR: a) 3D distribution of heat fluxes on the plasma facing components of the KSTAR tokamak due to fast ion losses. b) V-KSTAR 3D tracings of radio frequency waves injected for plasma heating and current drive in KSTAR.

instance, V-KSTAR can calculate detailed footprints of equilibrium magnetic fields on plasma facing components based on detailed 3D CAD models. Although equilibrium magnetic fields confining fusion plasma in a tokamak have toroidal 2D symmetry, due to the 3D shapes of plasma facing components, there are highly non-trivial 3D features characterising plasma-wall interactions even under axisymmetric magnetic fields. Furthermore, there can be externally added 3D magnetic field perturbations, which intend to control plasma performances and stabilities by external means. All these imply the necessities of detailed 3D analyses of plasma-wall interactions based on detailed 3D models of a tokamak.

An example application of V-KSTAR is shown in Fig. 28a. In KSTAR, neutral beam injection results in a loss of fast ions, whose heating effect must be quantified. After calculating the trajectories of fast ions using a Monte Carlo particle simulation, the collisions between the ions and the tokamak structure, as defined by KSTAR CAD models, were detected in 3D. The collisions were then recorded and analyzed to calculate the resulting heat fluxes on the plasma facing components. A second example, in Fig. 28, is the accurate 3D tracing of RF-waves injected for plasma heating and current drive. Though the waves are injected with careful controls of both target plasma parameters and wave launchers, there can be some residual portions of RF-waves, which are not absorbed by plasma and therefore affecting plasma facing components by multiple reflections. As demonstrated by these functionalities of V-KSTAR, digital shadows enable accurate 3D mapping of the impact of plasma operation on materials in a fusion device. The present version of V-KSTAR is primarily focused on plasma effects. For a more realistic representation of a fusion device and its plasma operation, however, it is critical that the digital twins also use accurate models for fusion materials. Fusion digital twins such as V-KSTAR provide a natural 3D platform for integrating physics simulation, engineering analysis, experiments, and machine operation.

Here it would be appropriate to note the pivotal significance of the availability of high-quality data for AI-related developments, which are taking central roles with the explosive growths of their complexity and applicability to broad scientific areas. Fusion digital twins are expected to play an important part in stimulating and accelerating the AI-related developments for fusion material modelling in coming years.

The China Fusion Engineering Test Reactor (CFETR) was used as a test case for developing virtual reality (VR) tools for future operation, maintenance and decommissioning of fusion power plants [350]. In the US, simulations are starting to integrate plasma physics, neutron transport, computational fluid dynamics and structural mechanics in a single framework, FERMI, or a Fusion Energy Reactor Models Integrator to

shorten the design process of components such as the breeding blanket [351].

It is clear that modelling frameworks are becoming increasingly multiscale and oriented towards the upcoming transition to exascale computing [352].

8.1. Structural modelling at the engineering level

The stress analysis of components for nuclear applications is impeded by the need to consider irradiation effects, which in fusion materials involve higher dose, neutron energies and hydrogen and helium production by transmutation [353]. One effect of irradiation important for structural considerations is macroscopic swelling, which for instance was studied in the context of breeding blanket design [242,354] and DEMO divertor monoblock simulations [355,356]. We now describe recent advances in modelling of swelling and irradiation creep, highlighting from the outset that it is an area where irradiation effects, materials science and structural engineering all appear to be severely underdeveloped.

8.2. Modelling of swelling and irradiation creep at nano- and micro-scales

Creep is broadly defined as plastic deformation below the elastic limit, facilitated by diffusional processes, enabled by relatively large thermal concentrations of vacancies. Under irradiation, defect concentrations are many orders of magnitude above those expected under the solely thermal operating conditions, effectively eliminating the need for high (homologous) temperature to observe creep. Creep is generally classified as a volume-preserving deformation mode. On the other hand, swelling implies the presence of dimensional (not just shape) changes, often quantified by the degree of volumetric expansion. No significant swelling typically occur under purely thermal conditions, even though the spontaneous production of vacancies at very high temperatures does give rise to the volumetric expansion of a material beyond the notion of conventional thermal expansion [357]. Hence, swelling is a uniquely typical irradiation effect. The very short duration of pulses where fusion had been achieved in the presently available experimental facilities implies that the structures of these devices have never experienced the level of fluence and temperature expected in an operating fusion power plant. Materials simultaneously subjected to stress and irradiation undergo irreversible deformation that is known as irradiation creep. Differently from thermal creep, irradiation creep is active at all temperatures. At low temperatures, where thermal diffusion of vacancies is frozen out, irradiation creep is directly driven by high-energy neutron impacts via defect generation and the subsequent stress-driven athermal migration of predominantly self-interstitial atom defects. At higher temperatures, ballistic neutron impact effects and effects of thermal motion of defects co-exist, although under the expected magnetic fusion-relevant irradiation dose rates, irradiation creep generally overwhelms thermal creep at moderate to high temperatures.

Creep and swelling are the manifestations of non-conservative irreversible deformation processes in materials. As such, they are formally defined by a plastic strain tensor whose hydrostatic part represents swelling while the deviatoric one represents creep. However, for the arguably dubious reasons of simplicity, it is often expressed as a linear combination of scalar strain rates:

$$\dot{\varepsilon} = \dot{\varepsilon}_{\text{thermal-creep}} + \dot{\varepsilon}_{\text{irradiation-creep}} + \dot{\varepsilon}_{\text{swelling/growth}} \tag{18}$$

which is the expression found in, e.g., as Eq. (1) in ref. [358]. A combination of irradiation, stress, and temperature brings about a rich and complex set of interactions that are challenging to observe in pure form experimentally and model computationally. These processes are generally thought to fall under the umbrella of the so-called SIPA (stress-induced preferential absorption) and SIPN (stress-induced preferential-nucleation) mechanisms. SIPA and SIPN are legacy terms intended to reflect the fact that, although produced in equal numbers during irradiation, self-interstitial atoms and vacancies behave in substantially different ways, giving rise to an asymmetry in dynamic behavior and total effect on the microstructure. Ultimately, SIPA and SIPN mechanisms are directly attributable to long-range elastic interaction between dislocations and SIA clusters, as well as to the elastic interaction between these defects and external stress, which may manifest itself as (i) stress-induced alignment of bulk SIA clusters, (ii) re-orientation of SIA clusters during nucleation within displacement cascades, (iii) changes in defect diffusivities due to elasto-diffusion, or (iv) modification of absorption bias coefficients due to stress. Not unexpectedly then, unravelling the relative weight of each of the SIPA/SIPN processes in irradiation creep is extremely challenging. This is compounded by a lack of systematic experimental studies involving the main irradiation variables (temperature, stress, irradiation dose, dose rate, and main microstructural features). As is often the case for fusion materials, two factors that severely limit the availability of experimental data are the cost of experimenting with neutron irradiation and, above all, the lack of a suitable fusion neutron source. Fusion devices capable of delivering substantial damage are not expected to be operational before the 2040s and the IFMIF-DONES irradiation facility [359] is going to come online before the mid-2030s. The effects of 14.1 MeV fusion neutrons on materials, and how different these effects are going to be in comparison with the effects of fission neutrons remains unknown. Leading up to IFMIF-DONES, the MYRRHA (Multi-Purpose hYbrid Research Reactor for High-tech Applications) research facilities are currently under development in Europe. These include a subcritical accelerator system driven by a 600 MeV superconducting linear proton accelerator coupled to a 100 MeV proton injector to be deployed by 2027, whose fast spectrum will enable, for instance, the investigation of He/H transmutation effects in structural steels and copper alloys [360].

The scarcity of experimental data stimulated some relatively limited but important effort in modelling irradiation creep and swelling under irradiation, using state-of-the-art simulation tools developed over the last 20 years [361–363]. The majority of existing models maintain a relatively large degree of empiricism [364,365] or rely on simplified assumptions that make the models amenable to analytical solutions [358,366].

Fig. 29 shows predictions based on a crystal-plasticity/stochastic cluster dynamics coupled model described in ref. [361]. The simulations predict the stress exponent of $n = 0.77$, which is below the expected value of 1.0 representative of SIPA conditions. This is indicative of gaps in the physical understanding and/or implementation of how the SIPA mechanisms manifest themselves on the macrosocopic scale.

At low temperatures, both irradiation creep and swelling exhibit saturation as a function of increasing dose. At low temperatures, thermal creep is not active and irradiation creep dominates. In the absence of thermally activated processes, irradiation creep can be quantified by means of MD simulations, as shown in Fig. 30 for tungsten from Ref. [148]. Radiation damage was simulated using the 'molten spheres' algorithm (see Section 4.2), where the irradiation-induced strain tensor was monitored while keeping a constant elastic stress. After diagonalising this strain tensor, the principal strains were found to be remarkably aligned with those of the original elastic strain tensor. On the other hand, at high temperatures, breakaway growth and swelling occur alongside the conventional thermal creep. An important issue with the conceptual separation illustrated by Eq. (18) is that in practice it is impossible to separate thermal and irradiation creep at high temperature.

Multiscale frameworks have been developed specifically for fusion-relevant irradiation, with the goal of quantifying the effect of point defects—self-interstitials and vacancies—on the macroscopic deformation via their interactions with existing dislocations. Dislocations can glide and climb, under irradiation, at a stress lower than the elastic limit and at a temperature lower than that of thermal creep. McElfresh et al. [368] studied the influence of vacancies produced by irradiation on dislocation climb. In particular, kinetic Monte-Carlo simulations have

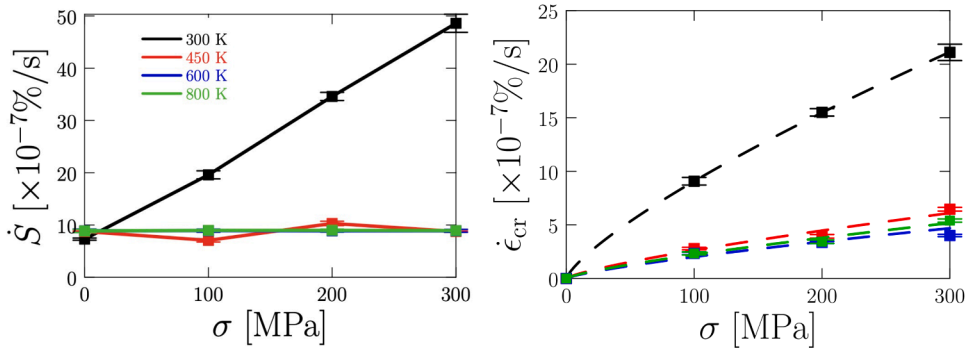

(a) Swelling rate, $\dot{S}$ (b) Creep rate, $\dot{\epsilon}_{cr}$

Fig. 29. Changes in dimensional stability as a function of temperature for Fe under DEMO helium-cooled pebble bed (HCPB) fusion blanket conditions [367], using a model developed in Ref. [361]. Fig. 29(a) Swelling rate. Fig. 29(b) Creep rate.

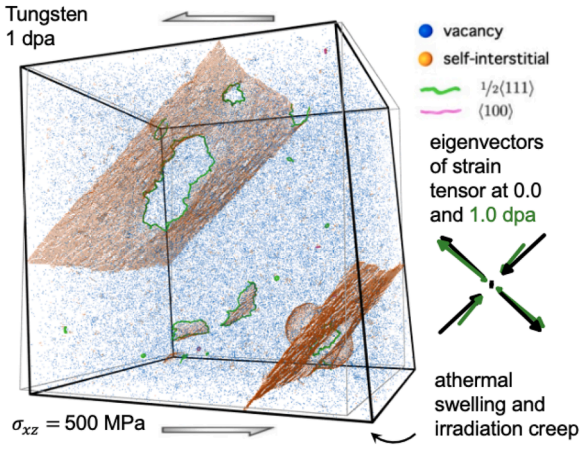

Fig. 30. Molecular dynamics simulation of low temperature irradiation creep in tungsten. Figure adapted from Ref. [148]. In the absence of thermally activated diffusion, vacancies remain immobile and isolated, while self-interstitial atom defects coalesce irrespectively of thermal activation, driven by elastic interactions. The irreversible deformation remains closely aligned with externally applied stress.

been used to parametrise discrete dislocation dynamics simulations as a function of pressure, temperature and vacancy concentration [368]. As the irradiation produces vastly greater vacancy concentrations than the concentrations corresponding to thermal equilibrium conditions [369], this is reflected in a very strong enhancement of the climb velocity. Self-interstitial atoms, on the other hand, both contribute to the nucleation of dislocation loops and are absorbed into existing ones. Yu et al. [361] coupled a stochastic cluster dynamics model for the defect generation and diffusion to a rate-dependent crystal plasticity representation of the dislocation structure. The defect production model included the effect of the recoil spectrum, using DEMO first wall conditions the study. As a result, curves for the swelling and creep rate in iron for various values of applied stress and temperature can be produced [361], see Fig. 29.

A separate approach is to directly use molecular dynamics data to quantify swelling and irradiation creep. The approach has been successfully applied to interpreting experimental observations of microstructural evolution and deuterium retention in irradiated tungsten [147], where parameter-free simulations have been able to match the experimental data at a quantitative level of accuracy. Still, the approaches based on direct atomistic simulations are presently limited to low temperatures where vacancy motion is inactive, an approximation that in tungsten spans a relatively large temperature interval from 0 to ~600 Kelvin [168]. It has also proved possible to make a direct quantitative comparison between experimental observations and MD-informed FEM simulations of irradiation creep [370]. In experiment, the stress relaxation in a micrometric tungsten wire was observed under heavy self-ion irradiation. In the calculations, the anisotropic swelling occurring under the expected recoil spectrum was extracted from MD and used as input to the FEM analysis that predicted the stress and dimensional changes in the wire due to the accumulation of radiation defects, even taking into account the depth-dependent effects associated with the shallow penetration of the incident energetic ions into the wire. At low temperatures, where irradiation defects do not diffuse thermally but evolve solely as a result of being driven by elastic interactions, and point defects are created and destroyed by the persistent melting and recrystallisation of materials by collision cascades, fcc copper and bcc tungsten show qualitatively similar irradiation creep and swelling behaviour [148]. Also, the low-temperature simulations, together with a combination of experimental observations and object kinetic Monte-Carlo simulations by Da Fonseca et al. [371] indicate that the pre-existing dislocations in the microstructure do not readily change even if they become elastically unfavourable under the conditions where elastic stress changes. Rather, it is the nucleation of new dislocation loops in the course of exposure to irradiation that is affected by the changing stress state [371].

It is important to stress that the available theoretical models for dimensional changes driven by irradiation fall short of the needs of multiscale simulation framework at the moment. Crystal plasicity-based and atomistic approaches both have limitations that must be addressed, bearing in mind that there is no immediate hope of being able to access the experimental data spanning the dose and recoil energy spectra corresponding to fusion conditions.

9. Future prospects

The number of areas in nuclear fusion where high performance computing (HPC) applications prove effective is increasing [372]. Beside the historically well-established and now well-trodden area of materials, simulated at very small length scales —this includes electronic structure and atomistic simulations —there are now other notable advances involving virtual reality and large-scale digital engineering. Progress is also being made in the development of multiscale models, e.g. coupling cluster dynamics and crystal plasticity to treat irradiation creep, or object kinetic Monte Carlo and cluster dynamics to study irradiation hardening. However, the classic multiscale paradigm, where multiple techniques are used at multiple length- and time-scales in a structured framework, has not yet been achieved, and this represents a major gap in fusion modelling capabilities. Exploiting HPC-based computer graphics is also important, because good visualisation assists with understanding a variety of complex aspects of fusion technology by both scientists and

engineers, working on the design and construction of new fusion devices with yet unknown operating parameters.

The need for an extensive deployment of HPC technology in fusion is well illustrated by the fact that ITER tokamak is expected to contain about a million of individual components, and as many as ten million individual parts. These components and parts are expected to operate - and deliver reliable performance - in a highly challenging environment involving high temperatures and stresses, and intense neutron irradiation. It is desirable, from the safety and investment protection perspectives, to have a tool capable of predicting and assessing the dynamics of interactions in a nuclear device involving such a high number of components and parts. Supercomputers provide the only presently available means matching the level of complexity of the task, potentially enabling the exploration of operating scenarios and identification of failure mitigation options.

What also appears clear from the above analysis is that the models for materials need to be made compatible with the digital input requirements of finite element codes used in structural engineering. A universal model for microstructural evolution of an irradiated material, suitable for performing finite element simulations, is still lacking.

It is undoubtedly important to have full mechanistic clarity about the microscopic phenomena involved in the transformation of materials occurring under intense irradiation, high temperatures, stress, and chemical environment of a fusion power plant. However, the objective of scientific understanding of the relevant phenomena is insufficient; the outcome of microstructural analysis needs to be presented in an appropriate digital form - not in the form of a pictorial illustration of the relevant phenomena - to ensure that a large scale FEM code, describing a full fusion reactor, could interrogate the model and use the microstructural information generated by the model to deliver predictions about the behaviour of the full device as it operates.

To achieve this, a realistic multiscale approach is expected to focus on advancing, on the one hand, the digital tools for modelling irradiated microstructures and, on the other hand, on the development of means of querying such microstructural simulations to return quantities such as a flow stress, swelling, thermal conductivity, fracture toughness, magnetization, or deuterium retention, at every location in the structure of the device where the FEM model needs them. A microscopic model for a material should also be sufficiently computationally efficient to be compatible with a simulation of a full fusion device, the digital FEM representation of which, as we now know, involves between 10^8 and 10^{10} finite elements [349].

This also implies that the multiscale problem of materials simulation is *not* hierarchical, with information propagating up the scales, but rather *self-consistent*, since in a holistic simulation of a fusion device the boundary conditions for a microscopic material simulation are set by the solutions generated by global finite element code. It is the global code that defines the stress, radiation field, temperature, hydrogen isotope content, magnetic field, and other parameters at each location in a device where a microscopic materials response needs to be computed. In turn, the location-dependent macroscopic parameters are evaluated by the global code that uses the microscopic input from the models for materials describing how each individual finite element evolves in the context of a holistic simulation.

What transpires from existing studies, reviewed above, is that often the models for materials are too narrowly focus on some specific phenomena, often just one type of irradiation effect, disregarding the fact that in reality, exposure to irradiation occurs in a representative volume element of a material that is subject not only to exposure to irradiation, but also is in triaxial stress state, at a high temperature, and is embedded in a complex chemical environment. There is therefore a clear need to either explore the option of collating the existing models, or develop a new class of models with broader validity and better compatibility with engineering simulations.

Given the multi-dimensional nature of the space of environmental operating parameters for materials and the lack of availability of a fusion neutron source, it is reasonable to expect that in the near future the observational experimental effort is going to concentrate on surrogate irradiation campaigns, involving fission neutron and ion irradiation. The data delivered by such experiments is often limited to results of mechanical tests or relatively fragmented electron microscope observations of microstructure. Interpolating these observations to fusion scenarios inevitably involves an element of uncertainty, and the assessment of confidence in the observational data themselves, and their transferability. This opens an interesting line of questions about the quantification of uncertainty of predictions made using the models trained solely on the fission neutron and ion irradiation data.

10. Overall conclusions

This article, co-authored by attendees of the 7th Fusion Materials Theory & Modelling Workshop held in 2024 in Incheon, Korea, reviews a selection of research studies of materials for fusion applications, focussing on the latest developments and attempting to identify the critical gaps in our knowledge. We highlight some recent advances in modelling and interpretation of experimental results, discuss how modelling can be targeted to the design of future power plants, and note the limitations of the presently available approaches.

Transmutation of the nuclides originally present in fusion materials is a concern. Tungsten is a notable example, because accurate inventory calculations are required to interpret experiments, to assess the effect of transmutation products on its properties, and to assist with its waste management. Here, further work is required particularly on quantification and propagation of uncertainties.

Over the past five years, substantial advances were made in simulations of high-dose radiation damage. There is still a gap between molecular dynamics and higher-length scale methods, despite some initial successes. For example, molecular dynamics accurately captures microstructural evolution occurring at low temperature whereas rate theory better applies at high temperature. Further work is also warranted on the precipitation and dissolution of second phases, and on the role of interstitial elements on the evolution of He and void formation.

At the other end of the length scale spectrum, the recent tendency has been to deploy virtual reality and develop digital representations of components and even full devices, either with the purpose of simulating plasma-wall interactions or to progress towards mechanical models that integrate neutron transport and materials simulations as a part of a unified platform. A challenge in this area is that tools for automatic meshing and contact enforcement are not yet sufficiently robust and still require excessive human supervision. Multi-scale approaches are also under development in the context of plasma-facing materials.

Even when structural engineering simulations are set up, a substantial gap exists between the theories of irradiation creep and swelling and their implementation in the form of numerical design rules specific to fusion applications, due to the lack of experimental data and the breadth of temperature, stress, dose and dose rates intervals that models are expected to encompass.

Given the importance of atomistic simulations for understanding radiation damage, there is considerable effort on the development of interatomic potentials based on machine learning, the MLPs, in order to retain, as much as possible, both the accuracy of density functional theory and the computational efficiency of empirical potentials. Fusion applications in particular need models for the Fe-Cr alloys and Fe-Cr-He systems, including the high temperature magnetic properties, Ta-Ti-V-W high-entropy alloys, and hydrogen isotope retention effects in metals. The main limitation is that MLPs remain much slower than conventional empirical potentials, thereby making their use in large scale simulations still challenging and generally beyond the reach of the available computer systems on typical research project timescales. Extensive further work is required before ceramic materials, or other materials containing ceramic elements, for example oxide dispersion-strengthened steels, can be studied using these potentials.

Finally, we note the outstanding issue stemming from the practical need to include models for materials in finite element structural engineering simulations. Although this objective was stated decades ago [373–375] as a foundational concept of multiscale materials modelling, relatively little has been done in practice to achieve this goal, and examples of application of multiscale modelling frameworks to problems of fusion engineering are still exceedingly rare. This is probably the most significant gap in the existing fusion materials modelling effort, and we hope that this review will help in directing future research towards addressing this outstanding scientific objective.

CRediT authorship contribution statement

Luca Reali: Writing - review & editing, Writing - original draft, Supervision, Conceptualization; **Mark R. Gilbert:** Writing - review & editing, Writing - original draft, Project administration, Conceptualization; **David Cereceda:** Writing - review & editing; **Krishna Chaitanya Pitike:** Writing - original draft; **Sergei L. Dudarev:** Writing - review & editing; **Philip Edmondson:** Writing - review & editing, Conceptualization; **Shin Kajita:** Writing - review & editing; **Jae-Min Kwon:** Writing - original draft; **Byeongchan Lee:** Writing - review & editing, Conceptualization; **Jaime Marian:** Writing - original draft, Conceptualization; **Daniel R. Mason:** Writing - review & editing, Writing - original draft; **Samuel T. Murphy:** Writing - original draft; **Duc Nguyen-Manh:** Writing - review & editing, Writing - original draft; **Takuji Oda:** Writing - review & editing, Writing - original draft; **Pär Olsson:** Writing - review & editing; **Wahyu Setyawan:** Writing - review & editing; **Sophia O. Von Tiedemann:** Writing - original draft; **Chenxu Wang:** Writing - review & editing; **Yugang Wang:** Writing - review & editing; **Andrew R. Warwick:** Writing - original draft; **Jan S. Wróbel:** Writing - original draft; **Hong-Bo Zhou:** Writing - review & editing; **Steven J. Zinkle:** Writing - review & editing, Writing - original draft.

Data availability

Data will be made available on request.

Declaration of competing interest

The authors declare that they have no known competing financial interests or personal relationships that could have appeared to influence the work reported in this paper.

Acknowledgments

The authors gratefully acknowledge stimulating discussions with M. Boleininger, R. J. Akers, M. J. Caturla, D. Borba, G. Federici, A. Ibarra, M.-C. Marinica, and T. D. Swinburne. UKAEA authors gratefully acknowledge funding from the EUROfusion Consortium, funded by the European Union via the Euratom Research and Training Programme (Grant Agreement No. 101052200–EUROfusion), and partially supported by the Broader Approach Phase II agreement under the PA of IFERC2-T2PA02. Views and opinions expressed are however those of the authors only and do not necessarily reflect those of the European Union or the European Commission. Neither the European Union nor the European Commission can be held responsible for them. Work at UKAEA was also partly funded by the UK Fusion Futures Programme and the UK EPSRC Energy Programme (Grant Number EP/W006839/1). PNNL authors acknowledge financial support from US DOE-FES under contract DE-AC05-76RL0-1830. J. M. thanks Dr Qianran Yu for assistance regenerating some of the plots related to the section on irradiation creep. J. S. W. acknowledges supported by the National Science Centre, Poland, under research project no UMO-2019/35/D/ST5/03526. D.C. acknowledges support from the U.S. Department of Energy, Office of Science, Fusion Energy Sciences Program Early Career Research Program under Award Number DE-SC0023072. Some of the numerical calculations were performed using resources provided by the Cambridge Service for Data Driven Discovery (CSD3) operated by the University of Cambridge Research Computing Service (https://www.csd3.cam.ac.uk). We thank the reviewers for their careful reading of the manuscript.

References

[1] M.R. Gilbert, K. Arakawa, Z. Bergstrom, M.J. Caturla, S.L. Dudarev, F. Gao, A.M. Goryaeva, S.Y. Hu, X. Hu, R.J. Kurtz, A. Litnovsky, J. Marian, M.-C. Marinica, E. Martinez, E.A. Marquis, D.R. Mason, B.N. Nguyen, P. Olsson, Y. Osetskiy, D. Senor, W. Setyawan, M.P. Short, T. Suzudo, J.R. Trelewicz, T. Tsuru, G.S. Was, B.D. Wirth, L. Yang, Y. Zhang, S.J. Zinkle, Perspectives on multiscale modelling and experiments to accelerate materials development for fusion, J. Nucl. Mater. 554 (2021) 153113. https://www.sciencedirect.com/science/article/pii/S0022311521003366. https://doi.org/10.1016/j.jnucmat.2021.153113

[2] A. Bhattacharya, S.J. Zinkle, Cavity swelling in irradiated materials, in: R.J.M. Konings, R.E. Stoller (Eds.), Comprehensive Nuclear Materials, 1, Elsevier, Oxford, 2nd ed., 2020, pp. 406–455. https://doi.org/10.1016/B978-0-12-803581-8.11599-1

[3] Y.-R. Lin, A. Bhattacharya, S.J. Zinkle, The effect of helium on cavity swelling in dual-ion irradiated Fe and Fe-10Cr ferritic alloys, J. Nucl. Mater. 569 (2022) 153907. https://doi.org/10.1016/j.jnucmat.2022.153907

[4] L.N. Clowers, Z. Jiao, G.S. Was, Synergies between H, He and radiation damage in dual and triple ion irradiation of candidate fusion blanket materials, J. Nucl. Mater. 565 (2022) 153722. https://doi.org/10.1016/j.jnucmat.2022.153722

[5] Y. Katoh, L.L. Snead, L.M. Garrison, X. Hu, T. Koyanagi, C.M. Parish, P.D. Edmondson, M. Fukuda, T. Hwang, T. Tanaka, et al., Response of unalloyed tungsten to mixed spectrum neutrons, J. Nucl. Mater. 520 (2019) 193–207.

[6] Y. Wang, J. Zhao, Understanding the thermal conductivity of pristine W and W-Re alloys from a physics-based model, J. Nucl. Mater. 529 (2020) 151931.

[7] J.R. Echols, L.M. Garrison, N. Reid, C.M. Parish, A. Hasegawa, A. Bhattacharya, W. Zhong, D. Morrall, M. Lance, Y. Katoh, Degradation of electrical resistivity of tungsten following shielded neutron irradiation, Acta Mater. 257 (2023) 119025.

[8] A. Perrin, D. Hamaguchi, J.W. Geringer, S. Zinkle, Y. Yang, S. Skutnik, J. Poplawsky, Y. Katoh, Microstructure, electrical resistivity, and tensile properties of neutron-irradiated Cu-Cr-Nb-Zr, Front. Nucl. Eng. 3 (2024) 1486694.

[9] L. Reali, M.R. Gilbert, M. Boleininger, S.L. Dudarev, Intense γ-photon and high-energy electron production by neutron irradiation: effects of nuclear excitations on reactor materials, PRX Energy 2 (2) (2023) 023008. https://doi.org/10.1103/PRXEnergy.2.023008

[10] L. Reali, M.R. Gilbert, M. Boleininger, S.L. Dudarev, γ-photons and high-energy electrons produced by neutron irradiation in nuclear materials, J. Nucl. Mater. 585 (2023) 154584. https://doi.org/10.1016/j.jnucmat.2023.154584

[11] T. Tanno, A. Hasegawa, J.C. He, M. Fujiwara, M. Satou, S. Nogami, K. Abe, T. Shishido, Effects of transmutation elements on the microstructural evolution and electrical resistivity of neutron-irradiated tungsten, J. Nucl. Mater. 386 (2009) 218–221.

[12] T. Tanno, M. Fukuda, S. Nogami, A. Hasegawa, Microstructure development in neutron irradiated tungsten alloys, Mater. Trans. 52 (2011) 1447–1451.

[13] M. Fukuda, T. Tanno, S. Nogami, A. Hasegawa, Effects of Re content and fabrication process on microstructural changes and hardening in neutron irradiated tungsten, Mater. Trans. 53 (12) (2012) 2145–2150.

[14] M. Fukuda, A. Hasegawa, T. Tanno, S. Nogami, H. Kurishita, Property change of advanced tungsten alloys due to neutron irradiation, J. Nucl. Mater. 442 (1–3) (2013) S273–S276.

[15] A. Hasegawa, T. Tanno, S. Nogami, M. Satou, Property change mechanism in tungsten under neutron irradiation in various reactors, J. Nucl. Mater. 417 (1–3) (2011) 491–494.

[16] A. Hasegawa, M. Fukuda, K. Yabuuchi, S. Nogami, Neutron irradiation effects on the microstructural development of Tungsten and Tungsten alloys, J. Nucl. Mater. 471 (2016) 175–183.

[17] M. Fujitsuka, B. Tsuchiya, I. Mutoh, T. Tanabe, T. Shikama, Effect of neutron irradiation on thermal diffusivity of Tungsten–Rhenium alloys, J. Nucl. Mater. 283 (2000) 1148–1151.

[18] L.M. Garrison, Y. Katoh, J.W. Geringer, M. Akiyoshi, X. Chen, M. Fukuda, A. Hasegawa, T. Hinoki, X. Hu, T. Koyanagi, et al., PHENIX US-Japan Collaboration investigation of thermal and mechanical properties of thermal Neutron–Shielded irradiated tungsten, Fusion Sci. Technol. 75 (6) (2019) 499–509.

[19] T. Hwang, A. Hasegawa, K. Tomura, N. Ebisawa, T. Toyama, Y. Nagai, M. Fukuda, T. Miyazawa, T. Tanaka, S. Nogami, Effect of neutron irradiation on rhenium cluster formation in tungsten and tungsten-rhenium alloys, J. Nucl. Mater. 507 (2018) 78–86.

[20] P.D. Edmondson, B. Gault, M.R. Gilbert, An atom probe tomography and inventory calculation examination of second phase precipitates in neutron irradiated single crystal tungsten, Nucl. Fusion 60 (12) (2020) 126013.

[21] T. Koyanagi, N. Kumar, T. Hwang, L.M. Garrison, X.X. Hu, L.L. Snead, Y. Katoh, Microstructural evolution of pure tungsten neutron irradiated with a mixed energy spectrum, J. Nucl. Mater. 490 (2017) 66–74.

[22] D. Nguyen-Manh, A.P. Horsfield, S.L. Dudarev, Self-interstitial atom defects in bcc transition metals: group-specific trends, Phys. Rev. B 73 (2) (2006) 020101.

[23] P.M. Derlet, D. Nguyen-Manh, S.L. Dudarev, Multiscale modeling of crowdion and vacancy defects in body-centered-cubic transition metals, Phys. Rev. B 76 (5) (2007) 054107.

[24] D. Nguyen-Manh, V. Vitek, A.P. Horsfield, Environmental dependence of bonding: a challenge for modelling of intermetallics and fusion materials, Prog. Mater. Sci. 52 (2–3) (2007) 255–298.

[25] D. Nguyen-Manh, M.Y. Lavrentiev, M. Muzyk, S.L. Dudarev, First-principles models for phase stability and radiation defects in structural materials for future fusion power-plant applications, J. Mater. Sci. 47 (21) (2012) 7385–7398.

[26] D. Cereceda, J.M. Perlado, J. Marian, Techniques to accelerate convergence of stress-controlled molecular dynamics simulations of dislocation motion, Comput. Mater. Sci 62 (2012) 272–275.

[27] S.L. Dudarev, Density functional theory models for radiation damage, Annu. Rev. Mater. Res. 43 (2013) 35–61.

[28] D. Cereceda, Multiscale Modeling of the Plastic Behaviour in Single Crystal Tungsten: from Atomistic to Crystal Plasticity Simulations, Univerisdad Politécnica de Madrid Ph. D. thesis (2015).

[29] F. Hofmann, D. Nguyen-Manh, M.R. Gilbert, C.E. Beck, J.K. Eliason, A.A. Maznev, W. Liu, D.E.J. Armstrong, K.A. Nelson, S.L. Dudarev, Lattice swelling and modulus change in a helium-implanted tungsten alloy: X-ray micro-diffraction, surface acoustic wave measurements, and multiscale modelling, Acta Mater. 89 (2015) 352–363.

[30] D. Nguyen-Manh, S.L. Dudarev, Trapping of He clusters by inert-gas impurities in tungsten: first-principles predictions and experimental validation, Nucl. Instrum. Methods Phys. Res. Sect. B 352 (2015) 86–91.

[31] D. Cereceda, M. Diehl, F. Roters, D. Raabe, J.M. Perlado, J. Marian, Unraveling the temperature dependence of the yield strength in single-crystal tungsten using atomistically-informed crystal plasticity calculations, Int. J. Plast. 78 (2016) 242–265.

[32] S.M. González De Vicente, J.-L. Boutard, S.J. Zinkle, H. Tanigawa, Materials testing facilities and programmes for fission and ion implantation damage, Nucl. Fusion 57 (9) (2017) 092011.

[33] R.G. Abernethy, Predicting the performance of tungsten in a fusion environment: a literature review, Mater. Sci. Technol. 33 (4) (2017) 388–399.

[34] J. Marian, C.S. Becquart, C. Domain, S.L. Dudarev, M.R. Gilbert, R.J. Kurtz, D.R. Mason, K. Nordlund, A.E. Sand, L.L. Snead, T. Suzudo, B.D. Wirth, Recent advances in modeling and simulation of the exposure and response of tungsten to fusion energy conditions, Nucl. Fusion 57 (9) (2017) 092008.

[35] D.R. Mason, D. Nguyen-Manh, C.S. Becquart, An empirical potential for simulating vacancy clusters in tungsten, J. Phys. Condens. Matter 29 (50) (2017) 505501.

[36] S.L. Dudarev, D.R. Mason, E. Tarleton, P.-W. Ma, A.E. Sand, A multi-scale model for stresses, strains and swelling of reactor components under irradiation, Nucl. Fusion 58 (12) (2018) 126002.

[37] D.R. Mason, D. Nguyen-Manh, M.-C. Marinica, R. Alexander, A.E. Sand, S.L. Dudarev, Relaxation volumes of microscopic and mesoscopic irradiation-induced defects in tungsten, J. Appl. Phys. 126 (7) (2019) 075112.

[38] K. Nordlund, Historical review of computer simulation of radiation effects in materials, J. Nucl. Mater. 520 (2019) 273–295.

[39] P.M. Derlet, S.L. Dudarev, Microscopic structure of a heavily irradiated material, Phys. Rev. Mater. 4 (2020) 023605.

[40] J. Marian, W. Setyawan, Y. Yang, A. Manzoor, W. Zhong, J.R. Trelewicz, J. Yu, E. Peterson, Y. Katoh, L. Snead, B.D. Wirth, Computational materials assessment of the D/Li-stripping neutron source as a prototypical facility for fusion materials testing, Curr. Opin. Solid State Mater. Sci. 38 (2025) 101231. https://doi.org/10.1016/j.cossms.2025.101231

[41] J.-Ch. Sublet, J.W. Eastwood, J.G. Morgan, M.R. Gilbert, M. Fleming, W. Arter, FISPACT-II: an advanced simulation system for activation, transmutation and material modelling, Nucl. Data Sheets 139 (2017) 77–137.

[42] M. Fleming, T. Stainer, M.R. Gilbert, The FISPACT-II User Manual, Technical Report UKAEA-R(18)001, UKAEA, 2018. Available from http://fispact.ukaea.uk.

[43] M.R. Gilbert, J.-C. Sublet, S.L. Dudarev, Spatial heterogeneity of tungsten transmutation in a fusion device, Nucl. Fusion 57 (4) (2017) 044002. https://doi.org/10.1088/1741-4326/aa5e2e

[44] A. Baker, The spherical tokamak for energy production (STEP) in context: UK public sector approach to fusion energy, Philos. Trans. R. Soc. A Math. Phys. Eng. Sci. 382 (2280) (2024) 20230401. https://royalsocietypublishing.org/rsta/article-pdf/doi/10.1098/rsta.2023.0401/1329105/rsta.2023.0401.pdfhttps://doi.org/10.1098/rsta.2023.0401

[45] C. Waldon, S.I. Muldrew, J. Keep, R. Verhoeven, T. Thompson, M. Kisbey-Ascott, Concept design overview: a question of choices and compromise, Philos. Trans. R. Soc. A Math. Phys. Eng. Sci. 382 (2280) (2024) 20230414. https://doi.org/10.1098/rsta.2023.0414

[46] T. Suzudo, M. Yamaguchi, A. Hasegawa, Stability and mobility of rhenium and osmium in tungsten: first principles study, Modell. Simul. Mater. Sci. Eng. 22 (7) (2014) 075006.

[47] Y. Shin, K. Kang, B. Lee, Reduced interstitial mobility through multicomponent alloying in bcc W, Fusion Eng. Des. 172 (2021) 112745.

[48] Y. Qian, M.R. Gilbert, L. Dezerald, D. Cereceda, Using first-principles calculations to predict the mechanical properties of transmuting tungsten under first wall fusion power-plant conditions, J. Phys. Condens. Matter 33 (34) (2021) 345901.

[49] Y. Qian, M.R. Gilbert, L. Dezerald, D. Nguyen-Manh, D. Cereceda, Ab initio study of tungsten-based alloys under fusion power-plant conditions, J. Nucl. Mater. (2023) 154422.

[50] L. Bellaiche, D. Vanderbilt, Virtual crystal approximation revisited: application to dielectric and piezoelectric properties of perovskites, Phys. Rev. B 61 (12) (2000) 7877.

[51] Y. Qian, M.R. Gilbert, L. Dezerald, D. Nguyen-Manh, D. Cereceda, First-principles study of the energetics and the local chemical ordering of tungsten-based alloys, arXiv preprint arXiv:2410.03998 (2024).

[52] M.R.K. Musa, Y. Qian, J. Peng, D. Cereceda, Accelerating the discovery of low-energy structure configurations: a computational approach that integrates first-principles calculations, Monte Carlo sampling, and machine learning, Scr. Mater. 259 (2025) 116535.

[53] J. Peng, Y. Qian, D. Cereceda, A first-principles study of the structural and thermo-mechanical properties of Tungsten-based plasma-Facing materials, Metals 14 (10) (2024) 1197.

[54] M.R. Gilbert, T. Eade, C. Bachmann, U. Fischer, N.P. Taylor, Activation, decay heat, and waste classification studies of the European DEMO concept, Nucl. Fusion 57 (4) (2017) 046015. https://iopscience.iop.org/article/10.1088/1741-4326/aa5bd7. https://doi.org/10.1088/1741-4326/aa5bd7

[55] M.R. Gilbert, T. Eade, C. Bachmann, U. Fischer, N.P. Taylor, Waste assessment of European DEMO fusion reactor designs, Fusion Eng. Des. 136 (2018) 42–48. https://linkinghub.elsevier.com/retrieve/pii/S0920379617309717. https://doi.org/10.1016/j.fusengdes.2017.12.019

[56] G.W. Bailey, O.V. Vilkhivskaya, M.R. Gilbert, Waste expectations of fusion steels under current waste repository criteria, Nucl. Fusion 61 (3) (2021) 036010. https://doi.org/10.1088/1741-4326/abc933

[57] M.R. Gilbert, Z. Zacharauskas, P. Almond, N. Scott-Mearns, S. Reynolds, M.Y. Lavrentiev, Fusion waste requirements for tritium control: perspectives and current research, Fusion Eng. Des. 202 (2024) 114296. https://linkinghub.elsevier.com/retrieve/pii/S0920379624001492. https://doi.org/10.1016/j.fusengdes.2024.114296

[58] S.O. von Tiedemann, D.M. Collins, M.R. Gilbert, I.A. Kodeli, Nuclear data uncertainty propagation and implications for radioactive waste management of fusion steels, Fusion Eng. Des. 188 (2023) 113409. https://linkinghub.elsevier.com/retrieve/pii/S0920379622003994. https://doi.org/10.1016/j.fusengdes.2022.113409

[59] P.K. Romano, N.E. Horelik, B.R. Herman, A.G. Nelson, B. Forget, K. Smith, OpenMC: a state-of-the-art Monte Carlo code for research and development, Ann. Nucl. Energy 82 (2015) 90–97. https://linkinghub.elsevier.com/retrieve/pii/S030645491400379X. https://doi.org/10.1016/j.anucene.2014.07.048

[60] I.A. Kodeli, XSUN-2022/SUSD3D n/gamma sensitivity-uncertainty code package with recent JEFF-3.3 and ENDF/B-VIII.0 covariance data, EPJ Web Conf. 281 (2023) 00013. https://doi.org/10.1051/epjconf/202328100013

[61] R.E. MacFarlane, TRANSX 2.15, Code system to produce neutron, photon, and particle transport tables for discrete- ordinates and diffusion codes from cross sections in MATXS format, RSICC Peripher. Shield. Rout. Collect. PSR- 317 (1995).

[62] R.E. Alcouffe, R.S. Baker, J.A. Dahl, S.A. Turner, R.C. Ward, PARTISN 5.97, 1-D, 2-D, 3-D time-dependent, multigroup deterministic parallel neutral particle transport code, LA-UR08-07258, NEA/Data Bank CCC-0760/01 Computer Code Collection (2008).

[63] I.A. Kodeli, S. Slavic, SUSD3D computer code as part of the XSUN-2017 windows interface environment for deterministic radiation transport and cross-section sensitivity-uncertainty analysis, Sci. Technol. Nucl. Install. 2017 (2017) 1–16. https://doi.org/10.1155/2017/1264736

[64] D.A. Brown, M.B. Chadwick, R. Capote, A.C. Kahler, A. Trkov, M.W. Herman, A.A. Sonzogni, Y. Danon, A.D. Carlson, M. Dunn, D.L. Smith, G.M. Hale, G. Arbanas, R. Arcilla, C.R. Bates, B. Beck, B. Becker, F. Brown, R.J. Casperson, J. Conlin, D.E. Cullen, M.-A. Descalle, R. Firestone, T. Gaines, K.H. Guber, A.I. Hawari, J. Holmes, T.D. Johnson, T. Kawano, B.C. Kiedrowski, A.J. Koning, S. Kopecky, L. Leal, J.P. Lestone, C. Lubitz, J.I. Márquez Damián, C.M. Mattoon, E.A. McCutchan, S. Mughabghab, P. Navratil, D. Neudecker, G.P.A. Nobre, G. Noguere, M. Paris, M.T. Pigni, A.J. Plompen, B. Pritychenko, V.G. Pronyaev, D. Roubtsov, D. Rochman, P. Romano, P. Schillebeeckx, S. Simakov, M. Sin, I. Sirakov, B. Sleaford, V. Sobes, E.S. Soukhovitskii, I. Stetcu, P. Talou, I. Thompson, S. van der Marck, L. Welser-Sherrill, D. Wiarda, M. White, J.L. Wormald, R.Q. Wright, M. Zerkle, G. Zerovnik, Y. Zhu, ENDF/B-VIII.0: the 8 th major release of the nuclear reaction data library with CIELO-project cross sections, new standards and thermal scattering data, Nucl. Data Sheets 148 (2018) 1–142. https://linkinghub.elsevier.com/retrieve/pii/S0090375218300206. https://doi.org/10.1016/j.nds.2018.02.001

[65] A.J.M. Plompen, O. Cabellos, C. De Saint Jean, M. Fleming, A. Algora, M. Angelone, P. Archier, E. Bauge, O. Bersillon, A. Blokhin, F. Cantargi, A. Chebboubi, C. Diez, H. Duarte, E. Dupont, J. Dyrda, B. Erasmus, L. Fiorito, U. Fischer, D. Flammini, D. Foligno, M.R. Gilbert, J.R. Granada, W. Haeck, F.-J. Hambsch, P. Helgesson, S. Hilaire, I. Hill, M. Hursin, R. Ichou, R. Jacqmin, B. Jansky, C. Jouanne, M.A. Kellett, D.H. Kim, H.I. Kim, I. Kodeli, A.J. Koning, A.Y. Konobeyev, S. Kopecky, B. Kos, A. Krása, L.C. Leal, N. Leclaire, P. Leconte, Y.O. Lee, H. Leeb, O. Litaize, M. Majerle, J.I. Márquez Damián, F. Michel-Sendis, R.W. Mills, B. Morillon, G. Noguère, M. Pecchia, S. Pelloni, P. Pereslavtsev, R.J. Perry, D. Rochman, A. Röhrmoser, P. Romain, P. Romojaro, D. Roubtsov, P. Sauvan, P. Schillebeeckx, K.H. Schmidt, O. Serot, S. Simakov, I. Sirakov, H. Sjöstrand, A. Stankovskiy, J.C. Sublet, P. Tamagno, A. Trkov, S. van der Marck, F. Álvarez Velarde, R. Villari, T.C. Ware, K. Yokoyama, G. Zerovnik, The joint evaluated fission and fusion nuclear data library, JEFF-3.3, Eur. Phys. J. A 56 (7) (2020) 181. https://doi.org/10.1140/epja/s10050-020-00141-9

[66] M.R. Gilbert, Nuclear data for fusion: inventory validation successes and future needs, J. Phys. Energy 5 (3) (2023) 034002. https://doi.org/10.1088/2515-7655/acd028

[67] K.C. Russell, Phase stability under irradiation, Prog. Mater. Sci. 28 (1984) 229–434.

[68] D. Nguyen-Manh, J.S. Wrobel, M. Klimenkov, M.J. Lloyd, L. Messina, S.L. Dudarev, First principles model for voids decorated by transmutation solutes: short range order effects and application to neutron irradiated tungsten, Phys. Rev. Mater. 5 (2021) 065401.

[69] D. Nguyen-Manhh, M. Klimenkov, M.J. Lloyd, J.S. Wrobel, L. Messina, J. Marian, G.D. Samolyuk, Y.N. Osetsky, E. Gaganidze, M. Dürrschnabel, M. Rieth, T.P. Davis, E. Martinez, C.S. Becquart, C. Domain, A.J. London, J. Haley, M.R. Gilbert, S.L.

Dudarev, D.E.J. Armstrong, An integrated experimental and multiscale modelling study of transmutation-induced defects in neutron irradiated tungsten, Nucl. Fusion (2025).
[70] A. Fernandez-Cabalerro, M. Fedorov, J.S. Wrobel, Mummery, D. Nguyen-Manh, Configurational entropyin multicomponent alloys: matrix formulatiion from ab initio based Hamiltonian and application to fcc Cr–Fe–Mn–Ni system, Entropy 21 (2019) 68.
[71] B.E. Warren, X-ray Diffraction, New York, Dover, 1990.
[72] J.M. Cowley, Short-range order and long-range order parameters, Phys. Rev. 138 (5A) (1965) 1384–1388.
[73] J.S. Wrobel, D. Nguyen-Manh, M. Muzyk, M.Y. Lavrentiev, K.J. Kurzydlowski, S.L. Dudarev, Phase stability of ternary fcc and bcc Fe-Cr-Ni alloys, Phys. Rev. B 91 (2015) 024108.
[74] M. Fedorov, J.S. Wrobel, A. Fernandez-Carabello, K. Kurzydlowski, D. Nguyen-Manh, Phase stability and magnetic properties in fcc Fe-Cr-Mn-Ni alloys from first-principles modeling, Phys. Rev. B 101 (2020) 174416.
[75] M.J. Lloyd, R.G. Abernethy, M.R. Gilbert, I. Griffiths, P.A.J. Bagot, D. Nguyen-Manh, M.P. Moody, D.E.J. Armstrong, Decoration of voids with rhenium and osmium transmutation products in neutron irradiated single crystal tungsten, Scr. Mater. 173 (2019) 96–100.
[76] J.M. Lloyd, Radiation Damage and Transmutation in Tungsten-Alloys for Nuclear Fusion Applications, DPhil thesis, University of Oxford (2021).
[77] M.J. Lloyd, A. London, J. Haley, M.R. Gilbert, C. Becquart, C. Domain, E. Martinez, M.P. Moody, P.A.J. Bagot, D. Nguyen-Manh, D.E.J. Armstrong, Interaction of transmutation products with precipitates, dislocations and grain boundaries in neutron irradiated W, Materialia 22 (2022) 101370. https://doi.org/10.1016/j.mtla.2022.101370
[78] M.J. Lloyd, J. Haley, B. Jim, R. Abernethy, M.R. Gilbert, E. Martinez, K. Hattar, O. El-Atwani, D. Nguyen-Manh, M.P. Moody, P.A.J. Bagot, D.E.J. Armstrong, Microstructural evolution and transmutation in tungsten under ion and neutron irradiation, Materialia 33 (2024) 101991. https://doi.org/10.1016/j.mtla.2023.101991
[79] D. Sobieraj, J.S. Wrobel, T. Rygier, K.J. Kurzydlowski, O. El-Atwani, E. Martinez Saez, D. Nguyen-Manh, Chemical short-range order in derivative Cr–Ta–Ti–V–W high entropy alloysd from first-principles thermodynamic study, Phys. Chem. Chem. Phys. 22 (2020) 23929.
[80] D. Sobieraj, J.S. Wrobel, M.R. Gilbert, K.J. Kurzydlowski, D. Nguyen-Manh, Co-segregation of Y and Zr in W-Cr-Y-Zr alloys: first-principles modeling at finite temperature and application to SMART materials, J. Alloys Mettalurg. Syst. 1 (2023) 100011.
[81] D. Sobieraj, Phase Stability and Short-Range Ordering of W-based SMART Materials and High-Entropy Alloys Predicted from the First-Principles Modelling, PhD thesis, Warsaw University of Technology (2025).
[82] D. Sobieraj, J.S. Wrobel, M.R. Gilbert, A. Litnovsky, F. Klein, K.J. Kurzydlowski, D. Nguyen-Manh, Composition stability and cr-rich phase formation in W-Cr-Y and W-Cr-Ti smart alloys, Metals 11 (2021) 743.
[83] A. Litnovsky, F. Klein, X. Tan, J. Ertmer, J.W. Coenen, C. Linsmeier, J. Gozalez-Julian, M. Bram, I. Povstugar, T. Morgan, Y.M. Gasparyan, A. Suchkov, D. Bachurina, D. Nguyen-Manh, M. Gilbert, D. Sobieraj, J.S. Wrobel, E. Tejado, J. Matejicek, H.U. Zoz, H. Benz, P. Bittner, A. Reuban, Advanced self-passivating alloys for an application under extreme condition, Metals 11 (2021) 1255.
[84] J. Chen, E. Tejado, A. Litnovsky, D. Nguyen-Manh, E. Prestat, T. Witfield, J.Y. Pastor, M. Bram, J.W. Coenen, C. Lismeiner, J. Gonzalez . Juilian, Influence of phase decomposition on mechanical properties and oxidation resistance of WCrY SMART material, J. Nucl. Mater. Energy 41 (2024) 101762. https://doi.org/10.1016/j.nme.2024.101762
[85] J. Chen, E. Tejado, M. Rasinski, A. Litnovsky, D. Nguyen-Manh, E. Prestat, T. Witfield, J.Y. Pastor, M. Bram, J.W. Coenen, C. Lismeiner, J. Gonzalez . Juilian, Effect of yttrium and yttria addition in self-passivating WCr SMART material for first-wall application in a fusion power plant, Metals 14 (2024) 1092. https://doi.org/10.3390/met14091092
[86] O. El-Atwani, N. Li, M. Li, A. Devaraj, J. Baldwin, M.M. Schneider, D. Sobieraj, J.S. Wróbel, D. Nguyen-Manh, S.A. Maloy, et al., Outstanding radiation resistance of tungsten-based high-entropy alloys, Sci. Adv. 5 (3) (2019) eaav2002.
[87] O. El Atwani, H.T. Vo, M.A. Tunes, C. Lee, A. Alvarado, N. Krienke, J.D. Poplawsky, A.A. Kohnert, J. Gigax, W.Y. Chen, M. Li, Y. Wang, J. Wrobel, D. Nguyen-Manh, J. Balwin, Q.U. Tukac, E. Aydogan, S. Fensin, M.J. Martinez, A quinary WTaCrVHf nanocrystalline refractory high-entropy alloy withholding extreme irradiation environments, Nat. Commun. 14 (1) (2023) 2516.
[88] M.A. Tunes, D. Parkison, B. Sun, P. Willenshofer, S. Samberger, B.K. Derby, S.K.S. Baldwin, S.J. Fensin, D. Sobieraj, J. Wróbel, J. S. Byggmästar, S. Pogatscher, E. Martinez, D. Nguyen-Manhh, O. El-Atwani, High radiation resistance in the binary W-Ta system through small V additions: a new paradigm for nuclear fusion materials, Adv. Sci. (2025) 2417659.
[89] J. Byggmastar, D. Sobieraj, J. Wrobel, D. K. Schreiber, M. J. Martinez, O. El Atwani, D. Nguyen-Manh, Segregation, ordering, and precipitation in WTaV-based concentrated refractory alloys, Acta Mater. 296 (2025) 121276.
[90] D. Nguyen-Manh, M.Y. Lavrentiev, S.L. Dudarev, Magnetic origin of nano-clustering and point defect interaction in Fe-Cr alloys: an ab-initio study, J. Comput.-Aided Mater. Des. 14 (2007) 159.
[91] D. Nguyen-Manh, M.Y. Lavrentiev, S.L. Dudarev, The Fe-Cr system: atomistic modelling of thermodynamics and kinetics of phase transformations, Compte Rendus Physique 9 (2008) 379.
[92] D. Nguyen-Manh, S.L. Dudarev, Model many-body stoner hamiltonian for binary FeCr alloys, Phys. Rev. B 80 (2010) 104440.
[93] M. Mrovec, D. Nguyen-Manh, C. Elsasser, P. Gumbsch, Magnetic bond-order potential for iron, Phys. Rev. Lett. 106 (2011) 246402.
[94] D. Nguyen-Manh, P.W. Ma, M.Y. Lavrentiv, S.L. Dudarev, Constrained non-collinear magnetism in disordered Fe and Fe-Cr alloys, Ann. Nucl. Energy 77 (2015) 020101(R).
[95] J.S. Wróbel, D. Nguyen-Manh, M.Y. Lavrentiev, M. Muzyk, S.L. Dudarev, Phase stability of ternary fcc and bcc Fe-Cr-Ni alloys, Phys. Rev. B 91 (2015) 024108. https://doi.org/10.1103/PhysRevB.91.024108
[96] M. Fedorov, J.S. Wróbel, A. Fernández-Caballero, K.J. Kurzydłowski, D. Nguyen-Manh, Phase stability and magnetic properties in fcc Fe-Cr-Mn-Ni alloys from first-principles modeling, Phys. Rev. B 101 (2020) 174416. https://doi.org/10.1103/PhysRevB.101.174416
[97] M. Fedorov, J.S. Wróbel, W. Chrominski, G. Cieslak, M. Plocinsla, K.J. Kurzydłowski, D. Nguyen-Manh, Composition stability of single fcc phase in Cr-Fe-Mn-Ni alloys: first-principles prediction and experimental validation, Acta Mater. 255 (2023) 119047.
[98] M. Fedorov, J.S. Wróbel, A. London, K.J. Kurzydłowski, C.C. Fu, T. Tadic, S.L. Dudarev, D. Nguyen-Manh, Precipitation of Cr-rich clusters in Fe-Cr alloys: effects of irradiation from first principles modeling and experimental observations, J. Nucl. Mater. 587 (2023) 154715. https://doi.org/10.1016/j.jnucmat.2023.154715
[99] M. Fedorov, Phase stability and properties of Fe-Cr-Mn-Ni alloys from firstprinciples modeling, PhD Thesis, Warsaw University of Technology (2024).
[100] M.J. Norgett, M.T. Robinson, I.M. Torrens, A proposed method of calculating displacement dose rates, Nucl. Eng. Des. 33 (1975) 50–54.
[101] K. Nordlund, S.J. Zinkle, A.E. Sand, F. Granberg, R.S. Averback, R.E. Stoller, T. Suzudo, L. Malerba, F. Banhart, W.J. Weber, F. Willaime, S.L. Dudarev, D. Simeone, Improving atomic displacement and replacement calculations with physically realistic damage models, Nat. Commun. 9 (2018) 1084.
[102] K. Nordlund, S.J. Zinkle, A.E. Sand, F. Granberg, R.S. Averback, R.E. Stoller, T. Suzudo, L. Malerba, F. Banhart, W.J. Weber, et al., Primary radiation damage: a review of current understanding and models, J. Nucl. Mater. 512 (2018) 450–479.
[103] S.J. Zinkle, Radiation-induced effects on microstructure, in: R. Konings, R.E. Stoller (Eds.), Comprehensive Nuclear Materials, 2nd Ed., 1, Elsevier, Oxford, 2020, pp. 91–129.
[104] S.J. Zinkle, R.E. Stoller, Quantifying defect production in solids at finite temperatures: thermally-activated correlated defect recombination corrections to DPA (CRC-DPA), J. Nucl. Mater. 577 (2023) 154292.
[105] S. Agarwal, S.J. Zinkle, 1.03 experimental studies on primary damage formation, in: R. Konings, R.E. Stoller (Eds.), Comprehensive Nuclear Materials, 2nd Ed., 1, Elsevier, Oxford, 2020, pp. 74–90.
[106] R.S. Nelson, J.A. Hudson, D.J. Mazey, Stability of precipitates in an irradiation environment, J. Nucl. Mater. 44 (1972) 318–330.
[107] G. Martin, Phase-stability under irradiation - ballistic effects, Phys. Rev. B 30 (1984) 1424–1436.
[108] K.H. Heinig, T. Muller, B. Schmidt, M. Strobel, W. Moller, Interfaces under ion irradiation: growth and taming of nanostructures, Appl. Phys. A Mater. Sci. Process. 77 (2003) 17–25.
[109] J. Ribis, 1.09 Phase stability in irradiated alloys, in: R. Konings, R.E. Stoller (Eds.), Comprehensive Nuclear Materials, 2nd Ed., 1, Elsevier, Oxford, 2020, pp. 265–309.
[110] S.M. Levine, C. Pareige, Z. Jiao, P.D. Edmondson, G.S. Was, S.J. Zinkle, A. Bhattacharya, Phase instabilities in austenitic steels during particle bombardment at high and low dose rates, Mater. Des. 217 (2022) 110588.
[111] Y. Zhao, A. Bhattacharya, C. Pareige, C.P. Massey, P. Zhu, J.D. Poplawsky, J. Henry, S.J. Zinkle, Effect of heavy ion irradiation dose rate and temperature on α' precipitation in high purity Fe-18%Cr alloy, Acta Mater. 231 (2022) 117888.
[112] Z.-K. Liu, Y.A. Chang, Evaluation of the thermodynamic properties of the Re-Ta and Re-W systems, J. Alloys Compd. 299 (2000) 153–162.
[113] B.N. Singh, S.J. Zinkle, Defect accumulation in pure fcc metals in the transient regime: a review, J. Nucl. Mater. 206 (1993) 212–229.
[114] L.K. Mansur, E.H. Lee, Theoretical basis for unified analysis of experimental data and design of swelling-resistant alloys, J. Nucl. Mater. 179–181 (1991) 105–110.
[115] A.A. Kohnert, M.A. Cusentino, B.D. Wirth, Molecular statics calculations of the biases and point defect capture volumes of small cavities, J. Nucl. Mater. 499 (2018) 480–489.
[116] Y. Wang, F. Gao, B.D. Wirth, Atomic modeling assessment of the interaction distance and effective bias for small defect clusters absorption at a void in BCC Fe, J. Nucl. Mater. 568 (2022) 153882.
[117] D. Woodley, S. Taller, Z. Jiao, K. Sun, G.S. Was, The role of co-injected helium on swelling and cavity evolution at high damage levels in ferritic-martensitic steels, J. Nucl. Mater. 550 (2021) 152912.
[118] A.K. Seeger, On the theory of radiation damage and radiation hardening, in: 2nd UN Conference on Peaceful Uses of Atomic Energy, 6, United Nations, New York, 1958, pp. 250–273.
[119] S.J. Zinkle, Y. Matsukawa, Observation and analysis of defect cluster production and interactions with dislocations, J. Nucl. Mater. 329–333 (2004) 88–96.
[120] L. Tan, J.T. Busby, Formulating the strength factor alpha for improved predictability of radiation hardening, J. Nucl. Mater. 465 (2015) 724–730.
[121] P. Zhu, Y. Zhao, S. Agarwal, J. Henry, S.J. Zinkle, Toward accurate evaluation of bulk hardness from nanoindentation testing at low indent depths, Mater. Des. 213 (2022) 110317.
[122] A.J.E. Foreman, M.J. Makin, Dislocation movement through random arrays of obstacles, Can. J. Phys. 45 (1967) 511–517.
[123] A.J. Ardell, Precipitation hardening, Metall. Trans. A 16 (1985) 2131–2165.

[124] N. Hansen, B. Ralph, Additive strengthening mechanisms in dispersion hardened polycrystals, Acta Metall. 34 (1986) 1955–1962.
[125] G.R. Odette, G.E. Lucas, Recent progress in understanding reactor pressure vessel embrittlement, Radiat. Eff. Defects Solids 144 (1998) 189–231.
[126] M. Hiratani, V.V. Bulatov, Solid-solution hardening by point-like obstacles of different kinds, Philos. Mag. Lett. 84 (2004) 461–470.
[127] S. Queyreau, G. Monnet, B. Devincre, Orowan strengthening and forest hardening superposition examined by dislocation dynamics simulations, Acta Mater. 58 (2010) 5586–5595.
[128] P. Zhu, Y. Zhao, Y.-R. Lin, J. Henry, S.J. Zinkle, Defect-specific strength factors and superposition model for predicting strengthening of ion irradiated Fe18Cr alloy, J. Nucl. Mater. 588 (2024) 154823.
[129] P. Zhu, Y.-R. Lin, S. Agarwal, V. Pauly, S. Taller, S.J. Zinkle, Comparison of hardening and microstructures of ferritic/martensitic steels irradiated with fast neutrons and dual ions, J. Nucl. Mater. 599 (2024) 155211.
[130] N. Mousseau, L.K. Béland, P. Brommer, J.-F. Joly, F. El-Mellouhi, E. Machado-Charry, M.-C. Marinica, P. Pochet, The activation-relaxation technique: ART Nouveau and Kinetic ART, J. Atom. Mol. Phys. 2012 (1) (2012) 925278. https://doi.org/10.1155/2012/925278
[131] H. Xu, Y.N. Osetsky, R.E. Stoller, Simulating complex atomistic processes: on-the-fly kinetic Monte Carlo scheme with selective active volumes, Phys. Rev. B 84 (2011) 132103. https://doi.org/10.1103/PhysRevB.84.132103
[132] S.I. Golubov, A.V. Barashev, R.E. Stoller, Radiation damage theory, Comprehens. Nucl. Mater. 1 (2012) 357–391.
[133] R.E. Stoller, S.I. Golubov, C. Domain, C.S. Becquart, Mean field rate theory and object kinetic Monte Carlo: a comparison of kinetic models, J. Nucl. Mater. 382 (2) (2008) 77–90. Microstructural Processes in Irradiated Materials, https://www.sciencedirect.com/science/article/pii/S0022311508004480. https://doi.org/10.1016/j.jnucmat.2008.08.047
[134] D.R. Mason, X. Yi, M.A. Kirk, S.L. Dudarev, Elastic trapping of dislocation loops in cascades in ion-irradiated tungsten foils, J. Phys. Condens. Matter 26 (37) (2014) 375701. https://doi.org/10.1088/0953-8984/26/37/375701
[135] D.R. Mason, A.E. Sand, X. Yi, S.L. Dudarev, Direct observation of the spatial distribution of primary cascade damage in tungsten, Acta Mater. 144 (2018) 905–917. https://www.sciencedirect.com/science/article/pii/S1359645417308893. https://doi.org/10.1016/j.actamat.2017.10.031
[136] N. Castin, A. Bakaev, D. Terentyev, M.I. Pascuet, G. Bonny, Understanding why dislocation loops are visible in transmission electron microscopy: the tungsten case, J. Nucl. Mater. 555 (2021) 153122. https://www.sciencedirect.com/science/article/pii/S0022311521003457. https://doi.org/10.1016/j.jnucmat.2021.153122
[137] D.R. Mason, A.E. Sand, S.L. Dudarev, Atomistic-object kinetic Monte Carlo simulations of irradiation damage in tungsten, Modell. Simul. Mater. Sci. Eng. 27 (5) (2019) 055003. https://doi.org/10.1088/1361-651X/ab1a1e
[138] F. Granberg, F. Djurabekova, E. Levo, K. Nordlund, Damage buildup and edge dislocation mobility in equiatomic multicomponent alloys, Nucl. Instrum. Methods Phys. Res. B 393 (2017) 114–117. https://doi.org/10.1016/j.nimb.2016.11.012
[139] F. Granberg, J. Byggmästar, K. Nordlund, Defect accumulation and evolution during prolonged irradiation of Fe and FeCr alloys, J. Nucl. Mater. 528 (2020) 151843. https://www.sciencedirect.com/science/article/pii/S0022311519305719. https://doi.org/10.1016/j.jnucmat.2019.151843
[140] Y. Limoge, A. Rahman, H. Hsieh, S. Yip, Computer simulation studies of radiation induced amorphization, J. Non Cryst. Solids 99 (1) (1988) 75–88. https://doi.org/10.1016/0022-3093(88)90459-0
[141] A. Chartier, M.C. Marinica, Rearrangement of interstitial defects in alpha-Fe under extreme condition, Acta Mater. 180 (2019) 141–148. Publisher: Elsevier Ltd, https://doi.org/10.1016/j.actamat.2019.09.007
[142] A.R. Warwick, M. Boleininger, S.L. Dudarev, Microstructural complexity and dimensional changes in heavily irradiated zirconium, Phys. Rev. Mater. 5 (11) (2021) 113604. Publisher: American Physical Society, https://doi.org/10.1103/PhysRevMaterials.5.113604
[143] M. Boleininger, D.R. Mason, A.E. Sand, S.L. Dudarev, Microstructure of a heavily irradiated metal exposed to a spectrum of atomic recoils, Sci. Rep. 13 (2023) 1684.
[144] E. Mansouri, P. Olsson, Modeling of irradiation-induced microstructure evolution in Fe: impact of frenkel pair distribution, Comput. Mater. Sci 236 (2024) 112852.
[145] E. Mansouri, P. Olsson, Microstructure and magnetization evolution in bcc iron via direct first-principles predictions of radiation effects, Phys. Rev. Mater. 7 (12) (2023) 123604.
[146] E. Mansouri, P. Olsson, First-principles predictions of structural and magnetic phase stability in irradiated α-Fe, Mater. Res. Lett. 12 (7) (2024) 477–483.
[147] D.R. Mason, F. Granberg, M. Boleininger, T. Schwarz-Selinger, K. Nordlund, S.L. Dudarev, Parameter-free quantitative simulation of high-dose microstructure and hydrogen retention in ion-irradiated tungsten, Phys. Rev. Mater. 5 (9) (2021) 095403.
[148] L. Reali, M. Boleininger, D.R. Mason, S.L. Dudarev, Atomistic simulations of athermal irradiation creep and swelling of copper and tungsten in the high dose limit, Acta Mater. 288 (2025) 120814. https://doi.org/10.1016/j.actamat.2025.120814
[149] L. Zepeda-Ruiz, A. Stukowski, T. Oppelstrup, V.V. Bulatov, Probing the limits of metal plasticity with molecular dynamics simulations, Nature 550 (2017) 492–495. https://doi.org/10.1038/nature23472
[150] J. Byggmästar, F. Granberg, A.E. Sand, A. Pirttikoski, R. Alexander, M.C. Marinica, K. Nordlund, Collision cascades overlapping with self-interstitial defect clusters in Fe and W, J. Phys. Condens. Matter 31 (24) (2019) 245402.
[151] T.D. Swinburne, Coarse-graining and forecasting atomic material simulations with descriptors, Phys. Rev. Lett. 131 (2023) 236101. https://doi.org/10.1103/PhysRevLett.131.236101
[152] M.R. Gilbert, J.C. Sublet, Differential dpa calculations with SPECTRA-PKA, J. Nucl. Mater. 504 (2018) 101–108. https://www.sciencedirect.com/science/article/pii/S0022311518302812. https://doi.org/10.1016/j.jnucmat.2018.03.032
[153] A. De Backer, A.E. Sand, K. Nordlund, L. Luneville, D. Simeone, S.L. Dudarev, et al., Subcascade formation and defect cluster size scaling in high-energy collision events in metals, Europhys. Lett. 115 (2) (2016) 26001. https://doi.org/10.1209/0295-5075/115/26001
[154] C.S. Becquart, A. Souidi, C. Domain, M. Hou, L. Malerba, R.E. Stoller, Effect of displacement cascade structure and defect mobility on the growth of point defect clusters under irradiation, J. Nucl. Mater. 351 (1) (2006) 39–46. Proceedings of the Symposium on Microstructural Processes in Irradiated Materials, https://www.sciencedirect.com/science/article/pii/S002231150600064X. https://doi.org/10.1016/j.jnucmat.2006.02.022
[155] A.E. Sand, D.R. Mason, A. De Backer, X. Yi, S.L. Dudarev, K. Nordlund, Cascade fragmentation: deviation from power law in primary radiation damage, Mater. Res. Lett. 5 (5) (2017) 357–363. https://doi.org/10.1080/21663831.2017.1294117
[156] W. Setyawan, G. Nandipati, K.J. Roche, H.L. Heinisch, B.D. Wirth, R.J. Kurtz, Displacement cascades and defects annealing in tungsten, part i: defect database from molecular dynamics simulations, J. Nucl. Mater. 462 (2015) 329–337. https://www.sciencedirect.com/science/article/pii/S0022311514009982. https://doi.org/10.1016/j.jnucmat.2014.12.056
[157] F. Granberg, J. Byggmästar, K. Nordlund, Molecular dynamics simulations of high-dose damage production and defect evolution in tungsten, J. Nucl. Mater. 556 (2021) 153158. https://www.sciencedirect.com/science/article/pii/S0022311521003810. https://doi.org/10.1016/j.jnucmat.2021.153158
[158] D.R. Mason, S. Das, P.M. Derlet, S.L. Dudarev, A.J. London, H. Yu, N.W. Phillips, D. Yang, K. Mizohata, R. Xu, F. Hofmann, Observation of transient and asymptotic driven structural states of tungsten exposed to radiation, Phys. Rev. Lett. 125 (2020) 225503. https://doi.org/10.1103/PhysRevLett.125.225503
[159] M. Boleininger, S.L. Dudarev, D.R. Mason, E. Martínez, Volume of a dislocation network, Phys. Rev. Mater. 6 (2022) 063601. https://doi.org/10.1103/PhysRevMaterials.6.063601
[160] S. Wang, W. Guo, T. Schwarz-Selinger, Y. Yuan, L. Ge, L. Cheng, X. Zhang, X. Cao, E. Fu, G.-H. Lu, Dynamic equilibrium of displacement damage defects in heavy-ion irradiated tungsten, Acta Mater. 244 (2023) 118578. https://www.sciencedirect.com/science/article/pii/S1359645422009533. https://doi.org/10.1016/j.actamat.2022.118578
[161] H. Yu, P. Karamched, S. Das, J. Liu, K. Mizohata, F. Hofmann, New perspectives on collision cascade damage in self-ion irradiated tungsten from HR-EBSD and ECCI, J. Nucl. Mater. 554 (2021) 153074. https://www.sciencedirect.com/science/article/pii/S002231152100297X. https://doi.org/10.1016/j.jnucmat.2021.153074
[162] S.L. Dudarev, M.R. Gilbert, K. Arakawa, H. Mori, Z. Yao, M.L. Jenkins, P.M. Derlet, Langevin model for real-time brownian dynamics of interacting nanodefects in irradiated metals, Phys. Rev. B 81 (2010) 224107. https://doi.org/10.1103/PhysRevB.81.224107
[163] S.L. Dudarev, K. Arakawa, X. Yi, Z. Yao, M.L. Jenkins, M.R. Gilbert, P.M. Derlet, Spatial ordering of nano-dislocation loops in ion-irradiated materials, J. Nucl. Mater. 455 (2014) 16–20. https://doi.org/10.1016/j.jnucmat.2014.02.032
[164] P.-W. Ma, D.R. Mason, S. Van Boxel, S.L. Dudarev, Nanocrystalline tungsten at high radiation exposure, Phys. Rev. Mater. 8 (8) (2024) 083601. Publisher: American Physical Society, https://doi.org/10.1103/PhysRevMaterials.8.083601
[165] L.K. Keys, J.P. Smith, J. Moteff, High-temperature recovery of tungsten after neutron irradiation, Phys. Rev. 176 (1968) 851–856. https://doi.org/10.1103/PhysRev.176.851
[166] C.-C. Fu, J.D. Torre, F. Willaime, J.-L. Bocquet, A. Barbu, Multiscale modelling of defect kinetics in irradiated iron, Nat. Mater. 4 (2005) 68–74. https://doi.org/10.1038/nmat1286
[167] S.L. Dudarev, J.-L. Boutard, R. Lässer, M.J. Caturla, P.M. Derlet, M. Fivel, C.-C. Fu, M.Y. Lavrentiev, L. Malerba, M. Mrovec, D. Nguyen-Manh, K. Nordlund, M. Perlado, R. Schäublin, H.V. Swygenhoven, D. Terentyev, J. Wallenius, D. Weygand, F. Willaime, The EU programme for modelling radiation effects in fusion reactor materials: an overview of recent advances and future goals, J. Nucl. Mater. 386–388 (2009) 1–7. https://doi.org/10.1016/j.jnucmat.2008.12.301
[168] M.W. Thompson, The damage and recovery of neutron irradiated tungsten, Philos. Mag. 5 (1960) 278–296. https://doi.org/10.1080/14786436008235842
[169] J.N. Mundy, S.T. Ockers, L.C. Smedskjaer, Vacancy migration enthalpy in tungsten at high temperatures, Philos. Mag. A 56 (6) (1987) 851–860. https://doi.org/10.1080/01418618708204493
[170] M. Muzyk, D. Nguyen-Manh, K.J. Kurzydłowski, N.L. Baluc, S.L. Dudarev, Phase stability, point defects, and elastic properties of W-V and W-Ta alloys, Phys. Rev. B 84 (2011) 104115. https://doi.org/10.1103/PhysRevB.84.104115
[171] A.D. Brailsford, R. Bullough, The theory of sink strengths, Philos. Trans. R. Soc. Lond. Ser. A Math. Phys. Sci. 302 (1465) (1981) 87–137. https://doi.org/10.1098/rsta.1981.0158
[172] C.H. Woo, B.N. Singh, The concept of production bias and its possible role in defect accumulation under cascade damage conditions, Physica Status Solidi (b) 159 (2) (1990) 609–616. https://doi.org/10.1002/pssb.2221590210
[173] M.J. Caturla, Object kinetic Monte Carlo methods applied to modeling radiation effects in materials, Comput. Mater. Sci. 156 (2019) 452–459. https://www.sciencedirect.com/science/article/pii/S0927025618303318. https://doi.org/10.1016/j.commatsci.2018.05.024
[174] I. Martin-Bragado, A. Rivera, G. Valles, J.L. Gomez-Selles, M.J. Caturla, MMonCa: an object kinetic Monte Carlo simulator for damage irradiation evolution and defect diffusion, Comput. Phys. Commun. 184 (12) (2013) 2703–2710. https://www.sciencedirect.com/science/article/pii/S0010465513002397. https://doi.

org/10.1016/j.cpc.2013.07.011
[175] J. Marian, V.V. Bulatov, Stochastic cluster dynamics method for simulations of multispecies irradiation damage accumulation, J. Nucl. Mater. 415 (1) (2011) 84–95.
[176] A.A. Kohnert, B.D. Wirth, L. Capolungo, Modeling microstructural evolution in irradiated materials with cluster dynamics methods: a review, Comput. Mater. Sci 149 (2018) 442–459. https://www.sciencedirect.com/science/article/pii/S0927025618301381. https://doi.org/10.1016/j.commatsci.2018.02.049
[177] C.A. Hirst, F. Granberg, B. Kombaiah, P. Cao, S. Middlemas, R.S. Kemp, J. Li, K. Nordlund, M.P. Short, Revealing hidden defects through stored energy measurements of radiation damage, Sci. Adv. 8 (31) (2022) eabn2733. https://doi.org/10.1126/sciadv.abn2733
[178] F. Granberg, D.R. Mason, J. Byggmästar, Effect of simulation technique on the high-dose damage in tungsten, Comput. Mater. Sci 217 (2023) 111902. https://www.sciencedirect.com/science/article/pii/S0927025622006139. https://doi.org/10.1016/j.commatsci.2022.111902
[179] C.D. Meyer, Matrix Analysis and Applied Linear Algebra, SIAM: Society for Industrial and Applied Mathematics, 2001.
[180] L.K. Béland, P. Brommer, F. El-Mellouhi, J.-F. m.c. Joly, N. Mousseau, Kinetic activation-relaxation technique, Phys. Rev. E 84 (2011) 046704. https://doi.org/10.1103/PhysRevE.84.046704
[181] J. Wu, J.-P. Balbuena, Z. Hu, V. Jantunen, M.-F. Barthe, M.J. Caturla, F. Granberg, High-dose long-time defect evolution in tungsten studied by atomistically informed object kinetic Monte Carlo simulations, (2024) 15856. https://doi.org/10.48550/arXiv.2409.15856
[182] M. Boleininger, D.R. Mason, T. Schwarz-Selinger, P.-W. Ma, Atomistic simulations of irradiation damage on the engineering timescale: examining the dose rate effect in tungsten, Mater. Adv. 6 (2025) 7379–7394. https://doi.org/10.1039/D5MA00677E
[183] D.R. Mason, M. Boleininger, J. Haley, E. Prestat, G. He, F. Hofmann, S.L. Dudarev, Simulated TEM imaging of a heavily irradiated metal, Acta Mater. 277 (2024) 120162. https://doi.org/10.1016/j.actamat.2024.120162
[184] M.-C. Marinica, F. Willaime, J.-P. Crocombette, Irradiation-induced formation of nanocrystallites with laves phase structure in bcc iron, Phys. Rev. Lett. 108 (2012) 025501.
[185] R. Alexander, M.-C. Marinica, L. Proville, F. Willaime, K. Arakawa, M. Gilbert, S.L. Dudarev, Ab initio scaling laws for the formation energy of nanosized interstitial defect clusters in iron, tungsten, and vanadium, Phys. Rev. B 94 (2016) 024103.
[186] P.-W. Ma, S.L. Dudarev, Universality of point defect structure in body-centered cubic metals, Phys. Rev. Mater. 3 (2019) 013605. https://doi.org/10.1103/PhysRevMaterials.3.013605
[187] P.-W. Ma, S.L. Dudarev, Nonuniversal structure of point defects in face-centered cubic metals, Phys. Rev. Mater. 5 (2021) 013601. https://doi.org/10.1103/PhysRevMaterials.5.013601
[188] A.R. Warwick, P.-W. Ma, S.L. Dudarev, Point defect structures in hexagonal close packed metals and across the periodic table, Phys. Rev. Mater. 252 (2025) 116276.
[189] J. Wu, D.R. Mason, F. Granberg, Atomistic study of irradiation-induced plastic and lattice strain in tungsten 251 (2025) 113738. https://www.sciencedirect.com/science/article/pii/S0927025625000813. https://doi.org/10.1016/j.commatsci.2025.113738
[190] A.R. Warwick, R. Thomas, M. Boleininger, Koç, G. Zilahi, G. Ribárik, Z. Hegedues, U. Lienert, T. Ungar, C. Race, M. Preuss, P. Frankel, S.L. Dudarev, Dislocation density transients and saturation in irradiated zirconium, Int. J. Plast. (2023) 103590. https://www.sciencedirect.com/science/article/pii/S0749641923000761. https://doi.org/10.1016/j.ijplas.2023.103590
[191] J. Marian, T. Hoang, M. Fluss, L.L. Hsiung, A review of helium-hydrogen synergistic effects in radiation damage observed in fusion energy steels and an interaction model to guide future understanding, J. Nucl. Mater. 462 (2015) 409–421.
[192] E. Waikai, Effect of helium production on swelling of F82H irradiated in HFIR, J. Nucl. Mater. 283–287 (2000) 799–805.
[193] F.A. Garner, D.S. Gelles, L.R. Greenwood, T. Okita, N. Sekimura, W.G. Wolfer, Synergistic influence of displacement rate and helium/dpa ratio on swelling of Fe-(9, 12)Cr binary alloys in FFTF at 400 degC, J. Nucl. Mater. 329–333 (2004) 1008–1012.
[194] Y.-R. Lin, A. Bhattacharya, D. Chen, Y. Zhao, J.-J. Kai, J. Henry, S.J. Zinkle, The role of cr concentration and temperature on cavity swelling with co-injected helium in dual-ion irradiated fe and fe-Cr alloys, Materials & Design 223 (2022) 111134.
[195] K. Farrell, M.B. Lewis, N.H. Packan, Simultaneous bombardment with helium, hydrogen, and heavy-ions to simulate microstructural damage from fission or fusion neutrons, Scr. Metall. 12 (12) (1978) 1121–1124.
[196] Y.E. Kupriiyanova, V.V. Bryk, O.V. Borodin, A.S. Kalchenko, V.N. Voyevodin, G.D. Tolstolutskaya, F.A. Garner, Use of double and triple-ion irradiation to study the influence of high levels of helium and hydrogen on void swelling of 8–12% Cr ferritic-martensitic steels, J. Nucl. Mater. 468 (2016) 264–273.
[197] A.M. Monterrosa, Z. Jiao, G.S. Was, The influence of helium on cavity evolution in ion-irradiated T91, J. Nucl. Mater. 509 (2018) 707–721.
[198] O.V. Borodin, V.V. Bryk, A.S. Kalchenko, V.V. Melnichenko, V.N. Voyevodin, F.A. Garner, Synergistic effects of helium and hydrogen on self-ion-induced swelling of austenitic 18Cr10NiTi stainless steel, J. Nucl. Mater. 442 (1, Supplement 1) (2013) S817–S820.
[199] T. Tanaka, K. Oka, S. Ohnuki, S. Yamashita, T. Suda, S. Watanabe, E. Wakai, Synergistic effect of helium and hydrogen for defect evolution under multi-ion irradiation of Fe-Cr ferritic alloys, J. Nucl. Mater. 329–333 (2004) 294–298.
[200] E. Wakai, T. Sawai, K. Furuya, A. Naito, S. Jistukawa, Effect of triple ion beams in ferritic/martensitic steel on swelling behavior, J. Nucl. Mater. 307 (3) (2002) 278–282.
[201] E. Wakai, K. Kikuchi, S. Yamamoto, T. Aruga, M. Ando, H. Tanigawa, T. Taguchi, T. Sawai, K. Oka, S. Ohnuki, Swelling behavior of F82H steel irradiated by triple/dual ion beams, J. Nucl. Mater. 318 (2003) 267–273.
[202] L.N. Clowers, G.S. Was, The effect of hydrogen co-injection on the microstructure of triple ion irradiated F82H, J. Nucl. Mater. 601 (2024) 155331.
[203] L. Malerba, N. Anento, J.P. Balbuena, C.S. Becquart, N. Castin, M.J. Caturla, C. Domain, C. Guerrero, C.J. Ortiz, B. Pannier, A. Serra, Physical mechanisms and parameters for models of microstructure evolution under irradiation in Fe alloys - Part I: pure Fe, Nucl. Mater. Energy 29 (2021) 101069.
[204] C.-C. Fu, F. Willaime, Ab initio study of helium in Fe: dissolution, migration, and clustering with vacancies, Phys. Rev. B 72 (6) (2005) 064117.
[205] E. Hayward, C.C. Fu, Interplay between hydrogen and vacancies in -Fe, Phys. Rev. B 87 (17) (2013) 174103.
[206] S. Echeverri Restrepo, H. Lambert, A.T. Paxton, Effect of hydrogen on vacancy diffusion, Phys. Rev. Mater. 4 (11) (2020) 113601.
[207] D. Terentyev, N. Juslin, Fast three dimensional migration of He clusters in bcc Fe and Fe-Cr alloys, J. Appl. Phys. 105 (2009) 103509.
[208] T. Jourdan, J.P. Crocombette, A variable-gap model for calculating free energies of helium bubbles in metals, J. Nucl. Mater. 418 (1–3) (2011) 98–105.
[209] C. Jiang, Y. Zhang, L.K. Aagesen, A.M. Jokisaari, C. Sun, J. Gan, Noble gas bubbles in bcc metals: Ab initio-based theory and kinetic Monte Carlo modeling, Acta Mater. 213 (2021) 116961.
[210] F. Luo, B. Zhang, Z. Gao, J. Huang, H.-B. Zhou, G.-H. Lu, F. Gao, Y. Wang, C. Wang, Quantitative method to predict the energetics of helium-nanocavities interactions in metal systems based on electrophobic interaction, J. Materiom. 10 (3) (2024) 725–737.
[211] F. Luo, Q. Liu, J. Huang, H. Xiao, Z. Gao, W. Ge, F. Gao, Y. Wang, C. Wang, Effects of lattice strain on hydrogen diffusion, trapping and escape in bcc iron from ab-initio calculations, Int. J. Hydrogen Energy 48 (22) (2023) 8198–8215.
[212] J. Hou, X.-S. Kong, X. Wu, J. Song, C.S. Liu, Predictive model of hydrogen trapping and bubbling in nanovoids in bcc metals, Nat. Mater. 18 (8) (2019) 833–839.
[213] W.T. Geng, L. Wan, J.-P. Du, A. Ishii, N. Ishikawa, H. Kimizuka, S. Ogata, Hydrogen bubble nucleation in -iron, Scr. Mater. 134 (2017) 105–109.
[214] E. Hayward, C. Deo, Energetics of small hydrogen-vacancy clusters in bcc iron, J. Phys. Condens. Matter 23 (42) (2011) 425402.
[215] F. Luo, J. Huang, Q. Liu, Z. Gao, W. Ge, F. Gao, Y. Wang, C. Wang, Dynamic investigations on hydrogen-helium interaction around the vacancy in BCC iron from ab-initio calculations, Nucl. Fusion 63 (4) (2023) 046005.
[216] C.J. Ortiz, R. Vila, Ab initio study of helium and hydrogen interactions in -Fe, arXiv preprint arXiv:1205.6374 (2012).
[217] E. Hayward, C. Deo, Synergistic effects in hydrogen-helium bubbles, J. Phys. Condens. Matter 24 (2012) 265402.
[218] N. Castin, D. Terentyev, A. Bakaev, A. Stankovskiy, G. Bonny, On the equivalence of irradiation conditions on present and future facilities for fusion materials research and qualification: a computational study, J. Nucl. Mater. 562 (2022) 153589.
[219] D. Brimbal, L. Fournier, A. Barbu, Cluster dynamics modeling of the effect of high dose irradiation and helium on the microstructure of austenitic stainless steels, J. Nucl. Mater. 468 (2016) 124–139.
[220] A.P. Thompson, H.M. Aktulga, R. Berger, D.S. Bolintineanu, W.M. Brown, P.S. Crozier, P.J. i.t. Veld, A. Kohlmeyer, S.G. Moore, T.D. Nguyen, R. Shan, M.J. Stevens, J. Tranchida, C. Trott, S.J. Plimpton, LAMMPS - a flexible simulation tool for particle-based materials modeling at the atomic, meso, and continuum scales, Comp. Phys. Comm. 271 (2022) 108171. https://doi.org/10.1016/j.cpc.2021.108171
[221] A.P. Bartók, R. Kondor, G. Csányi, On representing chemical environments, Phys. Rev. B 87 (18) (2013) 184115. https://doi.org/10.1103/PhysRevB.87.184115
[222] W.J. Szlachta, A.P. Bartók, G. Csányi, Accuracy and transferability of Gaussian approximation potential models for tungsten, Phys. Rev. B 90 (10) (2014) 104108. https://doi.org/10.1103/PhysRevB.90.104108
[223] D. Dragoni, T.D. Daff, G. Csányi, N. Marzari, Achieving DFT accuracy with a machine-learning interatomic potential: thermomechanics and defects in bcc ferromagnetic iron, Phys. Rev. Mater. 2 (1) (2018) 013808. https://doi.org/10.1103/PhysRevMaterials.2.013808
[224] A.P. Thompson, L.P. Swiler, C.R. Trott, S.M. Foiles, G.J. Tucker, Spectral neighbor analysis method for automated generation of quantum-accurate interatomic potentials, J. Comput. Phys. 285 (2015) 316–330. https://doi.org/10.1016/j.jcp.2014.12.018
[225] C. Chen, Z. Deng, R. Tran, H. Tang, I.-H. Chu, S.P. Ong, Accurate force field for molybdenum by machine learning large materials data, Phys. Rev. Mater. 1 (4) (2017) 043603. https://doi.org/10.1103/PhysRevMaterials.1.043603
[226] X.-G. Li, C. Hu, C. Chen, Z. Deng, J. Luo, S.P. Ong, Quantum-accurate spectral neighbor analysis potential models for Ni-Mo binary alloys and fcc metals, Phys. Rev. B 98 (9) (2018) 094104. https://doi.org/10.1103/PhysRevB.98.094104
[227] Z. Deng, C. Chen, X.-G. Li, S.P. Ong, An electrostatic spectral neighbor analysis potential for lithium nitride, npj Comput. Mater. 5 (1) (2019) 75. https://doi.org/10.1038/s41524-019-0212-1
[228] A.V. Shapeev, Moment tensor potentials: a class of systematically improvable interatomic potentials, Multiscale Model. Simul. 14 (3) (2016) 1153–1173. https://doi.org/10.1137/15M1054183
[229] E.V. Podryabinkin, A.V. Shapeev, Active learning of linearly parametrized interatomic potentials, Comput. Mater. Sci. 140 (2017) 171–180. https://doi.org/10.1016/j.commatsci.2017.08.031
[230] K. Gubaev, E.V. Podryabinkin, G.L.W. Hart, A.V. Shapeev, Accelerating high-throughput searches for new alloys with active learning of interatomic potentials, Comput. Mater. Sci. 156 (2019) 148–156. https://doi.org/10.1016/j.commatsci.

2018.09.031
[231] I.S. Novikov, K. Gubaev, E.V. Podryabinkin, A.V. Shapeev, The MLIP package: moment tensor potentials with MPI and active learning, Mach. Learn. Sci. Technol. 2 (2) (2021) 025002. https://doi.org/10.1088/2632-2153/abc9fe
[232] N. Artrith, A. Urban, An implementation of artificial neural-network potentials for atomistic materials simulations: performance for TiO_2, Comp. Mater. Sci. 114 (2016) 135–150. https://doi.org/10.1016/j.commatsci.2015.11.047
[233] N. Artrith, A. Urban, G. Ceder, Efficient and accurate machine-learning interpolation of atomic energies in compositions with many species, Phys. Rev. B 96 (1) (2017) 014112. https://doi.org/10.1103/PhysRevB.96.014112
[234] A.M. Cooper, J. Kästner, A. Urban, N. Artrith, Efficient training of ANN potentials by including atomic forces via Taylor expansion and application to water and a transition-metal oxide, npj Comput. Mater. 6 (1) (2020) 54. https://doi.org/10.1038/s41524-020-0323-8
[235] M.S. Chen, T. Morawietz, H. Mori, T.E. Markland, N. Artrith, AENET-LAMMPS and AENET-TINKER: interfaces for accurate and efficient molecular dynamics simulations with machine learning potentials, J. Chem. Phys. 155 (7) (2021) 074801. https://doi.org/10.1063/5.0063880
[236] H. Wang, L. Zhang, J. Han, W. E, DeePMD-kit: a deep learning package for many-body potential energy representation and molecular dynamics, Comput. Phys. Commun. 228 (2018) 178–184. https://doi.org/10.1016/j.cpc.2018.03.016
[237] L. Zhang, J. Han, H. Wang, W. Saidi, R. Car, W. E, End-to-end symmetry preserving inter-atomic potential energy model for finite and extended systems, in: S. Bengio, H. Wallach, H. Larochelle, K. Grauman, N. Cesa-Bianchi, R. Garnett (Eds.), Advances in Neural Information Processing Systems, 31, Curran Associates, Inc., 2018, pp. 4436–4446.
[238] J. Han, L. Zhang, R. Car, W. E, Deep potential: a general representation of a many-body potential energy surface, Commun. Comput. Phys. 23 (3) (2018). https://doi.org/10.4208/cicp.oa-2017-0213
[239] L. Zhang, J. Han, H. Wang, R. Car, W. E, Deep potential molecular dynamics: a scalable model with the accuracy of quantum mechanics, Phys. Rev. Lett. 120 (14) (2018) 143001. https://doi.org/10.1103/PhysRevLett.120.143001
[240] T. Wen, L. Zhang, H. Wang, W. E, D.J. Srolovitz, Deep potentials for materials science, Mater. Fut. 1 (2) (2022) 022601. https://doi.org/10.1088/2752-5724/ac681d
[241] K.C. Pitike, W. Setyawan, Accurate Fe-He machine learning potential for studying He effects in BCC-Fe, J. Nucl. Mater. 574 (2023) 154183. https://doi.org/10.1016/j.jnucmat.2022.154183
[242] L. Reali, M. Boleininger, M.R. Gilbert, S.L. Dudarev, Macroscopic elastic stress and strain produced by irradiation, Nucl. Fusion 62 (1) (2022) 016002.
[243] D. Sobieraj, J.S. Wróbel, T. Rygier, K.J. Kurzydłowski, O. El Atwani, A. Devaraj, E. Martinez, D. Nguyen-Manh, Chemical short-range order in derivative Cr-Ta-Ti-V-W high entropy alloys from the first-principles thermodynamic study, Phys. Chem. Chem. Phys. 22 (2020) 23929. https://doi.org/10.1039/d0cp03764h
[244] L. Tan, K. Ali, P.S. Ghosh, A. Arya, Y. Zhou, R. Smith, P. Goddard, D. Patel, H. Shahmir, A. Gandy, Design principles of low-activation high entropy alloys, J. Alloys Compd. 907 (2022) 164526. https://doi.org/10.1016/j.jallcom.2022.164526
[245] J.S. Wróbel, A. Zhong, A.M. Goryaeva, D. Nguyen-Manh, A.E. Poisvert, M. Athènes, M.C. Marinica, Data-driven prediction of thermoelastic and defect properties of Ti-V-Ta-W high-entropy alloys up to the melting point, Physical Review B 112 (2025) 224110. https://doi.org/10.1103/6xkw-m6s3
[246] R.P. Feynman, A.R. Hibbs, Quantum Mechanics and Path Integrals, McGraw-Hill College, 1965. https://doi.org/10.1093/acprof:oso/9780198749349.003.0013
[247] D. Chandler, P.G. Wolynes, Exploiting the isomorphism between quantum theory and classical statistical mechanics of polyatomic fluids, J. Chem. Phys. 74 (7) (1981) 4078–4095. https://doi.org/10.1063/1.441588
[248] A.P. Thompson, H.M. Aktulga, R. Berger, D.S. Bolintineanu, W.M. Brown, P.S. Crozier, P.J. in 't Veld, A. Kohlmeyer, S.G. Moore, T.D. Nguyen, R. Shan, M.J. Stevens, J. Tranchida, C. Trott, S.J. Plimpton, LAMMPS - a flexible simulation tool for particle-based materials modeling at the atomic, meso, and continuum scales, Comput. Phys. Commun. 271 (February) (2022) 108171. https://linkinghub.elsevier.com/retrieve/pii/S0010465521002836. https://doi.org/10.1016/j.cpc.2021.108171
[249] M. Shiga, M. Tachikawa, S. Miura, A unified scheme for ab initio molecular orbital theory and path integral molecular dynamics, J. Chem. Phys. 115 (20) (2001) 9149–9159. https://doi.org/10.1063/1.1407289
[250] I.R. Craig, D.E. Manolopoulos, Quantum statistics and classical mechanics: real time correlation functions from ring polymer molecular dynamics, J. Chem. Phys. 121 (8) (2004) 3368–3373. https://doi.org/10.1063/1.1777575
[251] J. Cao, G.A. Voth, The formulation of quantum statistical mechanics based on the feynman path centroid density. II. dynamical properties, J. Chem. Phys. 100 (7) (1994) 5106–5117. https://pubs.aip.org/jcp/article/100/7/5106/482720/The-formulation-of-quantum-statistical-mechanics. https://doi.org/10.1063/1.467176
[252] M.J. Gillan, Quantum simulation of hydrogen in metals, Phys. Rev. Lett. 58 (6) (1987) 563–566. https://doi.org/10.1103/PhysRevLett.58.563
[253] H. Kimizuka, B. Thomsen, M. Shiga, Artificial neural network-based path integral simulations of hydrogen isotope diffusion in palladium, J. Phys. Energy 4 (3) (2022) 034004. https://doi.org/10.1088/2515-7655/ac7e6b
[254] H. Kwon, M. Shiga, H. Kimizuka, T. Oda, Accurate description of hydrogen diffusivity in bcc metals using machine-learning moment tensor potentials and path-integral methods, Acta Mater. 247 (February) (2023) 118739. https://doi.org/10.1016/j.actamat.2023.118739
[255] A.V. Shapeev, Moment tensor potentials: a class of systematically improvable interatomic potentials, Multiscale Model. Simul. 14 (3) (2016) 1153–1173. https://doi.org/10.1137/15M1054183
[256] J. Behler, M. Parrinello, Generalized neural-network representation of high-dimensional potential-Energy surfaces, Phys. Rev. Lett. 98 (14) (2007) 146401. https://doi.org/10.1103/PhysRevLett.98.146401
[257] S. Park, T. Oda, Efficient calculations of impurity diffusivity in metals by linearized multi-band embedded atom method potentials, Phys. Chem. Chem. Phys. 27 (25) (2025) 13390–13402. https://doi.org/10.1039/D5CP01224D
[258] H. Kimizuka, S. Ogata, M. Shiga, Unraveling anomalous isotope effect on hydrogen diffusivities in fcc metals from first principles including nuclear quantum effects, Phys. Rev. B 100 (2) (2019) 024104. https://doi.org/10.1103/PhysRevB.100.024104
[259] K. Kiuchi, R.B. McLellan, The solubility and diffusivity of hydrogen in well-annealed and deformed iron, Acta Metall. 31 (7) (1983) 961–984. https://doi.org/10.1016/0001-6160(83)90192-X
[260] K. Heinola, T. Ahlgren, Diffusion of hydrogen in bcc tungsten studied with first principle calculations, J. Appl. Phys. 107 (11) (2010) 113531. https://doi.org/10.1063/1.3386515
[261] T. Oda, Thermodynamic model for grain boundary effects on hydrogen solubility, diffusivity and permeability in poly-crystalline tungsten, Fusion Eng. Des. 112 (2016) 102–116. https://doi.org/10.1016/j.fusengdes.2016.08.001
[262] T. Oda, D. Zhu, Y. Watanabe, Kinetic Monte Carlo simulation on influence of vacancy on hydrogen diffusivity in tungsten, J. Nucl. Mater. 467 (2015) 439–447. https://linkinghub.elsevier.com/retrieve/pii/S0022311515301409. https://doi.org/10.1016/j.jnucmat.2015.07.054
[263] D.R. Mason, D. Nguyen-Manh, V.W. Lindblad, F.G. Granberg, M.Y. Lavrentiev, An empirical potential for simulating hydrogen isotope retention in highly irradiated tungsten, J. Phys. Condens. Matter 35 (49) (2023) 495901. https://link.aps.org/doi/10.1103/PhysRevMaterials.7.093601. arXiv:2305.10814https://doi.org/10.1088/1361-648X/acf25f
[264] X.Y. Wang, Y.N. Wang, K. Xu, F.Z. Dai, H.F. Liu, G.H. Lu, H. Wang, Deep neural network potential for simulating hydrogen blistering in tungsten, Phys. Rev. Mater. 7 (9) (2023) 1–20. https://doi.org/10.1103/PhysRevMaterials.7.093601
[265] K. Xu, S. Jin, G.-H. Lu, Predicting hydrogen segregation energy distributions in strained regions of tungsten using artificial neural network, Nucl. Mater. Energy 39 (9) (2024) 101637. https://linkinghub.elsevier.com/retrieve/pii/S2352179124000607. https://doi.org/10.1016/j.nme.2024.101637
[266] S. Yang, S. Kim, T. Oda, Sticking, reflection, and abstraction behavior of hydrogen irradiated on (110) tungsten surfaces at 0.1–100 eV by molecular dynamics simulations using a machine learning potential, Acta Mater. (2025) 121306. https://doi.org/10.1016/j.actamat.2025.121306
[267] Y. Liu, X. He, Y. Mo, Discrepancies and error evaluation metrics for machine learning interatomic potentials, npj Comput. Mater. 9 (1) (2023) 174. arXiv:2306.11639https://doi.org/10.1038/s41524-023-01123-3
[268] D. Torsello, D. Gambino, L. Gozzelino, A. Trotta, F. Laviano, Expected radiation environment and damage for YBCO tapes in compact fusion reactors, Supercond. Sci. Technol. 36 (1) (2022) 014003. https://doi.org/10.1088/1361-6668/aca369
[269] B. Mundet, S.T. Hartman, R. Guzman, J.C. Idrobo, X. Obradors, T. Puig, R. Mishra, J. Gázquez, Local strain-driven migration of oxygen vacancies to apical sites in YBa2Cu3O7x, Nanoscale 12 (2020) 5922–5931. https://doi.org/10.1039/D0NR00666A
[270] S.T. Murphy, A point defect model for YBa2Cu3O7 from density functional theory, J. Phys. Commun. 4 (11) (2020) 115003. https://doi.org/10.1088/2399-6528/abc9a7
[271] G. Liu, Y. Shang, B. Jia, X. Guan, L. Han, X. Zhang, H. Song, P. Lu, First-principles calculation of the optical properties of the YBa2Cu3O7-δ oxygen vacancies model, RSC Adv. 13 (2023) 18927–18933. https://doi.org/10.1039/D3RA01921G
[272] A. Umezawa, G.W. Crabtree, J.Z. Liu, H.W. Weber, W.K. Kwok, L.H. Nunez, T.J. Moran, C.H. Sowers, H. Claus, Enhanced critical magnetization currents due to fast neutron irradiation in single-crystal $YBa_2Cu_3O_{7-\delta}$, Phys. Rev. B 36 (13) (1987) 7151.
[273] F.M. Sauerzopf, H.P. Wiesinger, W. Kritscha, H.W. Weber, G.W. Crabtree, J.Z. Liu, Neutron-irradiation effects on critical current densities in single-crystalline $YBa_2Cu_3O_{7-\delta}$, Phys. Rev. B 43 (4) (1991) 3091.
[274] F.M. Sauerzopf, H.P. Wiesinger, W. Kritscha, H.W. Weber, M.C. Frischherz, H. Gerstenberg, Fast neutron irradiation and flux pinning in single crystalline high temperature superconductors, Cryogenics 33 (1) (1993) 8–13.
[275] F.M. Sauerzopf, H.P. Wiesinger, H.W. Weber, G.W. Crabtree, Analysis of pinning effects in $YBa_2Cu_3O_{7-\delta}$ single crystals after fast neutron irradiation, Phys. Rev. B 51 (9) (1995) 6002.
[276] M. Eisterer, R. Fuger, M. Chudy, F. Hengstberger, H.W. Weber, Neutron irradiation of coated conductors, Supercond. Sci. Technol. 23 (1) (2009) 014009.
[277] R. Prokopec, D.X. Fischer, H.W. Weber, M. Eisterer, Suitability of coated conductors for fusion magnets in view of their radiation response, Supercond. Sci. Technol. 28 (1) (2014) 014005.
[278] D.X. Fischer, R. Prokopec, J. Emhofer, M. Eisterer, The effect of fast neutron irradiation on the superconducting properties of REBCO coated conductors with and without artificial pinning centers, Supercond. Sci. Technol. 31 (4) (2018) 044006.
[279] S.L. Chaplot, Interatomic potential, phonon spectrum, and molecular-dynamics simulation up to 1300 K in $YBa_2Cu_3O_{7-\delta}$, Phys. Rev. B 42 (1990) 2149–2154. https://doi.org/10.1103/PhysRevB.42.2149
[280] R.C. Baetzold, Atomistic simulation of ionic and electronic defects in $YBa_2Cu_3O_7$, Phys. Rev. B 38 (1988) 11304–11312. https://doi.org/10.1103/PhysRevB.38.11304
[281] F.Z. Cui, J. Xie, H.D. Li, Preferential radiation damage of the oxygen sublattice in $YBa_2Cu_3O_7$: a molecular-dynamics simulation, Phys. Rev. B 46 (1992) 11182–11185. https://doi.org/10.1103/PhysRevB.46.11182

[282] Y. Zheng, J. Zheng, X. Wang, Y. Lu, D. Wang, Study of high-temperature superconducting material radiation damage based on molecular dynamics under uniaxial strain, Supercond. Sci. Technol. 38 (5) (2025) 055001. https://doi.org/10.1088/1361-6668/adc8e0

[283] R.L. Gray, M.J.D. Rushton, S.T. Murphy, Molecular dynamics simulations of radiation damage in YBa2Cu3O7, Supercond. Sci. Technol. 35 (3) (2022) 035010. https://doi.org/10.1088/1361-6668/ac47dc

[284] R.J. Nicholls, S. Diaz-Moreno, W. Iliffe, Y. Linden, T. Mousavi, M. Aramini, M. Danaie, C.R.M. Grovenor, S.C. Speller, Understanding irradiation damage in high-temperature superconductors for fusion reactors using high resolution X-ray absorption spectroscopy, Commun. Mater. 3 (1) (2022) 52. https://doi.org/10.1038/s43246-022-00272-0

[285] W. Iliffe, N. Peng, G. Brittles, R. Bateman, R. Webb, C. Grovenor, S. Speller, In-situ measurements of the effect of radiation damage on the superconducting properties of coated conductors, Supercond. Sci. Technol. 34 (9) (2021) 09LT01. https://doi.org/10.1088/1361-6668/ac1523

[286] A.M. Stoneham, L.W. Smith, Defect phenomena in superconducting oxides and analogous ceramic oxides, J. Phys. Condens. Matter 3 (3) (1991) 225. https://doi.org/10.1088/0953-8984/3/3/001

[287] A. Yamaji, S. Maeno, M. Tomizawa, M. Arai, T. Adachi, Oxygen-ion diffusion in YBa2Cu3O7 ceramics, Physica C 335 (1) (2000) 264–267. https://doi.org/10.1016/S0921-4534(00)00181-7

[288] M. D. Vázquez-Navarro, A. Kursumovic, J. E. Evetts, Study and modelling of oxygen diffusion in YBa2Cu3O7- under isothermal conditions, Supercond. Sci. Technol. 12 (12) (1999) 1117. https://doi.org/10.1088/0953-2048/12/12/320

[289] X. Zhang, C.R.A. Catlow, Molecular-dynamics study of oxygen diffusion in $YBa_2Cu_3O_{6.91}$, Phys. Rev. B 46 (1992) 457–462. https://doi.org/10.1103/PhysRevB.46.457

[290] D. Torsello, G. Celentano, L. Civale, V. Corato, M. Eisterer, D. Gambino, S. Murphy, S. Speller, F. Laviano, Roadmap for the investigation of irradiation effects in HTS for fusion, Supercond. Sci. Technol. 38 (5) (2025) 053501. https://doi.org/10.1088/1361-6668/adce40

[291] M.M.G. Alemany, J. Souto-Casares, L.E. González, D.J. González, Static structure, collective dynamics and transport coefficients in the liquid Li-Pb alloy. an ab initio molecular dynamics study, J. Mol. Liq. 344 (2021) 117775. https://www.sciencedirect.com/science/article/pii/S0167732221025009. https://doi.org/10.1016/j.molliq.2021.117775

[292] A.S. Al-Awad, L. Batet, L. Sedano, Parametrization of embedded-atom method potential for liquid lithium and lead-lithium eutectic alloy, J. Nucl. Mater. 587 (2023) 154735. https://www.sciencedirect.com/science/article/pii/S0022311523005020. https://doi.org/10.1016/j.jnucmat.2023.154735

[293] E. Álvarez Galera, D. Laria, F. Mazzanti, L. Batet, J. Martí, Henry's constant of helium in liquid lead-lithium alloys, J. Mol. Liq. 432 (2025) 127719. https://www.sciencedirect.com/science/article/pii/S0167732225008955. https://doi.org/10.1016/j.molliq.2025.127719

[294] A. Fraile, T. Polcar, Volume and pressure of helium bubbles inside liquid Pb16Li. a molecular dynamics study, Nucl. Fusion 60 (4) (2020) 046018. https://doi.org/10.1088/1741-4326/ab73c2

[295] H. Wang, B. Yue, L. Yan, T. Jiang, S. Peng, First-principles molecular dynamics study of the behavior of tritium in molten LiF-BeF2 eutectic, J. Mol. Liq. 345 (2022) 117027. https://doi.org/10.1016/j.molliq.2021.117027

[296] S.T. Lam, Q.-J. Li, R. Ballinger, C. Forsberg, J. Li, Modeling LiF and FLiBe molten salts with robust neural network interatomic potential, ACS Appl. Mater. Interf. 13 (21) (2021) 24582–24592. https://doi.org/10.1021/acsami.1c00604

[297] G. Zhou, F.A. Hernández, P. Pereslavtsev, B. Kiss, A. Retheesh, L. Maqueda, J.H. Park, The European DEMO helium cooled pebble bed breeding blanket: design status at the conclusion of the pre-concept design phase, Energies 16 (14) (2023). https://doi.org/10.3390/en16145377

[298] K.N. Goswami, S.T. Murphy, Influence of lithium vacancy defects on tritium diffusion in β-Li2TiO3, J. Phys. Chem. C 124 (23) (2020) 12286–12294. https://doi.org/10.1021/acs.jpcc.0c02551

[299] N. Kuganathan, A. Kordatos, M.E. Fitzpatrick, R.V. Vovk, A. Chroneos, Defect process and lithium diffusion in Li2TiO3, Solid State Ionics 327 (2018) 93–98. https://www.sciencedirect.com/science/article/pii/S0167273818307185. https://doi.org/10.1016/j.ssi.2018.10.030

[300] Y.-L. Lee, J. Holber, H.P. Paudel, D.C. Sorescu, D.J. Senor, Y. Duan, Density functional theory study of the point defect energetics in γ-LiAlO2, Li2ZrO3 and Li2TiO3 materials, J. Nucl. Mater. 511 (2018) 375–389. Special Section on "18th International Conference on Fusion Reactor Materials", https://www.sciencedirect.com/science/article/pii/S0022311518308870. https://doi.org/10.1016/j.jnucmat.2018.09.030

[301] S.T. Murphy, N.D.M. Hine, Point defects and non-stoichiometry in Li2TiO3, Chem. Mater. 26 (4) (2014) 1629–1638. https://doi.org/10.1021/cm4038473

[302] X. Xiang, W. Zhu, T. Lu, T. Gao, Y. Shi, M. Yang, Y. Gong, X. Yu, L. Feng, Y. Wei, Z. Lu, Density functional theory calculations of point defects and hydrogen isotopes in Li4SiO4, AIP Adv. 5 (10) (2015) 107136. https://pubs.aip.org/aip/adv/article-pdf/doi/10.1063/1.4934935/12985799/107136_1_online.pdfhttps://doi.org/10.1063/1.4934935

[303] A.W. Davies, W.D. Neilson, R.T. Bedford, S.T. Murphy, High-Temperature intrinsic defect chemistry of Li8PbO6 ceramic breeding material, J. Phys. Chem. C 127 (45) (2023) 22265–22276. https://doi.org/10.1021/acs.jpcc.3c04186

[304] N. Kuganathan, J. Dark, E.N. Sgourou, Y. Panayiotatos, A. Chroneos, Atomistic simulations of the defect chemistry and self-diffusion of Li-ion in LiAlO2, Energies 12 (15) (2019). https://doi.org/10.3390/en12152895

[305] K.A. Rex, P. Iyngaran, N. Kuganathan, A. Chroneos, Defect properties and lithium incorporation in Li2ZrO3, Energies 14 (13) (2021). https://doi.org/10.3390/en14133963

[306] F.A. Kröger, H.J. Vink, Relations between the Concentrations of Imperfections in Crystalline Solids, 3 of *Solid State Physics*, Academic Press, 1956, pp. 307–435. https://doi.org/10.1016/S0081-1947(08)60135-6

[307] M. Sanjeev, M.R. Gilbert, S.T. Murphy, Thermal conductivity of non-stoichiometric Li2TiO3, J. Nucl. Mater. 572 (2022) 154037. https://www.sciencedirect.com/science/article/pii/S0022311522005220. https://doi.org/10.1016/j.jnucmat.2022.154037

[308] Ģ. Vītiņš, G. Ķizāne, A. Lūsis, J. Tīliks, Electrical conductivity studies in the system Li2TiO3-Li1.33Ti1.67O4, J. Solid State Electrochem. 6 (5) (2002) 311–319. https://doi.org/10.1007/s100080100239

[309] C.-L. Yu, D.-P. Gao, K. Yanagisawa, Vacancy and substitution defects of -Li2TiO3 prepared by hydrothermal method, Chem. Lett. 43 (3) (2013) 369–370. https://academic.oup.com/chemlett/article-pdf/43/3/369/55635977/cl.130951.pdfhttps://doi.org/10.1246/cl.130951

[310] L. Padilla-Campos, A theoretical investigation of occupation sites for tritium atoms in lithium titanate, J. Mol. Struct. THEOCHEM 621 (1) (2003) 107–112. 2001 Quitel S.I., https://www.sciencedirect.com/science/article/pii/S0166128002005389. https://doi.org/10.1016/S0166-1280(02)00538-9

[311] L. Padilla-Campos, Theoretical study of two possible occupation sites for tritium atoms in lithium titanate, J. Mol. Struct. THEOCHEM 580 (1) (2002) 101–105. https://doi.org/10.1016/S0166-1280(01)00600-5

[312] S.T. Murphy, Tritium solubility in Li2TiO3 from first-principles simulations, J. Phys. Chem. C 118 (51) (2014) 29525–29532. https://doi.org/10.1021/jp508875y

[313] A.W. Davies, S.T. Murphy, Tritium accommodation and diffusion in Li8PbO6 from first-principles simulations, J. Phys. Chem. C 129 (4) (2025) 2274–2287. https://doi.org/10.1021/acs.jpcc.4c08016

[314] Y. Shi, T. Lu, T. Gao, X. Xiang, Y. Gong, M. Yang, L. Feng, H. Wang, C. Dang, First principle study of tritium trapping at oxygen vacancies in Li4SiO4, J. Nucl. Mater. 508 (2018) 257–264. https://www.sciencedirect.com/science/article/pii/S002231151731365X. https://doi.org/10.1016/j.jnucmat.2018.05.055

[315] Y. Shi, T. Lu, T. Gao, X. Xiang, Q. Zhang, X. Yu, Y. Gong, M. Yang, Density functional study of lithium vacancy in Li4SiO4: trapping of tritium and helium, J. Nucl. Mater. 467 (2015) 519–526. https://www.sciencedirect.com/science/article/pii/S0022311515302063. https://doi.org/10.1016/j.jnucmat.2015.09.017

[316] Y. Shi, J. Qi, Y. Han, T. Lu, Anisotropic diffusion of a charged tritium interstitial in Li_2TiO_3 from first-principles calculations, Phys. Rev. Appl. 10 (2018) 024021. https://doi.org/10.1103/PhysRevApplied.10.024021

[317] Z. Lu, Y. Shi, X. Wang, H. Guo, J. Qi, T. Lu, Diffusion of a tritium interstitial in Li4TiO4 from first-principles calculations, Ceram. Int. 48 (22) (2022) 33474–33484. https://www.sciencedirect.com/science/article/pii/S0272884222027110. https://doi.org/10.1016/j.ceramint.2022.07.293

[318] Z. Lu, Y. Shi, G. Wang, X. Wang, C. Zhang, J. Qi, T. Lu, The diffusion and desorption of tritium on Li2TiO3 (-133) surface from first-principles calculations, J. Nucl. Mater. 603 (2025) 155373. https://www.sciencedirect.com/science/article/pii/S0022311524004744. https://doi.org/10.1016/j.jnucmat.2024.155373

[319] S.T. Murphy, Mechanisms of helium accommodation in lithium metatitanate, Fusion Eng. Des. 101 (2015) 94–100. https://www.sciencedirect.com/science/article/pii/S0920379615302945. https://doi.org/10.1016/j.fusengdes.2015.10.007

[320] L. Zhou, W. Deng, Y. Li, A DFT + U study on diffusion and aggregation behavior of he atoms in Li2TiO3, Comput. Mater. Sci 227 (2023) 112296. https://doi.org/10.1016/j.commatsci.2023.112296

[321] L. Zhou, L. He, D. Yang, Y. Li, He atoms diffusion and aggregation in Li2TiO3: a molecular dynamics study, Nucl. Eng. Des. 413 (2023) 112567. https://doi.org/10.1016/j.nucengdes.2023.112567

[322] S. Kajita, A.M. Ito, K. Ibano, Growth of fiberform nanostructures on metal surfaces by helium plasma irradiation, J. Appl. Phys. 132 (18) (2022). https://doi.org/10.1063/5.0123430

[323] K. Heinola, F. Djurabekova, T. Ahlgren, On the stability and mobility of di-vacancies in tungsten, Nucl. Fusion 58 (2) (2017) 026004.

[324] J. Hou, Y.-W. You, X.-S. Kong, J. Song, C.S. Liu, Accurate prediction of vacancy cluster structures and energetics in bcc transition metals, Acta Mater. 211 (2021) 116860.

[325] C. Song, J. Hou, X.-S. Kong, L. Chen, S. Wang, C.S. Liu, Structures and energetics of multiple helium atoms in a tungsten monovacancy, J. Nucl. Mater. 561 (2022) 153577.

[326] J. Wang, Q. Hou, B.L. Zhang, Migration behavior of self-interstitial defects in tungsten and iron, Solid State Commun. 325 (2021) 114158.

[327] W. Setyawan, G. Nandipati, R.J. Kurtz, Ab initio study of interstitial cluster interaction with Re, Os, and Ta in W, J. Nucl. Mater. 484 (2017) 30–41.

[328] F.-F. Ma, P.-W. Hou, Z.-Z. Li, Y.-H. Li, Y.-Z. Niu, H.-Z. Ma, Q.-Y. Ren, F. Gao, G.-H. Lu, H.-B. Zhou, Collaborative motion of helium and self-interstitial atoms enhanced self-healing efficiency of irradiation-induced defects in tungsten, Nucl. Fusion 61 (10) (2021) 106017.

[329] A. Bakaev, G. Bonny, N. Castin, D. Terentyev, V.A. Bakaev, Impact of interstitial impurities on the trapping of dislocation loops in tungsten, Sci. Rep. 11 (1) (2021) 12333.

[330] A. Fellman, A.E. Sand, J. Byggmästar, K. Nordlund, Radiation damage in tungsten from cascade overlap with voids and vacancy clusters, J. Phys. Condens. Matter 31 (40) (2019) 405402.

[331] W. Setyawan, G. Nandipati, K.J. Roche, H.L. Heinisch, B.D. Wirth, R.J. Kurtz, Displacement cascades and defects annealing in tungsten, part i: defect database from molecular dynamics simulations, J. Nucl. Mater. 462 (2015) 329–337.

[332] J. Fu, Y. Chen, J. Fang, N. Gao, W. Hu, C. Jiang, H.-B. Zhou, G.-H. Lu, F. Gao, H. Deng, Molecular dynamics simulations of high-energy radiation damage in W and W–Re alloys, J. Nucl. Mater. 524 (2019) 9–20.

[333] Y. Shin, K. Kang, B. Lee, Temperature-dependent electron–phonon coupling changes the damage cascades in neutron-irradiation molecular dynamics simulation in W, Nucl. Fusion 64 (10) (2024) 106001.
[334] L. Liu, R. Qiu, Y. Chen, M. Jiang, N. Gao, B. Huang, F. Gao, W. Hu, H. Deng, Displacement cascades database from molecular dynamics simulations in tungsten, J. Nucl. Mater. 580 (2023) 154415.
[335] L. Liu, N. Gao, Y. Chen, R. Qiu, W. Hu, F. Gao, H. Deng, Formation mechanism of ⟨111⟩ interstitial dislocation loops from irradiation-induced C15 clusters in tungsten, Phys. Rev. Mater. 5 (9) (2021) 093605.
[336] S. Huang, J. Marian, Rates of diffusion controlled reactions for one-dimensionally-moving species in 3D space, Philos. Mag. 99 (20) (2019) 2562–2583.
[337] H.-Z. Ma, Y.-H. Li, Y.-Z. Niu, D. Terentyev, Z. Yang, H.-B. Zhou, G.-H. Lu, Initial microstructure and temperature dependence of irradiation defects evolution in tungsten, J. Nucl. Mater. 591 (2024) 154932.
[338] N. Castin, G. Bonny, A. Bakaev, C.J. Ortiz, A.E. Sand, D. Terentyev, Object kinetic Monte Carlo model for neutron and ion irradiation in tungsten: impact of transmutation and carbon impurities, J. Nucl. Mater. 500 (2018) 15–25.
[339] P. Wang, Q. Cao, J. Hou, X.-S. Kong, L. Chen, Z.M. Xie, Implantation and desorption of H isotopes in W revisited by object kinetic Monte Carlo simulation, J. Nucl. Mater. 561 (2022) 153576.
[340] P.-W. Hou, Y.-H. Li, Z.-Z. Li, L.-F. Wang, X. Gao, H.-B. Zhou, H. Song, G.-H. Lu, Influence of helium on the evolution of irradiation-induced defects in tungsten: an object kinetic Monte Carlo simulation, Chin. Phys. B 30 (8) (2021) 086108.
[341] N. Castin, A. Dubinko, G. Bonny, A. Bakaev, J. Likonen, A. De Backer, A.E. Sand, K. Heinola, D. Terentyev, The influence of carbon impurities on the formation of loops in tungsten irradiated with self-ions, J. Nucl. Mater. 527 (2019) 151808.
[342] Y.-Z. Niu, Y.-H. Li, Q.-Y. Ren, Z.-Z. Li, D. Terentyev, H.-Z. Ma, H.-B. Zhou, G.-H. Lu, Influence of carbon on the evolution of irradiation defects in tungsten, J. Nucl. Mater. 579 (2023) 154393.
[343] Z.-Z. Li, Y.-H. Li, D. Terentyev, N. Castin, A. Bakaev, G. Bonny, Z. Yang, L. Liang, H.-B. Zhou, F. Gao, et al., Investigating the formation mechanism of void lattice in tungsten under neutron irradiation: from collision cascades to ordered nanovoids, Acta Mater. 219 (2021) 117239.
[344] J. Wu, J.-P. Balbuena, Z. Hu, V. Jantunen, M.-F. Barthe, M.J. Caturla, F. Granberg, High-dose long-time defect evolution in tungsten studied by atomistically informed Object Kinetic Monte Carlo simulations, arXiv preprint arXiv:2409.15856 (2024).
[345] C.-H. Huang, M.R. Gilbert, J. Marian, Simulating irradiation hardening in tungsten under fast neutron irradiation including *Re* production by transmutation, J. Nucl. Mater. 499 (2018) 204–215.
[346] X. Chen, Y. Zhang, L. Wei, Q. Zheng, C. Zhang, Y. Li, Cluster dynamics modeling of hydrogen retention and desorption in tungsten with saturation and multi-trapping effect of sinks, Nucl. Fusion 64 (9) (2024) 096037.
[347] J.-M. Kwon, H. Choi, J. Ki, S.Y. Park, S.H. Park, Y.J. Kim, H. Cho, S. Kim, H.S. Chae, K.-S. Lee, et al., Development of a virtual tokamak platform, Fusion Eng. Des. 184 (2022) 113281. https://doi.org/10.1016/j.fusengdes.2022.113281
[348] J.-M. Kwon, C. Lee, T. Rhee, M. Woo, J. Park, C. Lee, D. Kim, J. Ki, H. Choi, C. Park, et al., Progress in digital twin development of virtual tokamak platform, IEEE Trans. Plasma Sci. 52 (9) (2024) 3910–3916.
[349] W.M.E. Ellis, L. Reali, A. Davis, H.M. Brooks, I. Katramados, A.J. Thornton, R.J. Akers, S.L. Dudarev, Mechanical model for a full fusion tokamak enabled by supercomputing, Nucl. Fusion 65 (2025) 036033. https://doi.org/10.1088/1741-4326/adb443
[350] S. Qin, Q. Wang, X. Chen, Application of virtual reality technology in nuclear device design and research, Fusion Eng. Des. 161 (2020) 111906.
[351] V. Badalassi, A. Sircar, J.M. Solberg, J.W. Bae, K. Borowiec, P. Huang, S. Smolentsev, E. Peterson, FERMI: fusion energy reactor models integrator, Fusion Sci. Technol. 79 (3) (2023) 345–379.
[352] A. Lasa, S. Blondel, M.A. Cusentino, D. Dasgupta, P. Hatton, J. Marian, D. Perez, W. Setyawan, B.P. Uberuaga, Q. Yu, et al., Development of multi-scale computational frameworks to solve fusion materials science challenges, J. Nucl. Mater. 594 (2024) 155011.
[353] J. Knaster, A. Moeslang, T. Muroga, Materials research for fusion, Nat. Phys. 12 (5) (2016) 424–434.
[354] A. Ghazari, R. Forte, T. Yamamoto, R. Odette, N. Ghoniem, Radiation effects on stress evolution and dimensional stability of large fusion energy structures, Fusion Eng. Des. 172 (2021) 112756.
[355] M. Fursdon, J.H. You, Towards reliable design-by-analysis for divertor plasma facing components-guidelines for inelastic assessment (part II: irradiated), Fusion Eng. Des. 160 (2020) 111831.
[356] L. Reali, S.L. Dudarev, Finite element models for radiation effects in nuclear fusion applications, Nucl. Fusion 64 (5) (2024) 056001.
[357] R.O. Simmons, R.W. Balluffi, Measurements of equilibrium vacancy concentrations in aluminum, Phys. Rev. 117 (1960) 52–61. https://doi.org/10.1103/PhysRev.117.52
[358] F. Onimus, T. Jourdan, C. Xu, A.A. Campbell, M. Griffiths, Irradiation creep in materials, Comprehens. Nucl. Mater. 1 (2021) 310–366.
[359] A. Ibarra, W. Królas, D. Bernardi, D. Cano-Ott, S. Becerril, I. Álvarez Castro, Y. Qiu, DONES performance, experimental capabilities and perspectives, Nucl. Fusion (2025). https://doi.org/10.1088/1741-4326/adcd86
[360] G. Van Oost, D. Terentyev, H.A. Abderrahim, Contributions of MYRRHA to the European fusion energy roadmap, Fusion Eng. Des. 198 (2024) 114098.
[361] Q. Yu, G. Po, J. Marian, Physics-based model of irradiation creep for ferritic materials under fusion energy operation conditions, J. Appl. Phys. 132 (22) (2022).
[362] S. Chatterjee, Q. Yu, Y. Li, K. Roche, J. Marian, G. Po, A spatially-resolved model of neutron-irradiated tungsten coupling stochastic cluster dynamics and finite deformation plasticity, J. Nucl. Mater. 605 (2025) 155526.
[363] C.K.C. Lieou, B.D. Wirth, A thermodynamic theory of coupling between point-defect diffusion and dislocation plasticity, J. Appl. Phys. 137 (15) (2025).
[364] J.R. Matthews, M.W. Finnis, Irradiation creep models-an overview, J. Nucl. Mater. 159 (1988) 257–285.
[365] Y.S. Garud, Low temperature creep and irradiation creep in nuclear reactor applications: a critical review, Int. J. Press. Vessels Pip. 139 (2016) 137–145.
[366] G.S. Was, Fundamentals of Radiation Materials Science: Metals and Alloys, Springer, 2007.
[367] M.R. Gilbert, S.L. Dudarev, D. Nguyen-Manh, S. Zheng, L.W. Packer, J.C. Sublet, Neutron-induced dpa, transmutations, gas production, and helium embrittlement of fusion materials, J. Nucl. Mater. 442 (1–3) (2013) S755–S760. https://doi.org/10.1016/j.jnucmat.2013.03.085
[368] C. McElfresh, Y. Cui, S.L. Dudarev, G. Po, J. Marian, Discrete stochastic model of point defect-dislocation interaction for simulating dislocation climb, Int. J. Plast. 136 (2021) 102848.
[369] Y. Kraftmakher, Equilibrium vacancies and thermophysical properties of metals, Phys. Rep. (1998). https://doi.org/10.1016/S0370-1573(97)00082-3
[370] A. Feichtmayer, M. Boleininger, J. Riesch, D.R. Mason, L. Reali, T. Höschen, M. Fuhr, T. Schwarz-Selinger, R. Neu, S.L. Dudarev, Fast low-temperature irradiation creep driven by athermal defect dynamics, Commun. Mater. 5 (2024) 218. https://doi.org/10.1038/s43246-024-00655-5
[371] D. Da Fonseca, F. Mompiou, T. Jourdan, J.-P. Crocombette, A. Chartier, F. Onimus, Evidence of dislocation loop preferential nucleation in irradiated aluminum under stress, Scr. Mater. 233 (2023) 115510. https://doi.org/10.1016/j.scriptamat.2023.115510
[372] F. Jenko, Accelerating fusion research via supercomputing, Nat. Rev. Phys. 7 (2025) 365–377. https://doi.org/10.1038/s42254-025-00837-1
[373] N.M. Ghoniem, K. Cho, The emerging role of multiscale modeling in nano- and micro-mechanics of materials, Comput. Model. Eng. Sci. 3 (2002) 147–174. https://doi.org/10.3970/cmes.2002.003.147
[374] S. Yip, Synergistic science, Nat. Mater. 2 (2003) 3–5. https://doi.org/10.1038/nmat778
[375] N.M. Ghoniem, E. Busso, N. Kioussis, H. Huang, Multiscale modelling of nanomechanics and micromechanics: an overview, Philos. Mag. 83 (2003) 3475–3528. https://doi.org/10.1080/14786430310001607388